IODP
INTERNATIONAL OCEAN DISCOVERY PROGRAM

# International Ocean Discovery Program Expedition 398 Preliminary Report

## Hellenic Arc Volcanic Field

**11 December 2022–10 February 2023**

Timothy H. Druitt, Steffen Kutterolf, Thomas A. Ronge, and the Expedition 398 Scientists

## Publisher's notes

Core samples and the wider set of data from the science program covered in this report are under moratorium and accessible only to Science Party members until 30 July 2024.

This publication was prepared by the *JOIDES Resolution* Science Operator (JRSO) at Texas A&M University (TAMU) as an account of work performed under the International Ocean Discovery Program (IODP). This material is based upon work supported by the JRSO, which is a major facility funded by the National Science Foundation Cooperative Agreement Number OCE1326927. Funding for IODP is provided by the following international partners:

National Science Foundation (NSF), United States
Ministry of Education, Culture, Sports, Science and Technology (MEXT), Japan
European Consortium for Ocean Research Drilling (ECORD)
Ministry of Science and Technology (MOST), People's Republic of China
Australia-New Zealand IODP Consortium (ANZIC)
Ministry of Earth Sciences (MoES), India

Portions of this work may have been published in whole or in part in other IODP documents or publications.

### Disclaimer



### Copyright



### Citation

Druitt, T.H., Kutterolf, S., Ronge, T.A., and the Expedition 398 Scientists, 2024. Expedition 398 Preliminary Report: Hellenic Arc Volcanic Field. International Ocean Discovery Program. https://doi.org/10.14379/iodp.pr.398.2024

### ISSN

World Wide Web: 2372-9562

January 2024

# Expedition 398 participants

## Expedition 398 scientists

**Timothy H. Druitt**
**Co-Chief Scientist**
Laboratoire Magmas et Volcans
Université Clermont Auvergne
France
**tim.druitt@uca.fr**

**Steffen Kutterolf**
**Co-Chief Scientist**
Dynamics of the Ocean Floor Research Division
GEOMAR Helmholtz Centre for Ocean Research Kiel
Germany
**skutterolf@geomar.de**

**Thomas A. Ronge**
**Expedition Project Manager/Staff Scientist**
International Ocean Discovery Program
Texas A&M University
USA
**ronge@iodp.tamu.edu**

**Sarah Beethe**
**Physical Properties/Downhole Measurements Specialist**
College of Earth, Ocean, and Atmospheric Sciences
Oregon State University
USA
**beethes@oregonstate.edu**

**Alexis Bernard**
**Inorganic/Igneous Geochemist**
Laboratoire des Fluides Complexes et leurs Réservoirs
Université de Pau et des Pays de l'Adour
France
**alexis.bernard@univ-pau.fr**

**Carole Berthod**
**Sedimentologist/Volcanologist**
Institut De Physique Du Globe De Paris
Université Paris Cité
France
**berthod@ipgp.fr**

**Hehe Chen**
**Structural Geologist**
School of Ocean Sciences
China University of Geosciences
China
**hehechen89@gmail.com**

**Shun Chiyonobu**
**Micropaleontologist (nannofossils)**
Faculty of International Resource Sciences
Akita University
Japan
**chiyo@gipc.akita-u.ac.jp**

**Acacia Clark**
**Sedimentologist/Volcanologist**
School of Natural Sciences/CODES
University of Tasmania
Australia
**acacia.clark@utas.edu.au**

**Susan DeBari**
**Igneous Petrologist/Volcanologist**
Geology Department
Western Washington University
USA
**debari@wwu.edu**

**Tatiana I. Fernandez Perez**
**Organic Geochemist**
Department of Geology
Kent State University
USA
**tfernan6@kent.edu**

**Ralf Gertisser**
**Sedimentologist/Volcanologist**
School of Geography, Geology and the Environment
Keele University
United Kingdom
**r.gertisser@keele.ac.uk**

**Christian Hübscher**
**Seismologist/Stratigraphic Correlator**
Institute of Geophysics
University of Hamburg
Germany
**christian.huebscher@uni-hamburg.de**

**Raymond M. Johnston**
**Sedimentologist/Volcanologist**
School of Geosciences
University of South Florida, Tampa
USA
**raymj@tampabay.rr.com**

**Christopher Jones**
**Inorganic Geochemist**
Department of Earth and Planetary Sciences
University of California, Riverside
USA
**cjone095@ucr.edu**

**K. Batuk Joshi**
**Inorganic/Igneous Geochemist**
Solid Earth Research Group
National Centre for Earth Science Studies
India
**kr.batukjoshi@ncess.gov.in**

**Gunther Kletetschka**
**Paleomagnetist**
Geophysical Institute
University of Alaska Fairbanks
USA
**gkletetschka@alaska.edu**

**Olga Koukousioura**
**Micropaleontologist (foraminifera/nannofossils)/Observer**
School of Geology
Aristotle University of Thessaloniki
Greece
**okoukous@geo.auth.gr**

**Xiaohui Li**
**Igneous Petrologist**
Key Laboratory of Submarine Geoscience and Prospecting Techniques
Ocean University of China
China
**xiaohuili@ouc.edu.cn**

**Michael Manga**
**Physical Properties/Downhole Measurements Specialist**
Department of Earth and Planetary Science
University of California, Berkeley
USA
**mmanga@berkeley.edu**

**Molly McCanta**
**Inorganic/Igneous Geochemist**
Department of Earth and Planetary Sciences
University of Tennessee
USA
**mmccanta@utk.edu**

**Iona McIntosh**
**Physical Properties/Downhole Measurements Specialist**
Japan Agency for Marine-Earth Science and Technology
Japan
**i.m.mcintosh@jamstec.go.jp**

**Antony Morris**
**Paleomagnetist**
School of Geography, Earth and Environmental Sciences
Plymouth University
United Kingdom
**A.Morris@plymouth.ac.uk**

**Paraskevi Nomikou**
**Physical Properties/Downhole Measurements Specialist/Observer**
Department of Geology and Geoenvironment
National and Kapodistrian University of Athens
Greece
**evinom@geol.uoa.gr**

**Katharina Pank**
**Sedimentologist/Volcanologist**
Dynamics of the Ocean Floor Research Division
GEOMAR Helmholtz Centre for Ocean Research Kiel
Germany
**kpank@geomar.de**

**Ally Peccia**
**Igneous Petrologist**
Lamont-Doherty Earth Observatory
Columbia University
USA
**asp2201@columbia.edu**

**Paraskevi N. Polymenakou**
**Microbiologist/Observer**
Institute of Marine Biology, Biotechnology and Aquaculture
Hellenic Centre for Marine Research (HCMR)
Greece
**polymen@hcmr.gr**

**Jonas Preine**
**Seismologist/Stratigraphic Correlator**
Institute of Geophysics
University of Hamburg
Germany
**jonas.preine@uni-hamburg.de**

**Masako Tominaga**
**Physical Properties/Downhole Measurements Specialist**
Department of Geology and Geophysics
Woods Hole Oceanographic Institution
USA
**mtominaga@whoi.edu**

**Adam Woodhouse**
**Micropaleontologist (planktic foraminifera)**
Institute for Geophysics
University of Texas
USA
**adam.woodhouse@austin.utexas.edu**

**Yuzuru Yamamoto**
**Structural Geologist**
Graduate School of Science
Kobe University
Japan
**yuzuru-y@harbor.kobe-u.ac.jp**

## Outreach

**Sara E. Whitlock**
**Onboard Outreach Officer**
American Association for the Advancement of Science
USA
**saraewhitlock@protonmail.com**

**Susan Schnur**
**Onshore Outreach Officer**
Washington Geological Survey
USA
**schnurs@gmail.com**

# Operational and technical staff

## Siem Offshore AS officials

**Harm Nienhuis**
Master of the Drilling Vessel

**Wayne Lambert**
Drilling Supervisor

## JRSO shipboard personnel and technical representatives

**Heather Barnes**
Assistant Laboratory Officer

**Erick Bravo**
Imaging Specialist

**Michael Cannon**
Marine Computer Specialist

**Oscar Cavazos**
Marine Laboratory Specialist

**Bridgette Cervera**
Marine Laboratory Specialist

**Etienne Claassen**
Marine Instrumentation Specialist

**Douglas Cummings**
Publications Specialist

**David Fackler**
Applications Developer

**Kirby Garrett**
Schlumberger Engineer

**Luan Heywood**
Marine Laboratory Specialist

**Jan Jurie Kotze**
Marine Instrumentation Specialist

**Nicholas Logan**
Marine Computer Specialist

**Zenon Mateo**
Marine Laboratory Specialist

**Eric Moortgat**
Assistant Laboratory Officer

**Elisabetta Olivo**
Marine Laboratory Specialist

**Chieh Peng**
Laboratory Officer

**Doris Pinero**
Marine Laboratory Specialist

**William Rhinehart**
Operations Superintendent

**Alexander Roth**
Marine Laboratory Specialist

**Johanna Suhonen**
Marine Laboratory Specialist

**Kara Vadman**
Marine Laboratory Specialist

# Abstract

The objectives of International Ocean Discovery Program (IODP) Expedition 398, Hellenic Arc Volcanic Field (11 December 2022 to 10 February 2023), were to study the volcanic record of the central Hellenic island arc; document the links and feedbacks between volcanism/magmatism, crustal tectonics, and sea level; investigate the processes and products of shallow submarine eruptions of silicic magma; and groundtruth the seismic stratigraphy of Santorini caldera. Reconstructing the subsidence history of the southern Aegean Sea and searching for deep life inside and outside of Santorini caldera were additional objectives.

The expedition drilled 10 primary and alternate sites that were originally proposed, in addition to 2 extra sites that were requested during the expedition. Outside of Santorini caldera, drilling penetrated the thick basin fills of the crustal rift system hosting the Christiana-Santorini-Kolumbo volcanic field, identifying numerous pumice and ash layers, some known from on land and others hitherto unknown, pushing back the onset of volcanism in the area into the Early Pleistocene or even Pliocene. Significant events of mass wasting into the basins, accompanied by very high sedimentation rates, were also documented. These basin sites served to groundtruth the seismic stratigraphy of the basins and to open the way to unraveling relationships between volcanic activity and crustal rift pulses. Two sites of condensed sequences on the basin margins served to sample many volcanic layers within the detailed age-depth constraints provided mainly by biostratigraphy, as diagenetic effects complicated the magnetic reversal record significantly. Drilling penetrated the Alpine basement at three basin sites northeast of Santorini, whereas in the Christiana Basin to the southwest it penetrated a thick sequence of Messinian evaporites. Drilling inside Santorini caldera penetrated to ~120 meters below seafloor (mbsf), less than planned due to hole instability issues but deep enough to groundtruth the seismic stratigraphy and to sample the different layers. One intracaldera hole yielded a detailed tephra record of the history of the Kameni Islands, as well as possible evidence for deep bacterial colonies within the caldera. Despite variable recovery in the unstable pumice and ash deposits, the expedition was a significant success that may address almost all the science objectives once the laboratory work has been done.

A dense program of preexpedition and shipboard outreach during the expedition gave rise to 59 live ship-to-shore tours, reaching 6,400 people in 7 countries including many school children. A total of 51 journalists were contacted and 9 stories were written about the expedition, with a readership of almost 200,000 people. While in Santorini caldera, the ship hosted 12 documentarians and journalists, the future products of whom should include a 1.5 h documentary and a four-part TV series about Expedition 398. The expedition social media pages were active. Prior to the expedition, an exhibition, "In Search of Earth's Secrets," ran for a week on Santorini and was visited by more than 1,800 school children.


# Plain language summary

About 800 million people are threatened by volcanic eruptions around the globe: high plumes of ash, ground-hugging flows of hot ash and rock, earthquakes, and associated tsunamis. The Christiana, Santorini, and Kolumbo volcanic group in the Aegean Sea of Greece is particularly hazardous because the volcanoes have produced many eruptions in the past, and some of them were highly explosive. Santorini is an iconic volcano because of its well-known eruption in the Late Bronze Age, and it is a major tourist destination. Although much has been learned about the eruption history of the Aegean volcanoes on land, most of their volcanic products lie on the seafloor, requiring research to move offshore.

During International Ocean Discovery Program (IODP) Expedition 398 we drilled the submarine sediment sequences, including muds and volcanic products, that fill the marine basins around the volcanoes and inside of Santorini caldera at twelve sites. Outside of the caldera, we penetrated many layers of pumice and ash, representing eruptive products settled at the seafloor. Some of these layers represent hitherto unknown explosive eruptions whose products do not occur on land. The ages of the different layers were determined mainly from the assemblages of microfossils preserved in them. We also identified times in the past when large fault movements and earth-

quakes appear to have caused remobilization of previously deposited ash layers, causing them to pour into the actively deepening basins. In the Christiana Basin south of Santorini, we unexpectedly penetrated a thick sequences of evaporates, formed 5.3 million years ago during the so called "Messinian Salinity Crisis." Inside Santorini caldera, we drilled through sediments and volcanic products that have accumulated there since the Late Bronze Age eruption, offering a detailed record of the previously inaccessible prehistoric evolution of Kameni Volcano, inside the caldera. At two sites inside Santorini caldera and two others outside, we collected samples for microbiological and genetic analysis to identify and characterize any microbial life living in the muds below the sediment surface.

Despite variable recovery in the unstable pumice and ash deposits, the expedition was a great success that will enable us to address almost all of the original science objectives once detailed laboratory work has been done. Some particularly important aims will be to link the volcanic activity to ancient crustal tectonic processes, as well as to variations in sea level through time due to changes in Earth's climate, and see any governing feedbacks between these processes.

A dense program of preexpedition and shipboard outreach during the expedition gave rise to 59 live ship-to-shore tours, reaching 2.5 million (6,400 not including China) people in 7 countries including many school children. Nine news stories were written about the expedition, with a readership of almost 200,000 people. While in Santorini caldera, the ship hosted 12 documentarians and journalists, the future products of whom should include a 1.5 hour documentary and a four-part TV series about Expedition 398. The expedition social media pages were very active. Prior to the expedition, an exhibition, "In Search of Earth's Secrets," ran for a week on Santorini and was visited by over 1,800 school children.

# 1. Introduction

Volcanic hazards and risks lie at the heart of global geoscience, with about 800 million people threatened by eruptions (Loughlin et al., 2015). Volcanoes in island arc settings impact humans and the environment through explosive eruptions (both subaerial and submarine), tephra fallout, pyroclastic flows, earthquakes, tsunamis, and ocean acidification. Some large eruptions, such as the Late Bronze Age eruption of Santorini, may have destabilized entire civilizations (e.g., Bruins et al., 2008). On the other hand, volcanoes can host rich ecosystems and fertilize the oceans (Duggen et al., 2010; Christakis et al., 2018).

Better understanding of the processes governing arc volcanoes and their hazards is important as the twenty-first century unfolds (McGuire et al., 2017; National Academies of Sciences, Engineering, and Medicine, 2017). Crustal tectonics is one process that strongly influences volcanism, but it has rarely been studied at high spatial and temporal resolutions (e.g., Cembrano and Lara, 2009). Crustal thickness and thermal structure affect the production of magmas in the mantle and their subsequent evolution through crystal fractionation, crustal contamination, and magma mixing (e.g., Farner and Lee, 2017). Extensional crustal motions across many island arcs create space for magma ascent and influence the depths and sizes of magma storage regions (Acocella and Funiciello, 2010; Bachmann and Huber, 2016). Large earthquakes cause changes in crustal stresses sufficient to induce eruptions as far as several hundreds of kilometers away (e.g., Walter and Amelung, 2007). Changes in sea level driven by tectonics or climate modulate volcanic activity by loading or unloading the magma plumbing system (Kutterolf et al., 2013; Sternai et al., 2017; Satow et al., 2021).

The Christiana-Santorini-Kolumbo (CSK) volcanic field is an excellent region at which to address these fundamental questions (Nomikou et al., 2019). It is one of the most active in Europe, having produced more than 100 explosive eruptions in the last 360 ky (Druitt et al., 1999; Druitt and Vougioukalakis, 2019). Situated in a rift zone that cuts northeast–southwest across the island arc, the field includes the extinct Christiana Volcano, Santorini caldera with its intracaldera Kameni Volcano, Kolumbo Volcano, and the 22 submarine cones of the Kolumbo volcanic chain (Figure **F1**) (Hooft et al., 2017; Hübscher et al., 2015; Nomikou et al., 2012, 2013, 2019), all of which have discharged their volcanic products into adjacent marine basins, creating a rich archive of past erup-

tions. Santorini is one of the most explosive arc volcanoes in the world; its onland products have been mapped, dated, and chemically fingerprinted, and its historical eruptions are well documented (Druitt et al., 1999; Pyle and Elliott, 2006). Kolumbo Volcano has had at least five large explosive eruptions, the last in the year 1650 (Hübscher et al., 2015; Nomikou et al., 2016b).

Prior to Expedition 398 we had a record of Santorini volcanism going back to 650 ka, but it was only detailed since 360 ka (Druitt et al., 1999). Apart from the 1650 CE eruption, the past volcanism of Kolumbo Volcano was poorly documented and that of Christiana Volcano was largely unknown. Offshore drilling enabled us to use the thick volcano-sedimentary records of the rift basins and Santorini caldera as time capsules for reconstructing the volcanic and tectonic histories of the area since rift inception in the Pliocene (Nomikou et al., 2018). Drilling allowed (1) groundtruthing of marine seismic profiles, (2) characterization and dating of seismic packages, (3) measurements of the physical properties of submarine strata, and (4) sampling for any subsurface ecosystems.

Hazards from the CSK rift zone include earthquakes, eruptions, and tsunamis (Dimitriadis et al., 2009, 2010; Cantner et al., 2014; Ulvrova et al., 2016; Vougioukalakis et al., 2016). The level of seismicity is among the highest in Europe (Sachpazi et al., 2016; Brüstle et al., 2014), and the largest twentieth-century shallow earthquake in Europe (M 7.5) took place there in 1956 (Okal et al., 2009). The Late Bronze Age (LBA) eruption of Santorini of about 3.6 ka was one of the largest of the Holocene Epoch worldwide; it may have influenced the decline of the Minoan civilization on Crete and thus is an iconic event in both volcanology and archaeology (e.g., Bruins et al., 2008). The 1650 CE eruption of Kolumbo Volcano killed 70 people on Santorini through gas release and tsunami inundation (Fuller et al., 2018; Ulvrova et al., 2016; Dominey-Howes et al., 2010; Cantner et al., 2014). Santorini had an episode of bradyseism unrest in 2011–2012 (Newman et al., 2015; Parks et al., 2015), raising awareness of the eruption threat at these islands that are visited by 2 million tourists per year.

Drilling was carried out in the context of several new research initiatives in the marine environment of the volcanic field. A dense network of subseafloor seismic reflection profiles exists across the rift zones, giving high-resolution images of sedimentary fills and faults (Figure **F2**) (Sigurdsson et al., 2006; Hübscher et al., 2015; Nomikou et al., 2013, 2016a, 2018). Detailed correlations and interpretations of these profiles from northeast to southwest across the volcanic field had previously led to a detailed seismic stratigraphic model (Preine et al., 2022c) that was tested and refined now by deep drilling. In 2015, an active seismic tomography experiment of the CSK system was carried out (PROTEUS: Plumbing Reservoirs Of The Earth Under Santorini; Hooft et al., 2017). It identified an upper-crustal magma reservoir beneath Santorini and extending northeastward

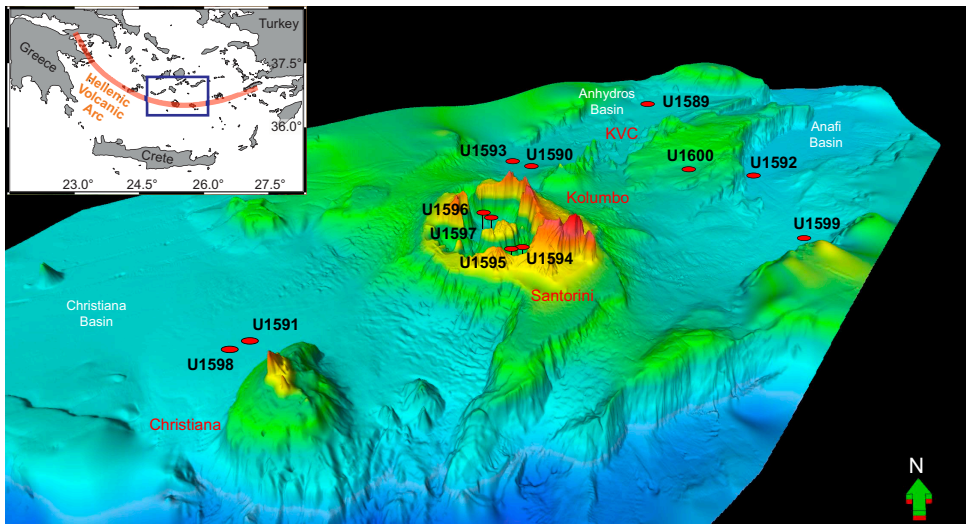


**Figure F1**. Three-dimensional view of the CSK volcanic field and its host rift basins, looking north, with the locations of Expedition 398 Sites U1589–U1600 (Nomikou et al., 2012, 2013; Hooft et al., 2017). KVC = Kolumbo volcanic chain.

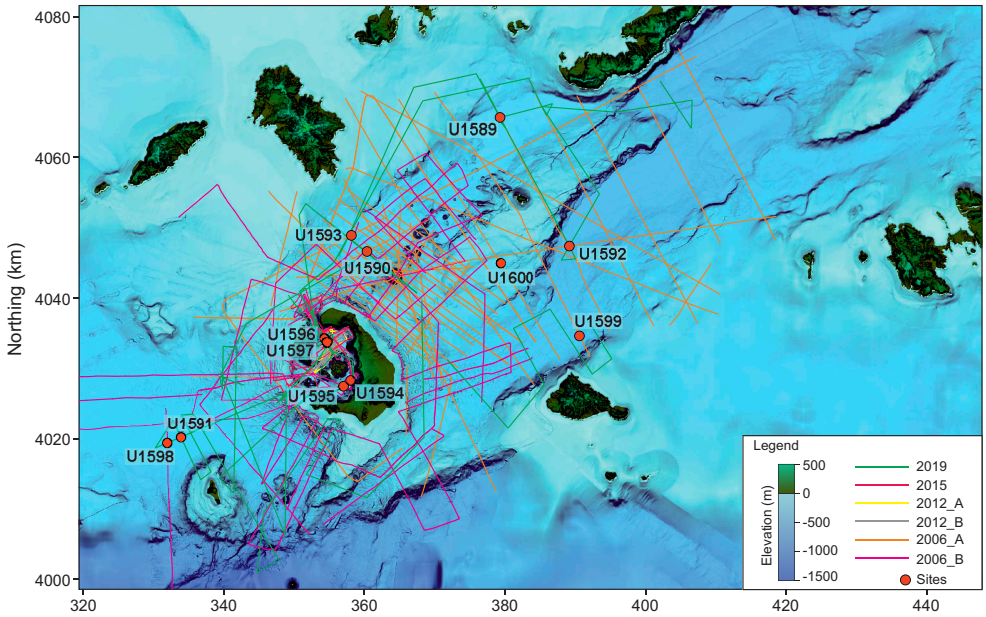


**Figure F2.** Seismic lines in and around CSK volcanic field with the locations of Expedition 398 drilling Sites U1589–U1600 (Hübscher et al., 2015; Preine et al., 2022b).

toward Kolumbo Volcano (McVey et al., 2020). Multibeam bathymetric surveys imaged submarine volcanic edifices and calderas (Nomikou et al., 2012, 2013, 2016a). Seismic reflection profiles inside Santorini caldera previously allowed recognition of several intracaldera layers (Johnston et al., 2015) that were sampled now by drilling. Seafloor volcanic products, hydrothermal deposits, and bacterial mounds were previously sampled (Hanert, 2002; Camilli et al., 2015), and the surface biosphere had been documented (Oulas et al., 2016; Polymenakou et al., 2021). Deep-sea ash layers were sampled by gravity coring across the Eastern Mediterranean, and many have been correlated with onshore products. The resulting preexpedition marine ash stratigraphy that extended back to 200,000 a included 12 ash deposits from CSK volcanoes and allowed estimation of the ages and masses of many of the tephra layers (Satow et al., 2015; Wulf et al., 2020; Kutterolf et al., 2021a, 2021b).

Expedition 398 started in Tarragona, Spain, on 11 December 2022 and ended in Heraklion, Greece, on 10 February 2023. Of the 12 drilled sites, 10 were primary or alternate sites proposed in the *Expedition 398 Scientific Prospectus* (Druitt et al., 2022); permission for the other two sites was granted during the expedition.

## 2. Geologic setting

The Hellenic volcanic arc owes its existence to subduction of the African plate beneath the European plate, which initiated in the Pliocene (Pe-Piper and Piper, 2005; Shaw and Jackson, 2010). The subducted slab descends at an angle of 10°–30°, and the back-arc Aegean region has been in extension since the Pliocene, a result of slab rollback (Jolivet et al., 2013; Papazachos, 2019). The convergence rate along the arc is 35 ± 8 mm/y, divided into 5–10 mm/y of relative motion between the Eastern Mediterranean and the Aegean and ~25 mm/y of slab rollback. Back-arc extension has thinned the Aegean continental crust, creating horsts and grabens (Le Pichon and Kreemer, 2010; Royden and Papanikolaou, 2011) (Figure **F1**). The Hellenic subduction system has one of the oldest (coolest) slabs and lowest convergence rates on Earth (Syracuse et al., 2010).

The island arc consists of five volcanic fields: Sousaki, Aegina-Poros-Methana, Milos, Christiana-Santorini-Kolumbo (CSK), and Kos-Nisyros-Yali, from west to east. The CSK volcanic field lies in the center of the arc on 18–20 km of thinned continental crust (Makris et al., 2013). It is located in a rift zone 100 km long × 45 km wide with three main northeast-southwest–oriented marine

basins and Pliocene–Quaternary sedimentary fills as thick as 800 m (Piper and Perissoratis, 2003; Nomikou et al., 2016b, 2018) (Figure **F1**). According to Heath et al. (2019) and Preine et al. (2020), the sediment infill in the Santorini-Anafi Basin is 1.4 km up to 2.0 km. The Anhydros Basin contains the Kolumbo volcanic chain, whereas the Anafi Basin lacks volcanoes. The Anhydros and Anafi Basins each contain six seismic stratigraphic units (here named Seismic Units U1–U6, upward), separated by onlap surfaces (Preine et al., 2022a). Thickness variations of the units record initial symmetric rifting (Units U1–U3) followed by northwest-tilted, more asymmetric rifting (Units U4–U6). Prior to Expedition 398, rifting was believed to have begun 3.8–5.3 My ago in the Pliocene (Nomikou et al., 2018).

The Christiana Basin, a broad, fault-bounded basin at the southwest entrance of the rift zone (Figure **F1**), contains Pliocene–Quaternary sediments and volcaniclastics divided into six major units, Seismic Units U1–U6 (Preine et al., 2022c).

Santorini caldera is a complex 11 km × 7 km structure caused by at least four collapse events over the last ~200,000 y, the last of which was the LBA eruption (Druitt and Francaviglia, 1992). It has a northern basin 390 m deep, a southern basin 280 m deep, and is connected to the sea via three breaches (Nomikou et al., 2014). The caldera's volcano-sedimentary fill is about 1 km thick (Budetta et al., 1984). The Kameni Islands are the subaerial summit of a 470 m high intracaldera edifice formed since the LBA eruption.

Preexpedition onland studies had suggested that volcanism at Santorini began 650,000 y ago with submarine, then subaerial, effusive activity and became highly explosive 360,000 y ago (Thera Pyroclastic Formation). There have since been about 12 Plinian eruptions (and ~100 less intense explosive eruptions), many of which generated high ash plumes and pyroclastic flows that entered the sea (Druitt et al., 1999). The LBA eruption of 3.6 ka (also called the Minoan eruption) discharged several tens of cubic kilometers of silicic magma as fallout and pyroclastic flows (Druitt, 2014), and the resulting subsidence deepened an already-existing caldera (Athanassis et al., 2016). After the caldera collapsed, the sea broke through the northwest breach, carving out a 2 km wide submarine channel (Nomikou et al. 2016a). Kameni Volcano has had nine subaerial effusive eruptions between 197 BCE and 1950, but bathymetry suggests a long previous submarine history (Pyle and Elliott, 2006; Nomikou et al., 2014).

Seismic profiles reveal three main units in the topmost caldera fill (here named Seismic Units S1–S3, downward; interpreted most recently as follows (Johnston et al., 2015; Nomikou et al., 2016a):

- S1: flat-lying sediments up to 40 m thick: mass wasting of the caldera cliffs;
- S2: sediments up to 100 m thick that merge into the clastic apron of Kameni edifice: tuffs and hyaloclastites from the submarine phase of Kameni; and
- S3: down-faulted deposits as thick as 250 m: uppermost levels of LBA intracaldera tuffs and/or sediments related to posteruptive flooding of the caldera. Sub-S3 deposits lack layering on seismic images and are interpreted as LBA intercaldera tuffs.

The extinct Christiana Volcano produced lavas and tuffs of unknown ages (Aarbourg and Frechen, 1999), but a particularly large ignimbrite found on neighboring islands is dated at ~1 Ma (Keller et al., 2010). The eroded remains of the volcano form two main islands: Christiani and Askani. Geochemical and $^{40}Ar/^{39}Ar$ dating studies of onland Christiana volcanics are in progress (Vrije Universiteit, Amsterdam). Prior to Expedition 398, very little was known about the volcanic history of Christiana.

Kolumbo Volcano rises 480 m above the surrounding seafloor, with a 1.7 km diameter summit crater formed in 1650 (Nomikou et al., 2012; Carey et al., 2013). Seismic profiles across it reveal five units interpreted as Kolumbo-derived volcaniclastics (Eruption Units K1–K5, from the base up); Unit K5 is the 1650 eruption (Hübscher et al., 2015). The submarine cones northeast of Kolumbo postdate Unit K2 on seismic profiles; they are much smaller than Santorini or Kolumbo, and their products are not expected to be prominent in our drill cores.

Based on the compiled seismic data set, Preine et al. (2022c) proposed that the entire CSK volcanic field evolved during four phases:

1. Phase 1—initiated in the Pliocene with formation of the Christiana Volcano.
2. Phase 2—formation of the current southwest-northeast–trending rift system associated with the evolution of two distinct volcanic centers, a proposed submarine Poseidon Center and the early Kolumbo Volcano.
3. Phase 3—a period of widespread volcanic activity throughout the entire rift.
4. Phase 4 (ongoing)—confined to Santorini caldera and Kolumbo Volcano.

## 2.1. Seismic studies/site survey data

A dense network of multichannel and single-channel seismic reflection profiles (campaigns in 2006–2015; Figure **F2**) from collaborating groups and publications have been interpreted in detail in the Santorini caldera (based on the volcanic history recorded on land; Johnston et al. 2015) and in the basins northeast of Santorini as well as to the southwest in the Christiana Basin (Sigurdsson et al., 2006; Hübscher et al., 2015; Nomikou et al., 2016a, 2016b, 2018; Tsampouraki-Kraounaki and Sakellariou, 2018). A further 620 km of new high-quality multichannel seismic profiles was shot in October 2019 (Karstens et al., 2020; Preine et al., 2022c). All profiles, which sum to 3350 km in length, were recorded with different sources and streamers and were merged into a homogeneous dataset at the University of Hamburg. All proposed primary drilling sites are situated at (or very close to) the intersections of multichannel seismic profiles. During the PROTEUS cruise in 2015 (Hooft et al., 2019), 3.5 kHz subbottom profiling and gravity and magnetic data were recorded.

In addition to the seismic survey and interpretations, fault distributions and throws have been mapped northeast of Santorini (Nomikou et al., 2016b; Hooft et al., 2017), and two-way traveltime (TWT) isopach maps have been constructed for each rift basin. High-resolution multibeam bathymetry is available inside and outside of Santorini caldera (Nomikou et al., 2014, 2016a; Hooft et al., 2017).

Shallow sediments at or close to the drill sites provide initial sediment properties and tephrochronostratigraphic interpretations (Kutterolf et al., 2021a, 2021b). A large database of radiometric ages (K-Ar, $^{40}Ar/^{39}Ar$, and $^{14}C$) and whole-rock chemical analyses exists for onland volcanic deposits from the CSK centers, particularly Santorini, along with glass major and trace element analyses for marine ash layers dating back to 200 ka (e.g., Druitt et al., 1999; Wulf et al., 2020; Kutterolf et al., 2021a, 2021b).

# 3. Scientific objectives

## 3.1. Objective 1. Arc volcanism in an active rift environment

Analysis of preexpedition seismic profiles northeast and southwest of Santorini led to an interpretation of the development of the volcanic field in space and time (Preine et al. 2022c). This interpretation invoked (in chronological order) the development of Christiana Volcano (Late Pliocene), followed by Kolumbo Volcano Eruption Units K1 and K2 and an offshore submarine center (Poseidon; early Quaternary), a mass transport deposit of unknown origin, deposits from the Akrotiri and Peristeria Volcanoes, Kolumbo Volcano Eruption Unit K3 and Kolumbo submarine cones (0.65–0.35 Ma), and the post-0.35 Ma explosive products of Santorini (Thera Pyroclastic Formation) and Eruption Units K4/K5 of Kolumbo Volcano. We planned to test this hypothesis using cores from all sites to reconstruct a complete volcanic stratigraphy of the CSK volcanic field since rift inception in the Pliocene, consistent with both onshore and offshore constraints.

It was anticipated that eruption products would be preserved in the rift basins not only as tephra fallout but also as turbidites channeled down the basin axes from volcanoes upslope (e.g., Schmincke and Sumita, 1998). Bed-to-bed and seismic unit-to-unit correlation between cores would use major and trace element compositions of juvenile blocks or lapilli, glasses, crystal-hosted glass inclusions (e.g.; Lowe, 2011; Brandl et al., 2017; Freundt et al., 2021), and phenocrysts. Correlation of volcaniclastics to source volcanoes would exploit established chemical and mineralogical differences between the different volcanic centers, extending chemical correlation databases already developed for the <0.2 Ma tephra layers (Kutterolf et al., 2021a, 2021b). Tephra fall

layers from other circum-Mediterranean volcanoes might serve as marker beds (Satow et al., 2015; Wulf et al., 2020). Absolute dates of cored volcanic layers based on (i) published onshore ages, (ii) published ages of marine tephra fall layers, and (iii) new radiometric age determinations of suitably fresh drilled pyroclasts as well as biostratigraphic constraints would refine the volcanic chronostratigraphy.

## 3.2. Objective 2. The volcano-tectonic connection

Studies of Miocene plutons, of fault patterns along the modern-day arc, and of relationships between regional seismicity and caldera unrest at Santorini in 2011–2012 all hint at intimate relationships between Aegean volcanism and crustal tectonics (Kokkalas and Aydin, 2013; Feuillet, 2013; Rabillard et al., 2018). We aimed to test this hypothesis by (i) reconstructing the histories of subsidence and tectonics of the Anhydros, Anafi, and Christiana Basins from our drill cores and seismic records, (ii) integrating them with our volcanic chronostratigraphy, (iii) seeking relationships between CSK volcanism and major crustal tectonic events, and finally (iv) investigating how sea level may modulate volcanic activity.

We planned to reconstruct the sedimentary and subsidence histories of the basins using sediment-focused chronostratigraphic techniques: biostratigraphy, sapropel records, and magnetostratigraphy. Inclusion of the volcanic record would then build a detailed rift-wide stratigraphy with multiple independent age markers, enabling construction of a Bayesian age model for each basin. Benthic foraminifera would provide estimates of paleowater depth and, via integration with seismic profiles and chronologic data, time-integrated basin subsidence rates (Pallikarakis et al., 2018).

## 3.3. Objective 3. Arc magmatism in a region of extending crust

Magmas of the CSK field have ascended through 18–20 km of rifted continental crust, which has influenced their chemical and isotopic evolution (e.g., Bailey et al., 2009; Elburg et al., 2014). Primitive basaltic melts rise into the crust, where they evolve to intermediate and silicic compositions through fractional crystallization, crustal melting/assimilation, and magma mixing (Cashman et al., 2017). It is likely that the structure of the rifted crust governs the polybaric ascent history of the CSK magmas, with evolving faults, density interfaces, and rheological transitions (Jolivet et al., 2013) controlling levels of magma storage and differentiation (Flaherty et al., 2018), as observed in the exhumed Miocene magmatic complexes of the Aegean (Rabillard et al., 2018).

We aimed to investigate magma genesis and the links with rifting history using major, trace, and multi-isotopic data on suitably fresh rocks. Volatile contents of crystal-hosted melt inclusions and mineral-barometry techniques would be used to quantify magma storage depths during ascent prior to eruption. These data will constrain how mantle source characteristics and heterogeneity (Bailey et al., 2009; Klaver et al., 2016b), degree of magma contamination by the crust, and the role of lower crustal amphibole have varied in space and time since the Pliocene across the volcanic field.

## 3.4. Objective 4. Unraveling an iconic caldera-forming eruption

The LBA eruption of Santorini has attracted attention for many decades (Friedrich, 2009), and the onland products have been studied in detail (Druitt, 2014). More recently, seismic studies have imaged the LBA products both outside (Sigurdsson et al., 2006) and inside (Johnston et al., 2015) the caldera, although their firm identification on seismic profiles is problematic due to the many other eruptions and tuffs with which they can be confused.

LBA tuffs accumulated outside the caldera are inferred from seismic profiles to be as thick as 80 m and have an estimated volume in the range of 30–60 $km^3$ (DRE: dense-rock equivalent; Pyle, 1990; Sigurdsson et al., 2006). Drilling enabled us to core the LBA deposits both outside and inside the caldera and to groundtruth the seismic profiles using downhole measurements of seismic velocities. Outside the caldera, drilling targeted the LBA submarine pyroclastic flows at Sites U1589, U1590, U1591, U1593, and U1598 to also test the published seismic interpretation.

Inside Santorini caldera, we planned to drill to 234 mbsf in the northern caldera basin (Sites U1596, U1597) and to 360 mbsf in the southern basin (Sites U1594, U1595). Our planned drilling targeted the top of the sub-S3 unit that is thought to possibly be intracaldera LBA tuffs. By drilling into the LBA tuffs in the caldera, we would have been able to estimate their minimum volume, contributing to volume estimates for LBA deposits on- and offshore (outside of the caldera) to make a new, much more precise (minimum) estimate of the erupted volume.

## 3.5. Objective 5. Volcanic hazards from submarine silicic eruptions

A potential future hazard at Santorini is a submarine eruption of Kameni or Kolumbo Volcanoes, similar to that of 1650 CE but possibly not as large. Better understanding of the dynamics of such eruptions will enable us to improve risk mitigation strategies in this highly populated and densely visited part of the Eastern Mediterranean (Vougioukalakis et al., 2016; Carey et al., 2018).

Studies of the products of the 1650 CE eruption of Kolumbo Volcano show that the eruption was driven mainly by primary degassing of the water-rich silicic magma, but with a component of phreatomagmatic fragmentation, and that the deposits were emplaced by a combination of subaerial plumes, submarine plumes, and density currents (Cantner et al., 2014). The planned drilling would enable us to traverse the products of at least three earlier explosive eruptions of Kolumbo Volcano (Eruption Units K1–K4). We would be able to compare these earlier submarine eruptions to that of 1650 CE, test the leading hypothesis, and arrive at a general model for this rarely accessible type of submarine volcanism.

Inside Santorini caldera, Seismic Unit S2 would provide access to a petrological time series of postcaldera volcanism that dates back to the birth of Kameni Volcano after the LBA eruption to its emergence in 197 BCE. Using similar methods as at Kolumbo Volcano, we could reconstruct the history of eruption styles over the growth of Kameni from 400 m water depth to the surface. It is rare to have a complete record of postcaldera volcanism at an arc caldera, as the magmatic transition and the long subsequent evolution of the new intracaldera volcano seldom are both preserved.

## 3.6. Objective 6. Transition from continental to marine environments in the southern Aegean

The drilling in the Christiana, Anhydros, and Anafi Basins will allow us to pierce the entire basin stratigraphy and reach the basement unconformity (presubsidence land surface). This provides the opportunity to reconstruct the environmental histories of the basins from continental to deep-marine stages, as well as the evolution of the Eastern Mediterranean paleoclimate since the Pliocene. Prior to Expedition 398 the subsidence history in the southern Aegean was poorly known due to the paucity of offshore studies. The plan was to build a high-resolution biostratigraphic framework for the recovered Expedition 398 cores then extract a time series of paleoenvironmental data from the cores using assemblages of calcareous nannofossils, benthic and planktonic foraminifera, dinoflagellates, and pollen, refined by stable oxygen and carbon isotopes, total organic carbon, major and trace elements, and organic biomarkers for selected depth intervals.

## 3.7. Objective 7. Biological systems reactions to volcanic eruptions and seawater acidification

The deep-marine biosphere hosts a large component of the world's microbial ecosystems, but little is known about them (Parkes et al., 2000; Schippers et al., 2005). Marine microbes have evolved to respond to environmental challenges, resulting in different survival mechanisms, growth strategies, and genetic adaptations. Knowing that Santorini caldera harbors highly diverse, metabolically complex microbial communities (Oulas et al., 2016; Christakis et al., 2018), we planned to use core material from inside the caldera (Sites U1594–U1597) and outside the caldera (Sites U1599 and U1600) to characterize the living and fossilized subseafloor biological communities present. This would enable us to document the sizes, genetic variabilities, and metabolic functions of subsurface ecosystems to 700 m depth, as well as explore for past anoxic events in the subsurface, extant biological activity, and trace fossils of extinct seafloor life.

Study of drill cores and pore fluids would moreover investigate the relationship between extant, or fossilized, subseafloor microbial communities and subseafloor biogeochemical and mineralization processes, particularly the relative importance of Fe released from hydrothermal activity in sustaining subseafloor biomes (Templeton, 2011).

### 3.8. Connections to the 2050 Science Framework

Overall, the results of Expedition 398 will address five of the seven Strategic Objectives of the 2050 Science Framework (Habitable and Life on Earth, The Ocean Life Cycle of Tectonic Plates, Earth's Climate System, Feedbacks in the Earth System, and Natural Hazards Impacting Society) and two of the Flagship Initiatives (Assessing Earthquake and Tsunami Hazards and Exploring Life and its Origins).

## 4. Site summaries

### 4.1. Site U1589

#### 4.1.1. Background and objectives

The principal aim at Site 1589 (Prospectus Site CSK-01A) was to reconstruct the evolution of the Anhydros Basin including its history of subsidence as well as to document the presence of volcanic event layers in the basin sediments and draw conclusions regarding the links between volcanism and crustal tectonics. The site is located about 10 km southwest of Amorgos Island in a water depth of 494 meters below sea level (mbsl). The drill site targeted the volcano-sedimentary fill of the Anhydros Basin. We received permission from the International Ocean Discovery Program (IODP) Environmental Protection and Safety Panel (EPSP) to touch Alpine basement using an advanced piston/extended core barrel/rotary core barrel (APC/XCB/RCB) drilling strategy.

The site was chosen because it is situated on a sediment distribution pathway that leads downstream from both Santorini and Kolumbo Volcanoes. It was therefore expected that the site would receive volcaniclastic material from both volcanic systems, both as turbidity currents directed by the basin bathymetry and as tephra fallout controlled by high-altitude wind patterns (Kutterolf et al., 2021a, 2021b). The aim of drilling at the site was (1) to fingerprint the volcaniclastic layers at the site, (2) correlate them using chemical and mineralogical criteria with their source volcanoes, (3) establish a complete stratigraphy for Santorini and Kolumbo Volcanoes and how they interrelate, and (4) seek links between volcanic activity and the tectonic history of the Anhydros Basin as recorded on seismic profiles. Drilling was very successful, with good recovery in the cores from all three holes (U1589A, U1589B, and U1589C), and Hole U1589C touched the limestone basement. The site transected all six seismic packages (Seismic Units U1–U6) of the Anhydros rift basin, as well as the onlap surfaces between them (Nomikou et al. 2016b, 2018; Preine et al., 2022a, 2022b).

#### 4.1.2. Operations

We started our 1241 nmi voyage across the Mediterranean to Aegean Sea Site U1589 at 1254 h local time on 16 December 2022 in Tarragona, Spain, and completed the transit to Site U1589 on 21 December at 0715 h.

##### 4.1.2.1. Hole U1589A

The bottom-hole assembly (BHA) and drill string were assembled and lowered to the seafloor at 484.3 mbsl. Using the APC, half-length APC (HLAPC), and XCB, Hole U1589A was cored to 446.7 m, recovering 350.55 m of volcanic, tuffaceous, and nonvolcanic sediments (Table **T1**).

##### 4.1.2.2. Hole U1589B

Hole U1589B was spudded in a water depth of 482.6 mbsl and recovered 331.46 m of volcaniclastic sediments, reaching a maximum depth of 381 meters below seafloor (mbsf) (all mbsf depths in this report are equivalent to core depth below seafloor, Method A [CSF-A]). At the base of Core 70F, the Sediment Temperature Tool (SET-2) probe was deployed to analyze the formation temperature at the bottom of the hole.

**Table T1.** Operations summary, Expedition 398.

| Hole | Latitude | Longitude | Water depth (m) | Penetration DSF (m) | Cored interval (m) | Recovered length (m) | Recovery (%) | Drilled interval (m) | Drilled interval (no.) | Total cores (no.) | APC cores (no.) | HLAPC cores (no.) | XCB cores (no.) | RCB cores (no.) | Other cores (no.) |
|---|---|---|---|---|---|---|---|---|---|---|---|---|---|---|---|
| U1589A | 36°43.7577′N | 25°38.8915′E | 484.3 | 446.7 | 446.7 | 350.55 | 78 | | 0 | 75 | 15 | 49 | 11 | 0 | 1 |
| U1589B | 36°43.7574′N | 25°38.9057′E | 482.6 | 381.0 | 381.0 | 331.46 | 87 | | 0 | 70 | 12 | 58 | 0 | 0 | 0 |
| U1589C | 36°43.7463′N | 25°38.9046′E | 482.6 | 621.9 | 261.9 | 62.08 | 24 | 360 | 1 | 27 | 0 | 0 | 0 | 27 | 0 |
| | | Site U1589 totals: | | 1449.6 | 1089.6 | 744.09 | | 360 | 1 | 172 | 27 | 107 | 11 | 27 | 1 |
| U1590A | 36°33.2938′N | 25°26.3888′E | 397.1 | 99.3 | 99.3 | 60.87 | 61 | | 0 | 11 | 11 | 0 | 0 | 0 | 0 |
| U1590B | 36°33.3129′N | 25°26.3644′E | 397.1 | 634.7 | 541.7 | 74.73 | 14 | 93 | 1 | 56 | 0 | 0 | 0 | 56 | 0 |
| | | Site U1590 totals: | | 734.0 | 641.0 | 135.60 | | 93 | 1 | 67 | 11 | | | 56 | |
| U1591A | 36°18.7615′N | 25°9.0057′E | 514.6 | 98.8 | 98.8 | 64.76 | 66 | | 0 | 11 | 11 | 0 | 0 | 0 | 0 |
| U1591B | 36°18.7621′N | 25°9.0190′E | 513.8 | 389.2 | 364.5 | 155.08 | 43 | 24.7 | 1 | 42 | 8 | 6 | 28 | 0 | 0 |
| U1591C | 36°18.7810′N | 25°8.9962′E | 513.8 | 902.9 | 668.6 | 384.47 | 58 | 234.3 | 2 | 69 | 0 | 0 | 0 | 69 | 0 |
| | | Site U1591 totals: | | 1390.9 | 1131.9 | 604.31 | | 259 | 3 | 122 | 19 | 6 | 28 | 69 | |
| U1592A | 36°33.9358′N | 25°45.6784′E | 693.1 | 339.2 | 339.2 | 240.45 | 71 | | 0 | 55 | 16 | 29 | 10 | 0 | 0 |
| U1592B | 36°33.9164′N | 25°45.7027′E | 693.1 | 527.8 | 234.8 | 117.04 | 50 | 293 | 1 | 25 | 0 | 0 | 0 | 25 | 0 |
| | | Site U1592 totals: | | 867.0 | 574.0 | 357.49 | | 293 | 1 | 80 | 16 | 29 | 10 | 25 | |
| U1593A | 36°34.5103′N | 25°24.8765′E | 402.5 | 250.6 | 250.6 | 149.55 | 60 | | 0 | 38 | 16 | 22 | 0 | 0 | 0 |
| U1593B | 36°34.4916′N | 25°24.9000′E | 404.0 | 232.8 | 232.8 | 156.78 | 67 | | 0 | 39 | 11 | 28 | 0 | 0 | 0 |
| U1593C | 36°34.5060′N | 25°24.8995′E | 404.0 | 192.6 | – | – | 0 | 192.6 | 1 | 0 | 0 | 0 | 0 | 0 | 0 |
| | | Site U1593 totals: | | 676.0 | 483.4 | 306.33 | | 192.6 | 1 | 77 | 27 | 50 | | | |
| U1594A | 36°23.3368′N | 25°25.0290′E | 291.0 | 51.7 | 51.7 | 47.94 | 93 | | 0 | 6 | 6 | 0 | 0 | 0 | 0 |
| | | Site U1594 totals: | | 51.7 | 51.7 | 47.94 | | | | 6 | 6 | | | | |
| U1595A | 36°22.8955′N | 25°24.3630′E | 291.6 | 98.6 | 98.6 | 72.30 | 73 | | 0 | 11 | 11 | 0 | 0 | 0 | 0 |
| U1595B | 36°22.8819′N | 25°24.3358′E | 291.4 | 127.1 | 127.1 | 74.02 | 58 | | 0 | 15 | 13 | 2 | 0 | 0 | 0 |
| U1595C | 36°22.8674′N | 25°24.3062′E | 291.3 | 95.3 | 46.1 | 21.37 | 46 | 49.2 | 1 | 10 | 1 | 9 | 0 | 0 | 0 |
| | | Site U1595 totals: | | 321.0 | 271.8 | 167.69 | | 49.2 | 1 | 36 | 25 | 11 | | | |
| U1596A | 36°26.5378′N | 25°22.5130′E | 382.1 | 41.9 | 41.9 | 38.00 | 91 | | 0 | 5 | 5 | 0 | 0 | 0 | 0 |
| U1596B | 36°26.5568′N | 25°22.4875′E | 381.9 | 42.2 | 42.2 | 36.63 | 87 | | 0 | 5 | 5 | 0 | 0 | 0 | 0 |
| | | Site U1596 totals: | | 84.1 | 84.1 | 74.63 | | | | 10 | 10 | | | | |
| U1597A | 36°26.2494′N | 25°22.7326′E | 382.4 | 43.6 | 43.6 | 40.84 | 94 | | 0 | 5 | 5 | 0 | 0 | 0 | 0 |
| | | Site U1597 totals: | | 43.6 | 43.6 | 40.84 | | | | 5 | 5 | | | | |
| U1598A | 36°18.2937′N | 25°7.7155′E | 521.5 | 79.6 | 79.6 | 54.50 | 68 | | 0 | 10 | 8 | 2 | 0 | 0 | 0 |
| U1598B | 36°18.2747′N | 25°7.6929′E | 521.5 | 98.8 | 23.5 | 7.91 | 34 | 75.3 | 1 | 5 | 0 | 5 | 0 | 0 | 0 |
| | | Site U1598 totals: | | 178.4 | 103.1 | 62.41 | | 75.3 | 1 | 15 | 8 | 7 | | | |
| U1599A | 36°26.9592′N | 25°46.8005′E | 591.2 | 245.4 | 245.4 | 204.57 | 83 | | 0 | 44 | 7 | 36 | 1 | 0 | 0 |
| U1599B | 36°26.9764′N | 25°46.8237′E | 592.7 | 241.0 | 241.0 | 199.13 | 83 | | 0 | 40 | 10 | 29 | 1 | 0 | 0 |
| U1599C | 36°26.9389′N | 25°46.7762′E | 592.7 | 688.2 | 465.2 | 234.37 | 50 | 223 | 1 | 48 | 0 | 0 | 0 | 48 | 0 |
| | | Site U1599 totals: | | 1184.2 | 961.2 | 647.88 | | 223 | 1 | 133 | 17 | 65 | 2 | 49 | |
| U1600A | 36°32.6277′N | 25°39.0553′E | 326.2 | 84.4 | 84.4 | 51.71 | 61 | | 0 | 13 | 4 | 6 | 3 | 0 | 0 |
| U1600B | 36°32.6092′N | 25°39.0311′E | 326.3 | 91.4 | 91.4 | 68.67 | 75 | | 0 | 19 | 1 | 18 | 0 | 0 | 0 |
| U1600C | 36°32.5890′N | 25°39.0066′E | 326.3 | 188.5 | 113.5 | 36.78 | 32 | 75 | 1 | 13 | 0 | 0 | 0 | 13 | 0 |
| | | Site U1600 totals: | | 364.3 | 289.3 | 157.16 | | 75 | 1 | 45 | 5 | 24 | 3 | 13 | |
| | | Expedition 398 totals: | | 7344.8 | 5724.7 | 3346.37 | | 1620.1 | 11 | 768 | 176 | 299 | 54 | 239 | 1 |

### 4.1.2.3. Hole U1589C

The RCB BHA was assembled and tripped back down to the mudline, spudding Hole U1589C in a water depth of 482.6 mbsl at 2304 h on 26 December. The uppermost 360 m of Hole U1589C was drilled without recovery and continued to a depth 20 m above the base of Hole U1589B, recovering Cores 2R–28R. Beginning at Core 25R, we began to recover pebbles of limestone. Coring continued to Core 28R, and all cores contained limestone pebbles. The basement depth was determined at a depth of 589 mbsf. Following Core 28R, coring in Hole U1589C was ended. In total, Hole U1589C recovered 62.08 m of volcanic, tuffaceous, and nonvolcanic sediments and limestone basement, reaching a total depth of 621.9 mbsf. Core recovery was good in Holes U1589A (78%) and U1589B (87%) but poor in Hole U1589C (24%).

Hole U1589C was prepared for downhole logging, the Triple Combo tool string—equipped with natural gamma radiation (HNGS), lithodensity (HLDS), electrical resistivity (HRLA), and magnetic susceptibility (MSS) sensors—was assembled. During logging Run 1, the tools encountered an obstruction at 544.9 mbsf that could not be passed. After a quick logging run up and down again, the tool got stuck at 227.7 mbsf. The remainder of the operations was spent retrieving the

**Table T1 (continued).**

| Hole | Date started | Time started UTC (h) | Date finished | Time finished UTC (h) | Time on hole (days) | Comments |
|---|---|---|---|---|---|---|
| U1589A | 21 Dec 2022 | 0545 | 24 Dec 2022 | 0615 | 3.02 | |
| U1589B | 24 Dec 2022 | 0615 | 26 Dec 2022 | 1430 | 2.34 | |
| U1589C | 26 Dec 2022 | 1430 | 31 Dec 2022 | 1615 | 5.07 | |
| U1590A | 31 Dec 2022 | 1815 | 1 Jan 2023 | 1945 | 1.06 | |
| U1590B | 10 Jan 2023 | 1730 | 14 Jan 2023 | 0030 | 3.29 | |
| U1591A | 1 Jan 2023 | 2215 | 2 Jan 2023 | 1500 | 0.70 | |
| U1591B | 2 Jan 2023 | 1500 | 5 Jan 2023 | 0745 | 2.70 | |
| U1591C | 5 Jan 2023 | 0745 | 10 Jan 2023 | 1445 | 5.29 | |
| U1592A | 14 Jan 2023 | 0215 | 16 Jan 2023 | 0915 | 2.29 | |
| U1592B | 16 Jan 2023 | 0915 | 18 Jan 2023 | 1900 | 2.41 | |
| U1593A | 18 Jan 2023 | 2130 | 20 Jan 2023 | 0545 | 1.34 | |
| U1593B | 20 Jan 2023 | 0545 | 21 Jan 2023 | 1200 | 1.26 | |
| U1593C | 21 Jan 2023 | 1200 | 22 Jan 2023 | 1500 | 1.13 | |
| U1594A | 22 Jan 2023 | 1645 | 23 Jan 2023 | 0245 | 0.42 | |
| U1595A | 23 Jan 2023 | 0330 | 23 Jan 2023 | 2100 | 0.73 | |
| U1595B | 2 Feb 2023 | 0245 | 2 Feb 2023 | 2115 | 0.77 | |
| U1595C | 2 Feb 2023 | 2115 | 3 Feb 2023 | 1230 | 0.64 | |
| U1596A | 24 Jan 2023 | 0130 | 24 Jan 2023 | 0900 | 0.31 | |
| U1596B | 3 Feb 2023 | 1415 | 4 Feb 2023 | 0000 | 0.41 | |
| U1597A | 24 Jan 2023 | 0930 | 24 Jan 2023 | 1630 | 0.29 | |
| U1598A | 24 Jan 2023 | 1815 | 25 Jan 2023 | 0515 | 0.46 | |
| U1598B | 25 Jan 2023 | 0515 | 25 Jan 2023 | 1530 | 0.43 | |
| U1599A | 25 Jan 2023 | 1915 | 27 Jan 2023 | 1945 | 2.02 | |
| U1599B | 27 Jan 2023 | 1945 | 29 Jan 2023 | 0130 | 1.24 | |
| U1599C | 30 Jan 2023 | 1315 | 1 Feb 2023 | 2345 | 2.44 | Reenter 2023-02-07 0230 h |
| U1600A | 29 Jan 2023 | 0245 | 29 Jan 2023 | 1700 | 0.59 | |
| U1600B | 29 Jan 2023 | 1700 | 30 Jan 2023 | 1000 | 0.60 | |
| U1600C | 4 Feb 2023 | 0200 | 5 Feb 2023 | 0400 | 1.08 | |

logging tools. After tool recovery, the drill string was found to be stuck. The decision was made to sever the string during the late evening on 30 December, and the line was successfully severed. At 1800 h, on 31 December, the rig floor was secured for transit. All thrusters were up and secured, and sea passage to Site U1590 (Prospectus Site CSK-03A) started at 1818 h.

### 4.1.3. Principal results

Cores from the three consecutive holes (U1589A–U1589C) recovered a coherent stratigraphy from 0 to 612 mbsf. Hole U1589A extended 0–446 mbsf, Hole 1589B extended 0–360 mbsf, and Hole 1589C extended 372–612 mbsf. There was very good overlap between Holes U1589A and U1589B. Hole U1589C began near the bottom of Holes U1589A and U1589B, and overlap was minimal with penetration to basement.

The drilled interval fill was divided into five lithostratigraphic units (I–V) (Figure **F3**).

- Lithostratigraphic Unit I (200 m thick) consisted primarily of tuffaceous mud intercalated with intervals of ash, lapilli-ash, and lapilli, punctuated by less abundant nontuffaceous mud and ooze intervals. It was divided into Subunits Ia, Ib and Ic.
- Unit II (170 m thick) primarily consisted of muds and oozes interspersed with intermittent volcanic layers and organic-rich sapropelitic (Figures **F4**, **F5**). Oozes ranged in color from dark gray, olive gray, and greenish gray to white depending on their organic matter content. Muds were generally darker in color and ranged from very dark gray, dark greenish gray, dark olive gray to greenish gray and several pale yellow layers. Five subunits of Unit II were recognized:

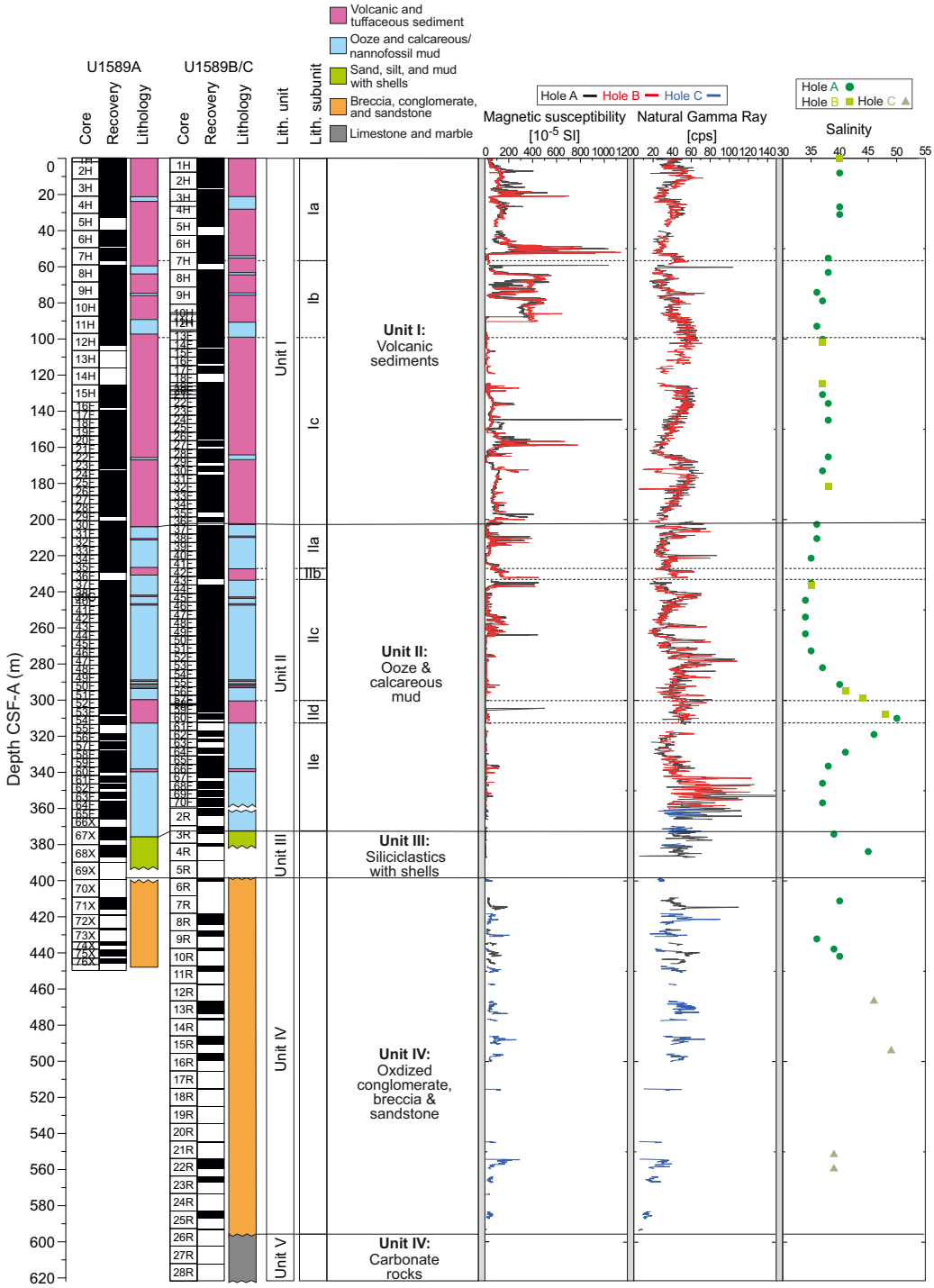


**Figure F3.** Simplified summary and overview for Site U1589, from Anhydros Basin, showing core recovery, stratigraphy, lithology, units, whole-round measurements of MS and NGR, and salinity in interstitial waters.

- Subunit IIa, ooze and mud with minor volcanic layers;
- Subunit IIb, tuffaceous sediments;
- Subunit IIc, ooze and mud with minor volcanics;
- Subunit IId, ash with minor lapilli and tuffaceous sediments; and
- Subunit IIe, ooze and mud with sapropels and minor volcanics.

- Unit III (20 m thick) was distinguished from Unit II by a gradual increase in both grain size and shell content. It consisted primarily of sand with ash and shells interspersed with calcareous mud and sapropels.
- Unit IV (190 m thick) consisted of intercalated sand and matrix-supported conglomerate of brown to reddish colors.

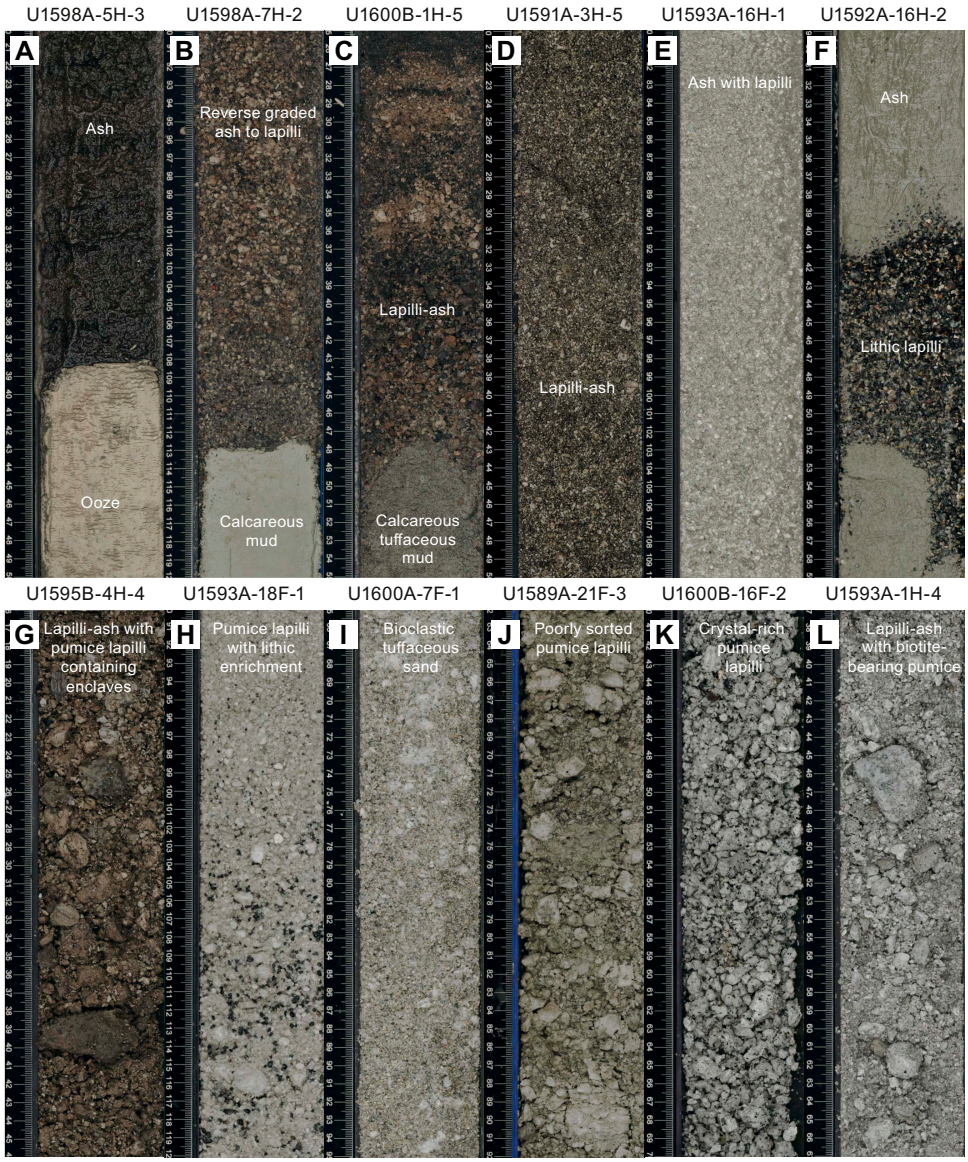


**Figure F4.** Representative images of volcanic lithologies, Sites U1589, U1591–U1593, U1595, U1598, and U1600. Note variable strong core disturbances (e.g., up-arching, sediment flowage, mid-core flow, fluidization) induced by the coring processes and seen in all Expedition 398 cores. A. Coarse black ash with sharp boundary to ooze. B. Reverse-graded colorful lithic- and mineral-rich ash to fine lapilli with sharp boundary to underlying calcareous mud. C. Multicolored lapilli-ash with variable thick horizons enriched in lapilli and ash. D. Black and white lapilli-ash. E. White ash with lapilli. F. Lithic lapilli layer embedded in fine white ash. G. Lapilli-ash layer with brown pumice containing mafic enclaves. H. Normal-graded pumice lapilli to ash with basal enrichment of lithics. I. Bioclastic tuffaceous sand. J. Poorly sorted pumice lapilli layer. K. Crystal-rich lapilli layer with amphibole-and-biotite-rich pumice. L. Lapilli-ash layer with biotite-bearing pumice.

- Unit V (22 m drilled to retraction at 612 mbsf) was lithified limestone/marble that is the basement rock on which the above-lying sediments were deposited. The samples collected from Unit V consisted of pluri-decimetric fragments of brecciated, carbonate-cemented, and nonbrecciated limestone/marble with large foraminifera (nummulites).

The upper and lower boundaries of each lithostratigraphic unit were defined by lithologic changes that were usually accompanied by a change in physical properties (e.g., magnetic susceptibility). Several types of core disturbance disrupted the lithostratigraphy at Site U1589: biscuiting, brecciation, fall-in, liquefaction to a soupy consistency, sediment flowage, sediment mixing, up-arching, and core voids.

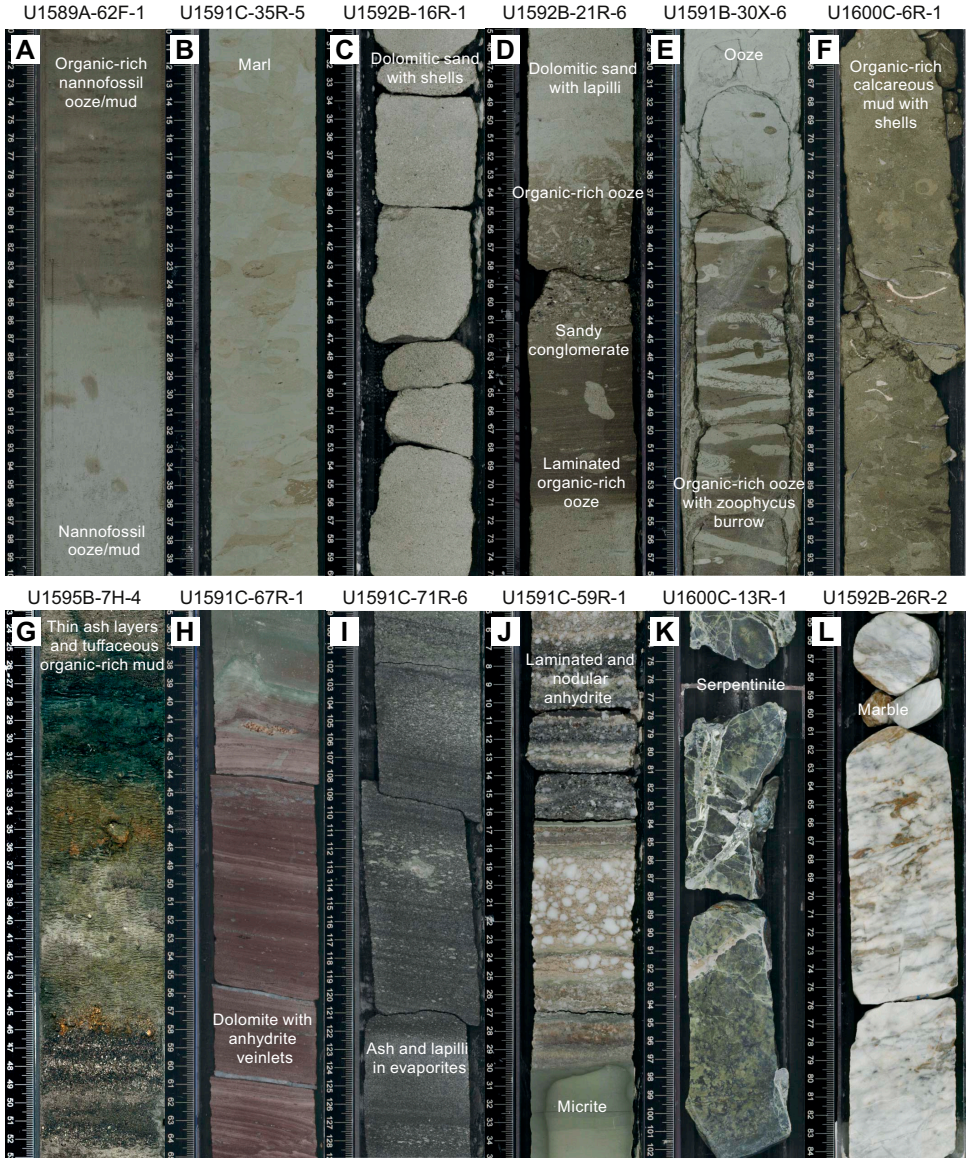


**Figure F5.** Representative images of nonvolcanic and tuffaceous lithologies, Sites U1589, U1591, U1592, U1595, U1598, and U1600. Note variable strong core disturbances (e.g., up-arching, biscuiting, brecciation) induced by the coring processes or bioturbation and seen in all Expedition 398 cores. A. Nannofossil ooze/mud with and without organics. B. Bioturbated marl. C. Dolomitic sand with shells. D. Dolomitic sand with lapilli with intercalated interval of laminated organic-rich ooze, sandy organic-rich conglomerate, and bioturbated organic-rich ooze. E. Bioturbated (*Zoophycus*) organic-rich ooze and overlying ooze. F. Organic-rich calcareous mud with shells. G. Thin ash layers intercalated in tuffaceous organic-rich mud. H. Laminated dolomite with anhydrite veinlets. I. Thinly bedded anhydrite and dolomite with horizons enriched in ash and lapilli. J. Laminated and nodular anhydrite above micrite. K. Serpentinite with veins filled with calcite and talc. L. Marble.

Structural measurements showed that the beds were horizontal to subhorizontal but that the dip decreased from the bottom to the top, with the median dip decreasing from 5.0° in Lithostratigraphic Unit IV to 4.2° in Unit I. The major change in the bedding dip was identified at the bottom of Unit II, whereas minor variation occurred between Units I and II. Some core sections contained faults that corresponded in orientation to the main basin structures.

Calcareous nannofossils, planktonic foraminifers, and benthic foraminifers recovered from core catcher samples and additional split-core samples from Holes U1589A, U1589B, and U1589C were used to develop a shipboard biostratigraphic framework for Site U1589. Calcareous nannofossils and planktonic foraminifers provided good age resolution throughout the Pleistocene sediments. Ages provided by benthic foraminifers were also consistent with those of calcareous nannofossils and planktonic foraminifers and showed that the basin fill at Site U1589 ranged from Holocene near the seafloor to Middle Pleistocene at ~400 mbsf (Figure **F6**). The data indicated highly variable sedimentation rates in different depth ranges of the basin fill, ranging from ~0.1 m/ky in Lithostratigraphic Unit III to up to ~1 m/ky in Units II and I. Owing to high sedimentation rates through some of the cored section, semiquantitative planktonic foraminiferal assemblage data were used in conjunction with calcareous nannofossil and planktonic foraminiferal biostratigraphic datums to tentatively recognize marine isotope Stages (MIS) 10 and 11. These were based primarily on fluctuations of the warm-water species *Globigerinoides ruber, Globigerinoides elongatus*, and *Globigerinoides pyramidalis*. Benthic foraminifers provided data on paleowater depths, which increased from 0 to 600–1000 m in Lithostratigraphic Unit II then stabilized at 200–600 m in Unit I. Oceanicity values (% planktonic foraminifers) gave paleodepths similar to those provided by benthic foraminifer assemblages.

To establish the core composite depth below seafloor (CCSF-A) depth scale, Holes U1589A and U1589B were analyzed for physical properties using the Whole-Round Multisensor Logger (WRMSL) for magnetic susceptibility (MS), gamma ray attenuation (GRA) density, and *P*-wave velocity; the Natural Gamma Radiation Logger (NGRL) for NGR intensity; and subsequently, the Section-Half Multisensor Logger (SHMSL) for point magnetic susceptibility (MSP) and color reflectance. Section-halves were photographed once the cores were split into working and archive halves. In general, MS was recognized to be the most reliable physical parameter for correlations, whereas NGR and GRA density measurements were often significantly overprinted by the irregu-

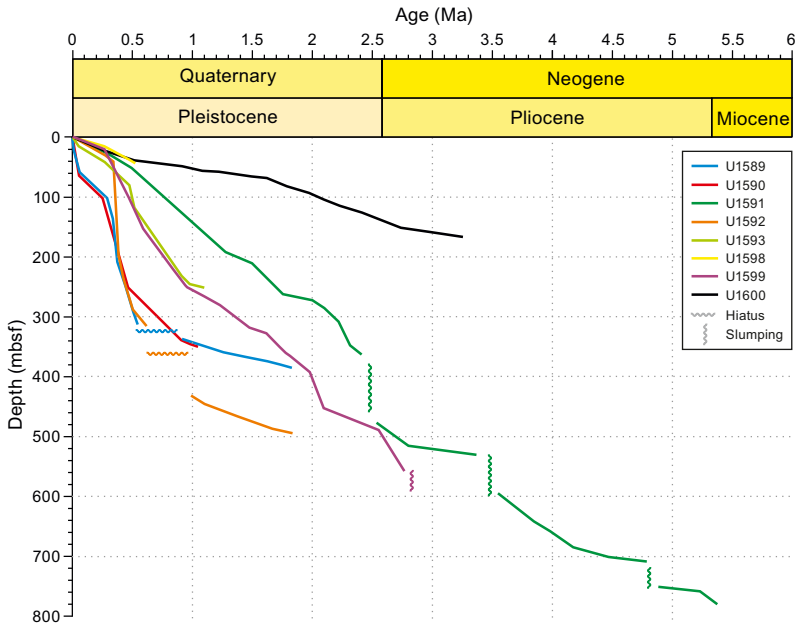


**Figure F6.** Early Pliocene to Holocene age-depth plot based on biochronologic events derived from foraminifers and nannofossils of Sites U1589, U1590, U1591, U1592, U1593, U1598, U1599, and U1600. Lines represent the interpolated sedimentation rates based on these datums. Unconformities in form of assumed hiatuses and slumping events are indicated.

lar distribution of core material in cores with low recovery and a high water content. MS also proved to be an excellent proxy for the presence of volcanic material in the cores (Figure **F3**). Once the composite depth scale was established, selected sequences from Holes U1589A and U1589B were spliced and the additional (but scattered) parts of Hole U1589C were added to create the most complete and representative section possible.

Downhole variations in physical properties (Figure **F3**) arise from changes in lithology, compaction, and other diagenetic processes. Differences between volcanic and other lithologies were most prominent in MS because of the abundance of ferromagnetic minerals (e.g., magnetite) in volcanic (high) and nonvolcanic (low) sediments. Whereas density was expected to increase progressively with increasing depth due to compaction, low-density pumice deposits and unconsolidated ash layers between compacted biogenic ooze created a more complex porosity structure throughout the drilled formation. Similarly, shear strength and thermal conductivity both increased with depth but were often lower in volcaniclastic units relative to adjacent materials. In general, at this site volcaniclastic units had higher MS, lower *P*-wave velocity, and lower density than other sediments at the same depth. Physical property measurements could thus be used to interpret downhole logging data and to help identify thin ash and pumice layers in mostly biogenic, compacted sediment.

The Triple Combo tool string provided whole-hole in situ NGR, resistivity, density, and MS measurements at various sampling rates. NGR downhole logs (total counts) confirmed the whole-hole trend of NGR measurements on whole-round core sections acquired by the shipboard NGRL. Resistivity logs showed a dichotomy in ranges of logged values between Lithostratigraphic Unit IV and the rest of the upper formation. Unit IV had the highest density values compared to the shallower formation, which was consistent with the trend observed by shipboard measurements. The magnetic susceptibility log had two distinctive intervals above and below ~380 mbsf (WMSF; wireline log matched depth below seafloor).

To determine the geochemistry of the volcanic layers, 17 tephra samples were hand-picked from various layers in Hole U1589A. Following cleaning, grinding, fusion, and dissolution, the volcaniclastic material was analyzed shipboard for major, minor, and trace elements using inductively coupled plasma–optical emission spectroscopy (ICP-OES) in atomic emission spectroscopy (AES) mode and are referred to as "ICP-AES" in this report. Of the volcaniclastic units sampled, 2 were classified as basaltic andesites, 4 as andesites, and 11 as dacites. Trace element ratios were used to broadly discriminate between the volcanic centers of Kolumbo and Santorini using published trace element data for onland volcanics. These correlations were tentative because the analytical precision of certain trace elements such as Nb are not very good on the shipboard ICP-AES instrument, limiting our ability to discriminate between compositionally similar volcanic sources. Salinity of the interstitial waters varied throughout the succession (Figure **F3**). Interstitial water concentrations of Ca, Mg, K, and $SO_4^{2-}$ showed downhole variations that strongly correlated with lithology. One layer exhibited a peak in $Ba^{2+}$ concentration at 246 mbsf in Lithostratigraphic Unit II that corresponded to the lowest $SO_4^{2-}$ concentrations observed. Salinity, $Cl^-$, $Br^-$, $SO_4^{2-}$, $Na^+$, and $K^+$ all peaked at ~320 mbsf in Unit II (Figure **F3**). Methane was the dominant hydrocarbon present at generally low concentrations (<4 ppmv). Ethane, propane, butane, and other heavier hydrocarbons were either low or below detection.

Natural remnant magnetism (NRM) intensities at Site U1589 were broadly normally distributed, but low-field susceptibilities displayed a bimodal distribution with peaks at $\sim 10 \times 10^{-5}$ SI and $\sim 60 \times 10^{-5}$ SI that suggested contributions from two distinct lithologic sources and/or magnetic minerals and/or magnetic grain sizes. When grouped into seven categories based on lithology, the data suggest the presence of two populations of magnetic grain assemblages, demarcated by susceptibilities higher than and lower than $\sim 20 \times 10^{-5}$ SI. We suspected that the low-susceptibility group included samples containing the diagenetic ferrimagnetic sulfide mineral greigite ($Fe_3S_4$) in lower intervals of the sampled section deeper than ~300 mbsf. The presence of greigite greatly complicated the use of the cores for creating a geomagnetic timescale. The core interval shallower than 300 mbsf could be confidently assigned to the Brunhes Chron, but recognition of the Bruhnes/Matuyama reversal was problematic. Comparison with the biostratigraphic age-depth curve predicted that the Brunhes/Matuyama should be seen at 330 mbsf and the Matuyama/

Jaramillo reversal at 342 mbsf, but the reversals were obscured by the effects of spurious magnetizations carried by greigite.

A preliminary synthesis of the data follows. The good recovery at Site U1589 led to the construction of a preliminary splice with few gaps. The age-depth model is very detailed, with a total of ~20 age constraints. Lithostratigraphic Unit V is Cretaceous–Eocene limestone that forms the Alpine basement. It is overlain by ~200 m of the intercalated brown to reddish sands and matrix-supported breccias of Unit IV, which is older than ~1.8 Ma and probably of terrestrial origin. Unit III is ~20 m thick and comprises a probable shoreline facies of 1.8–1.6 Ma age of sand with ash and shells interspersed with calcareous mud. It is overlain by the ~200 m thick Unit II, which is composed mainly of calcareous oozes with interleaved tuffaceous layers. It has an age of ~1.6–0.4 Ma, over which the water depth at Site U1589 increased from shoreline to as deep as 1000 m. At least one eruption laid down ash at this site during this period. Finally, Lithostratigraphic Unit I is ~200 m thick and is dominated by volcanic and tuffaceous sediments with ooze intervals. It was laid down from ~0.4 Ma to present day. Water depth during this period ranged from <250 to 500–750 m or more. The lower limit of Unit I coincides approximately with the boundary between MIS 11/10. This unit contains several volcanic units derived from both Santorini and Kolumbo Volcanoes. Detailed core-seismic integration awaits further work.

## 4.2. Site U1590

### 4.2.1. Background and objectives

Site U1590 (Prospectus Site CSK-03A) is located 5 km northwest of the submarine Kolumbo crater on its flank in the Anhydros Basin at a water depth of 397 mbsl.

The seismic profiles across the Kolumbo edifice reveal five units interpreted as Kolumbo-derived volcanics (Eruption Units K1–K5 from the base up), with Unit K5 representing the 1650 CE eruption (Hübscher et al., 2015; Preine et al., 2022c). The submarine cones northeast of Kolumbo postdate Unit K2 on seismic profiles, but their products are not expected to be prominent in our drill cores.

The aim of drilling on the flanks of Kolumbo Volcano was to penetrate the different seismically recognized volcanic eruption units from that volcano (K1–K5 or their thin, lateral equivalents), as well as many eruption units from Santorini and traces from the submarine cones northeast of Kolumbo Volcano. This would enable characterization of the products of the Kolumbo eruptions as well as construction of a coherent stratigraphy for Santorini and the submarine Kolumbo volcanic chain together. The anticipated lithologies were volcaniclastics, muds, and turbidites. Site U1590 at the foot of the Kolumbo edifice allows us to drill Seismic Units K1–K5, and therefore nearly the entire history of Kolumbo Volcano. Intercalated seismic units are believed to contain the products of Santorini eruptions, including potentially those of smaller magnitude than recorded at the more distal basin sites.

### 4.2.2. Operations

The transit to Site U1590 (proposed Site CSK-03A) started at 1818 h on 31 December 2022. The vessel arrived on location and started lowering the thrusters at 1946 h. All thrusters were down and secured at 2012 h. The vessel was switched to dynamic positioning (DP) mode and auto control at 2020 h, officially starting Site U1590. The transit to Site U1590 took only 1.9 h and covered 14.5 nmi at an average speed of 7.6 kt. The rig crew assembled the APC/XCB BHA in preparation to start Hole U1590A.

#### 4.2.2.1. Hole U1590A

At 0115 h on 1 January 2023, the trip in the hole started with the APC/XCB BHA. The sinker bars were loaded along with the APC barrel. Hole U1590A was spudded with Core 1H from 403 meters below rig floor (mbrf) at 36°33.2938′N, 25°26.3888′E. Recovery was 4.3 m, giving a calculated seafloor depth of 397.1 mbsl. Coring continued to 89.8 mbsf. Various levels of overpull were observed on the core barrels to a maximum of 50,000 lb. The Advanced Piston Corer Temperature (APCT-3) tool was run on Core 4H.

At 1200 h, the drill string took weight when trying to lower it, indicating ~8 m of fill that had fallen into the hole. Core 11H was retrieved, and the sinker bars were pulled.

The driller worked the drill string from 1230 to 1500 h with 50,000–70,000 lb overpull. Despite all efforts, the drill string was stuck—little to no vertical movement, no rotation, and 2,000 psi standpipe pressure immediately upon pumping. The driller continued to work the drill string while preparations for the severing operation began.

The severing tool was assembled and run into the hole to 4.6 mbsf. The BHA was severed at the top of the tapered drill collar (TDC) at 1700 h. The severing tool was retrieved, and the drill string was pulled up and clear of the seafloor at 1735 h. The drill string cleared the rotary table at 2025 h, and the vessel was secured for transit. All thrusters were raised at 2136 h, and the sea passage to Site U1591 (proposed alternate Site CSK-20A) began at 2148 h, ending Hole U1590A.

#### 4.2.2.2. Hole U1590B

Site U1590 was revisited on 10 January, with the intention of coring an RCB hole to the target depth of 566 mbsf. At 1852 h, the vessel came onto location at Site U1590. The transit of 20.3 nmi was completed in 2.4 h, for an average speed of 8.5 kt. All thrusters were down and secured at 1912 h. The ship was switched to DP control at 1924 h, marking the return to Site U1590. Despite fairly significant hole trouble early on, through careful coring and the liberal use of mud sweeps, the target of 566 mbsf was surpassed and went on to an EPSP-approved deepening to 634.7 mbsf (EPSP approved drilling to 850 mbsf).

The vessel was offset 50 m northwest of Hole U1590A. An RCB BHA with bit was again assembled and run in hole to 373.9 mbrf. Hole U1590B was spudded at 0030 h on 11 January and further drilled down to 93.0 mbsf. High torque was observed at 26.4 and 83.8 mbsf.

At 0700 h, RCB coring started with Core 2R from 93.0 mbsf. As expected, the recovery was extremely low in the upper sections, but the decision to use RCB was made to reach the target depth. However, because of the low recovery and as a precaution, a bit deplugger (tool to make sure no obstructions block the bit opening) was run before dropping the barrel for Core 12R, with no noticeable effect. Coring continued through 12 January; recovery was mostly very poor.

On 13 January, RCB coring was completed with Core 57R to 634.7 mbsf, the final depth for Hole U1590B. Coring was terminated in favor of other objectives at the following sites. The string was tripped up with the top drive from 634.7 to 546.5 mbsf. The top drive was racked back, and the trip continued, with the bit clearing the seafloor at 2355 h. On 14 January, the pipe trip continued, the bit cleared the rotary table at 0155 h, and the drill floor was secured at 0215 h. Overall, average core recovery in Hole U1590A was moderate (61%), but that in Hole U1590B was poor (14%).

The vessel was out of DP mode and under bridge control at 0224 h. All thrusters were brought up and secured. The sea passage started at 0230 h, ending Site U1590.

### 4.2.3. Principal results

Cores from Hole U1590A recovered a coherent stratigraphy from 0 to 91 mbsf; a partial stratigraphy was recovered in Hole U1590B from 93 to 628 mbsf. The recovered sediment succession in the uppermost ~90 m was dominated by volcanic ash, lapilli-ash, and lapilli, with minor tuffaceous muds and nannofossil oozes. The recovered material from the remaining 540 m was dominated by calcareous ooze/mud/sand and tuffaceous sediments with intermittent ash or lapilli layers (pumice and scoria). Four types of disturbance affected the cores: fall-in, sediment mixing, biscuiting, and cracking and breaking. We identified two lithostratigraphic units (Figure **F7**):

- Unit I was dominantly volcanic (Hole U1590A). Within Unit I, we identified three subunits based on the occurrence of tuffaceous muds and oozes within the predominantly volcanic succession:
  - Subunit Ia (20 m thick) was a biotite-bearing white and gray pumice-dominated unit with banded pumice;
  - Subunit Ib (26 m thick) consisted of lapilli, ash, and tuffaceous mud with dark coarse lithic-crystal ash;

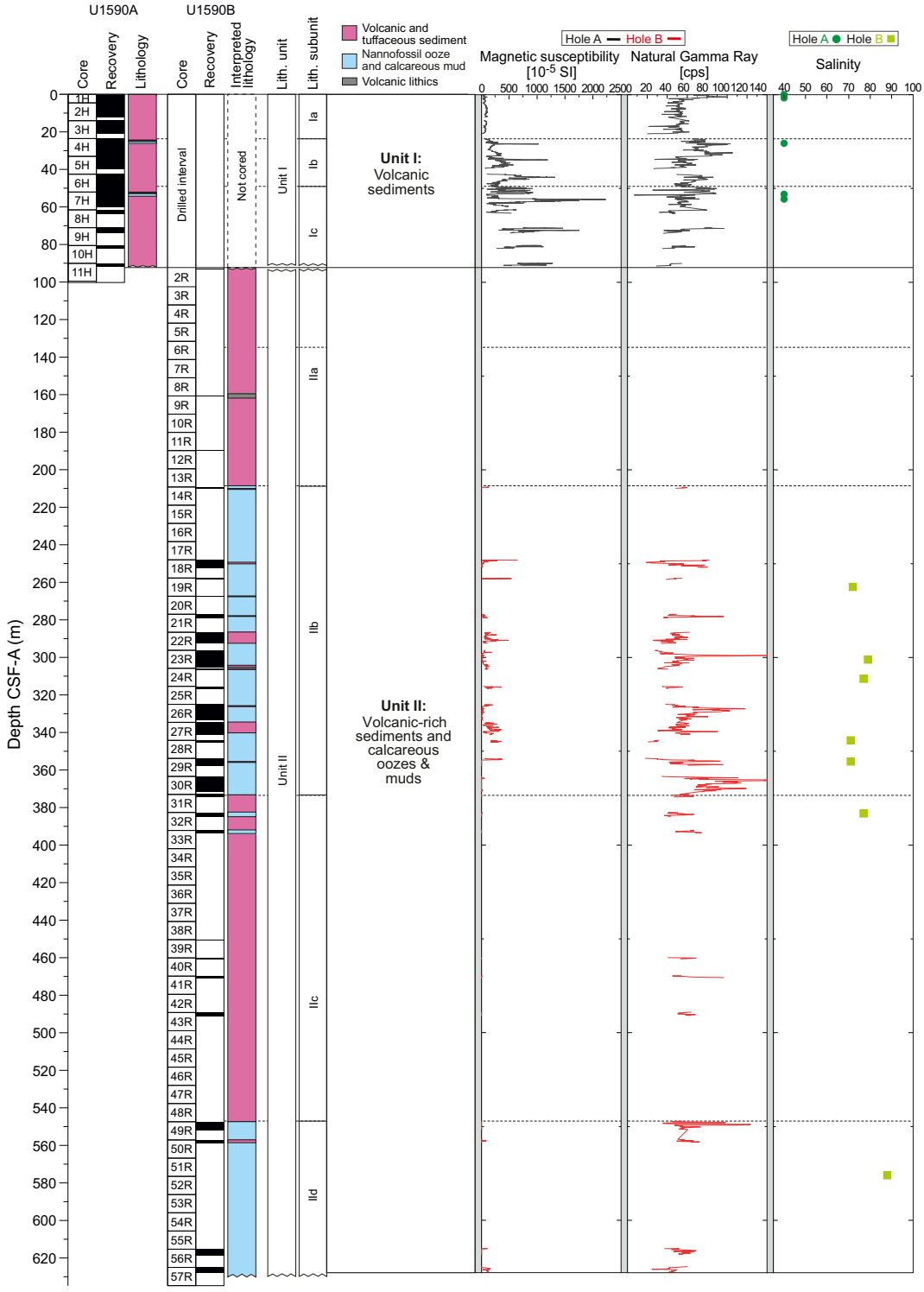


**Figure F7.** Simplified summary and overview for Site U1590, at the slope of Kolumbo Volcano, showing core recovery, stratigraphy, lithology, and units, whole-round measurements of MS and NGR, and salinity measurements from interstitial waters.

- Subunit Ic (42 m thick) comprised lapilli with white, biotite-bearing pumice and lithic lapilli that graded into tuffaceous to nannofossil mud.

- Unit II contained mixed nonvolcanic, tuffaceous, and minor volcanic intervals. Unit II was sampled in Hole U1590B, and four subunits were recognized:
  - Subunit IIa (117 m thick) consisted of tuffaceous mud, volcanic cobbles, ooze, and organic-rich ooze;
  - Subunit IIb (123 m thick) consisted primarily of ooze, organic-rich ooze/mud, ooze with ash/scoria lapilli, calcareous sand, tuffaceous ooze/mud, and minor ash and lapilli;
  - Subunit IIc (118 m thick) consisted of tuffaceous mud/ooze/sand, ash, lapilli, organic-rich ooze, and calcareous mud; and
  - Subunit IId (81 m thick) comprised ooze (±shells), mud (calcareous and noncalcareous), and calcareous sand.

X-ray diffraction (XRD) spectra of volcanic lithologies showed a characteristic hump at low °2θ indicating the presence of volcanic glass and characteristic mineral peaks of Ca-rich plagioclase, augitic or diopsidic clinopyroxene, and other phases such as glauconite, quartz, and halite. Nonvolcanic lithologies were characterized by calcium carbonate (calcite and aragonite), quartz, and clay minerals typical of the illite group. Additionally, Na-rich plagioclase, muscovite, zeolite, chlorite, and ankerite were identified in some samples.

Structural geology measurements showed that bedding planes were horizontal throughout the boreholes with dips ranging 0°–7°. Minor-scale slumps characterized by oblique foliation of sand-mud mixed layers were identified at 460 and 470 mbsf in Hole U1590B.

Calcareous nannofossils and planktonic and benthic foraminifers were used to develop a shipboard biostratigraphic framework for Site U1590. Additionally, benthic foraminifers provided data on paleowater depths, downslope reworking, and possible dissolution. Calcareous nannofossils were rare to abundant in samples from the Holocene to Early Pleistocene sequence. Preservation was generally good to moderate with sporadically poor to very poor intervals throughout the sequence; however, there was significant reworking of older material in most of the Pleistocene samples. The assemblages were characterized by the occurrence of warm-water species such as *Rhabdosphaera clavigera* and *Umbilicosphaera sibogae* throughout the sequence at Site U1590. The oldest calcareous nannofossil datum found was the basal occurrence of *Reticulofenestra asanoi* (1.078 Ma) at 481 mbsf. Planktonic foraminifer assemblages from the Holocene to Pleistocene section of Site U1590 were mostly well preserved, where specimens were rarely broken or exhibited partially dissolved shell walls. Foraminiferal faunas were sufficiently common to biostratigraphically divide the Pleistocene sediments into several Mediterranean planktonic foraminiferal biostratigraphic zones (Figure **F6**):

- Zone MPle2b (0–370 mbsf),
- Zone MPle2a (374–393 mbsf), and
- Zone MPle1c (450–627 mbsf).

The benthic foraminifer distributions indicated uppermost to upper bathyal (300–600 m) paleowater depths from 0 to 268 mbsf, mid to lower bathyal (600–1000 m) depths from 279 to 374 mbsf, and uppermost to upper bathyal (300–600 m) depths from 450 to 551 mbsf. Oceanicity values (% planktonic foraminifers) were generally in agreement with the benthic foraminiferal paleowater depth indicators.

Because of the very low recovery in the uppermost 17 cores of Hole U1590B, no stratigraphic correlation was possible using physical properties. Poor recovery in both holes limited the ability to document continuous variations in physical properties measurements over more than several tens of meters. MS was highly variable within the volcaniclastic deposits at Site U1590, from <100 SI to >1000 SI. Mean *P*-wave velocity was 1.63 km/s (standard deviation [SD] = 0.15 km/s), the largest value was 2.17 km/s. Moisture and density (MAD) measurements gave porosities of 53–73 vol%, bulk densities of 1.2–1.7 g/cm$^3$, and grain densities of 1.7–2.8 g/cm$^3$. Of a total of 5 thermal conductivity measurements, the mean value was 0.86 W/(m·K) (SD = 0.20 W/[m·K]). A temperature of 15.67° ± 0.17°C was measured downhole by APCT-3 at a depth of 33 mbsf.

Owing to potential hole instabilities in the ash- and pumice-rich lithologies, no wireline logging was possible at Site U1590.

Of 16 volcanic units sampled or analyzed by ICP-AES, 2 were classified as basaltic andesites and 10 as dacites. Trace element ratios were used to broadly discriminate between the volcanic centers of Kolumbo and Santorini, showing that the products of both volcanoes were present at this site. Interstitial water salinity values in Hole U1590A were 40 in all samples, which is close to the current average Aegean salinity value of 39; those in Hole U1590B ranged 71–88 and showed no correlation with depth (Figure F7). Values of alkalinity ranged 2.5–9.1 mM and pH ranged 7.1–7.9. Bromide, $Cl^-$, $Na^+$, B, $Ca^{2+}$, $Mg^{2+}$, and $SO_4^{2-}$ all followed similar trends, with lower values in the upper 53 m and increased concentrations at depth. Analyses of total organic carbon (TOC) content identified 1 sapropel with TOC values >2.0 wt% and 8 sapropelitic organic-rich layers for units with TOC values of 0.5–2.0 wt%. The data show low methane concentrations in Hole U1590A (<3 ppmv); values were below detection limit at all depths in Hole U1590B. Ethane concentrations were below the detection limit for all samples measured in both Holes U1590A and U1590B.

Paleomagnetic analysis at Site U1590 focused on measurement and demagnetization of archive section halves and 31 discrete samples to determine magnetostratigraphic age controls. The low overall recovery in Hole U1590B resulted in a restricted distribution of magnetic data downhole, and no reversal boundaries could be established. Nevertheless, by referring to biostratigraphic age constraints it was possible to make the following correlations with the Geomagnetic Polarity Timescale: (i) the interval 0–393 mbsf correlated with the Brunhes Chron (C1n) and was therefore <0.773 Ma age; (ii) the interval 470–491 mbsf corresponded to the Jaramillo Subchron (Chron C1r.1n) and was deposited within the period 1.008–1.076 Ma; and (iii) the interval 617–628 mbsf carried a reversed magnetization that was acquired during Chron C1r.2r (1.076–1.189 Ma).

We now provide a short synthesis of the findings at Site U1590. Owing to the poor recovery, particularly in Hole U1590B, any conclusions remain highly tentative. Detailed correlation of volcanic units by geochemical fingerprinting will be required to fully understand the stratigraphy. The volcanic layers of Lithostratigraphic Unit I are believed to include the pumice from the Kolumbo Volcano 1650 CE eruption (Eruption Unit K5) and the eruptions of the Thera Pyroclastic Formation of Santorini. Lithostratigraphic Unit II is believed to include the Eruption Units K1–K4 from Kolumbo Volcano, although identification is not yet possible based on the available data. It is possible that the volcanic units cored from Lithostratigraphic Unit II come from Kolumbo, Santorini, or both volcanoes. The cores penetrated to at least 1.08 Ma, showing that volcanism has persisted in this part of the volcanic field since the mid-Pleistocene.

## 4.3. Site U1591

### 4.3.1. Background and scientific objectives

Prior to arrival on site, it was decided to replace the original primary site (Prospectus Site CSK-13A) with an alternate site (Prospectus Site CSK-20A), the latter hence becoming definitive Site U1591. This was done to pass through a slightly more complete suite of reflectors in the 800–900 ms TWT interval.

Site U1591 is located ~8 km northwest of the Christiana Islands and ~20 km southwest of Santorini (Figure F1) in a water depth of 515 mbsl. The drill site targeted the Pliocene–Quaternary volcano-sedimentary fill of the Christiana Basin. This basin formed by subsidence along an east-northeast–west-southwest fault system in the Pliocene to Early Pleistocene, before the changing tectonic regime activated the current northeast–southwest rift system in which the CSK volcanic field lies (Tsampouraki-Kraounaki and Sakellariou, 2018; Preine et al., 2022a, 2022c; Heath et al., 2019).

The Christiana Basin is deeper than the Anhydros and Anafi Basins; its volcano-sedimentary fill potentially records the earlier volcanic history of the CSK volcanic field (including the products of Christiana Volcano and early Santorini), as well as younger Santorini and possibly Milos Volcano to the west along the Aegean volcanic arc. The now-extinct Christiana Volcano produced lavas

and tuffs of unknown ages (Aarbourg and Frechen, 1999), but an ignimbrite found on Christiani Island, Santorini, and the nonvolcanic island of Anafi, called the Christiani Ignimbrite (Keller et al., 2010), has the geochemical fingerprint of Christiana magmas.

Six seismic units have been identified in the Christiana Basin in previous work (Preine et al. 2022b, 2022c). Site U1591 was chosen to pass through Seismic Units U1–U6, including volcaniclastics from both Santorini and Christiana, and to target the top few meters of the prevolcanic basement below Seismic Unit 1. We received permission from the IODP EPSP to drill to Alpine basement at this site in an APC/XCB/RCB drilling strategy involving three holes.

The aims of Site U1591 were to (1) better date the volcanic activity of Christiana using biostratigraphic and magnetostratigraphic means and to determine whether the CSK volcanic field had Pliocene volcanism like Milos Volcano further west; (2) relate Christiana volcanism to subsidence along the east-northeast–west-southwest fault sets and to the activation of the northeast–southwest fault sets; and (3) seek the submarine equivalent of the Christiani Ignimbrite. By using deeper coring (and seismic profiles) to reconstruct the volcanic, sedimentary, and tectonic histories of Christiana Volcano, and possibly Milos Volcano, we would complement the Santorini and Kolumbo volcanic records of Sites U1589 and U1590, and therefore access a near-continuous time series of volcanism of the CSK volcanic field since rift inception. Site U1591 addresses scientific Objectives 1–4 and 6 of the *Expedition 398 Scientific Prospectus* (Druitt et al., 2022).

### 4.3.2. Operations

All thrusters were down and secured on 2 January 2023 at 0006 h. The vessel was switched to DP auto control mode at 0014 h, marking the start of Site U1591 (proposed Site CSK-20A). The transit from Site U1590 took only 2.3 h, covering 20.3 nmi at 8.8 kt.

The operations again involved three holes but with heavier use of the XCB and RCB because of the seemingly poor hole conditions when piston coring. Hole U1591A was piston cored with the APC until the hole became unstable at Core 398-U1591A-10H and was ended after Core 11H. Hole U1591B was piston cored to just above the trouble area, drilled down, and then primarily cored with XCB. Core 398-U1591B-43X saw the XCB shoe sheared off, ending the hole. Hole U1591C was an RCB-only hole, drilled to 149.3 mbsf and then cored to 902.9 mbsf. Average core recovery was similar in all three holes (U1591A = 66%, U1591B = 43%, U1591C = 58%).

The hole was terminated to move on to other objectives of the expedition.

#### 4.3.2.1. Hole U1591A

At 0740 h on 2 January, Hole U1591A was spudded at 36°18.7615′N, 025°09.0057′E, with a recovery of 3.8 m for Core 1H and a calculated seafloor at 514.6 mbsl. Coring with the APC continued to Core 11H at 98.8 mbsf. The string was pulled out of the hole, and the bit cleared the rotary table at 1700 h, ending Hole U1591A.

#### 4.3.2.2. Hole U1591B

Still on 2 January, a reconfigured APC/XCB BHA was assembled using the same drill bit. The TDC and nonmagnetic drill collar (NMDC) were removed and stored in the forward collar catwalk. Hole U1591B was spudded at 2150 h on 2 January at 36°18.7621′N, 025°09.0190′E. The recovery of 3.8 m indicated seafloor at 513.8 mbsl.

At 0245 h on the morning of 3 January, the APC was pulled and an XCB center bit was dropped. The intention was to drill through a previously identified pumice section. The driller established the slow circulation rates and proceeded to drill from 74.1 to 98.8 mbsf. On 5 January, XCB coring finished with Core 43X at 389.2 mbsf, the final depth for Hole U1591B, after the XCB cutting shoe sheared off in the hole. The reason for the failure was not clear. The bit cleared the rig floor at 0950 h, ending Hole U1591B.

#### 4.3.2.3. Hole U1591C

On 5 January at 1500 h, Hole U1591C was spudded at 36°18.7810′N, 025°08.9962′E, with an offset water depth of 524.9 mbrf. A drill-ahead section was completed to 149.3 mbsf. Coring began with the RCB, from Core 2R to 5R at 187.4 mbsf by midnight on 5 January. Coring continued, largely

uneventfully, into 10 January to Core 71R at 902.9 mbsf, the final depth for Hole U1591C. The decision was made to terminate coring in favor of other objectives. The bit cleared the rotary table at 1550 h, and the floor was secured for the transit. Deck hands started raising the thrusters at 1636 h. All thrusters were up and secured at 1648 h, and the sea passage to Site U1590 (proposed Site CSK-03A) began, ending Site U1591.

### 4.3.3. Principal results

The material recovered at Site U1591 is sedimentary and unlithified in all of Hole U1591A and Hole U1591B. A gradual transition to stiffer and more consolidated lithologies toward the bottom of Hole U1591B continues in Hole U1591C. Sediment in Hole U1591C in turn transitions gradually from consolidated sediment to sedimentary rock. The sedimentary succession in the upper 772 m is characterized by both volcanic lithologies (ash/tuff, lapilli-ash, lapilli, and tuffaceous mud/sand/mudstone/sandstone) and nonvolcanic calcareous mud/mudstone and ooze/marl (Figure **F8**). At 772 mbsf there is a sharp transition from marls, calcareous mudstones, and micrites to nodular anhydrite-bearing lithologies (± algal mats). Types of core disturbance include sediment mixing, up-arching, fall-in, brecciation, biscuiting, and sediment flowage.

Changes in relative abundances of volcanic lithologies and oozes/marls enables definition of the first two lithostratigraphic units at Site U1591, and the third unit is marked by the onset of lithologies containing anhydrite (Figure **F8**):

- Unit I is dominated by extensive volcanic intervals with lesser overall amounts of nonvolcanic material. This unit is divided into three subunits (Ia–Ic).
- Unit II is dominated by oozes/marls and calcareous muds/mudstones with lesser volcanic intervals. It is divided into six subunits (IIa–IIf).
- Unit III is dominated by lithologies containing anhydrite (evaporite sequence), clearly showing a distinct change in depositional environment. Unit III is divided into two subunits (IIIa and IIIb). A transition to ash- and lapilli-bearing volcanic material containing anhydrite (Subunit IIIb) marks the end of Hole U1591C.

XRD spectra obtained on lithologies from Units I and II were similar to those from Sites U1589 and U1590, with the majority of analyses carried out on oozes and organic-rich oozes in addition to samples from tuffaceous sediments (oozes and muds) and volcanic lithologies. Oozes and organic-rich oozes and muds are characterized by calcite and quartz, with most samples also containing Ca-rich or Na-rich plagioclase and clay minerals of the illite group and in some cases of the smectite group. Tuffaceous sediments and ash show characteristic XRD patterns of glass-rich (volcanic) material, with a characteristic hump at low °2θ, indicating the presence of an amorphous (noncrystalline) phase. Discrete samples from Unit III were analyzed by XRD to characterize the evaporite sequences that characterize Subunit IIIa. Anhydrite has been identified as one of the major evaporite minerals, occurring as laminated and nodular varieties and as veins and veinlets.

Observed and measured structures in the cores of Site U1591 were bedding, faults, and deformation bands, mineral veins, and sediment veins. Bedding planes were measured mainly on thin sand beds/laminae, sapropels, micrites, and anhydrite boundaries. They exhibited horizontal to subhorizontal dips shallower than 350 mbsf. However, steeper inclinations develop below 350 mbsf, where dips range 5°–85°. Slump deposits were frequently identified as (1) block-in-matrix occurrences, (2) flow/disturbed mud, and (3) folding of sandy laminae/beds in muddy matrices. Small-scale faults occurred on split-core surfaces; they showed displacements from a few millimeters to a centimeter. Sediment-filled veins and mineral veins were identified in specific intervals in the lower parts of Lithostratigraphic Units II and III, respectively.

Planktonic foraminifers, benthic foraminifers, and calcareous nannofossils were used to develop a shipboard biostratigraphic framework for Site U1591 (Figure **F6**). Calcareous nannofossils and planktonic foraminifers provided good resolution in the Holocene through Early Pliocene sediments. Seawater depths for Unit I and Subunit IIa derived from benthic foraminifer assemblages range 300–1000 m and were consistent with oceanicity values (ratio of planktonic to benthic foraminifers).

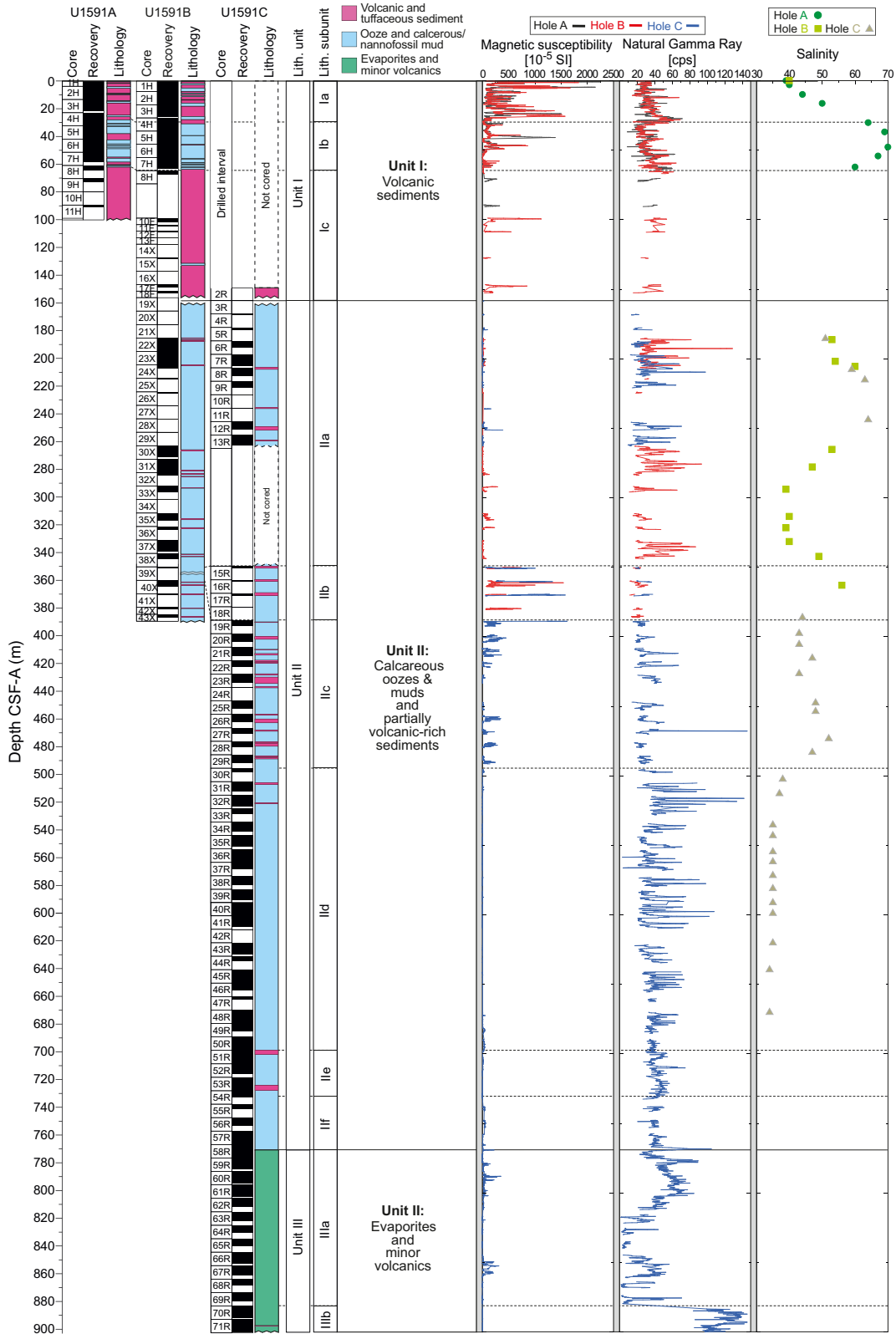


**Figure F8.** Simplified summary and overview for Site U1591, in the Christina Basin, showing core recovery, stratigraphy, lithology, and units, whole-round measurements of MS and NGR, and salinity measurements from interstitial waters.

Stratigraphic correlation mainly focused on the correlation of Holes U1591A and U1591B to identify coring gaps and to create a first, tentative splice between holes. Following this, the focus shifted to correlation of the small overlap between the deeper parts of Hole U1591B and the uppermost cores of Hole U1591C. The majority of the work done by the stratigraphic correlation group, however, was on remodeling seismic velocities based on *P*-wave analyses from the physical properties group.

Physical properties at Site U1591 correlated well with lithology. Thick volcaniclastic layers in Lithostratigraphic Unit I (ash, lapilli-ash, and lapilli) sometimes had low grain densities in coarse, pumice-rich subunits. Volcaniclastic deposits also exhibited large variations in MS and often had high MS compared to other sediments at this site. High-MS anomalies were most abundant and largest in amplitude at depths shallower than 490 mbsf (Figure **F8**). Unit II, which is dominated by nannofossil-rich oozes, often displayed cyclic variations in NGR that correlated with organic-rich layers (Figure **F8**). Volcaniclastic materials in Unit I had *P*-wave velocities of 1.5–1.7 km/s. Typical *P*-wave velocity of the oozes in Unit II increased with depth from ~1.7 km/s at the top of Unit II to ~2.1 km/s at its base. Lithostratigraphic Unit III had highly variable *P*-wave velocity; anhydrite-rich lithologies had velocities >5.0 km/s, whereas the background sediments had values similar to those of the overlying deposits of Unit II (2.1–2.8 km/s). The anhydrite-rich layers of Unit III also had higher thermal conductivity and bulk density and lower NGR than the surrounding sediments. Sediment porosity ranged 3–79 vol%, and bulk density ranged 1.2–2.9 g/cm$^3$. Some levels in Unit III had grain densities that exceeded 2.9 g/cm$^3$, consistent with anhydrite-dominated lithologies

Because of the instability of the formations encountered, downhole logging was not conducted at Site U1591.

Of the volcanic units sampled and analyzed by ICP-AES, 3 were classified as basaltic andesites, 5 as andesites, and 12 as dacites. Bulk chemistry values were less evolved than glass chemistry, as expected, due to bulk analyses including both minerals and glass. Trace element ratios were used to broadly discriminate between the volcanic centers of Kolumbo, Santorini, and Christiana, or indicate so-far unknown sources. A thick pumice layer between ~60 and 140 mbsf shows chemical affinities to Christiana magmas.

Salinities of interstitial water samples ranged 35–70 throughout the hole (most values were 35–60) (Figure **F8**). $Br^-$, $Cl^-$, B, $Na^+$, $K^+$, $Mg^{2+}$, $Ca^{2+}$, and $SO_4^{2-}$ trends all followed those of salinity. Lithium and strontium appeared to be roughly inversely correlated at depth. A total of 37 organic-rich units were identified; those with TOC values >2.0 wt% were identified as sapropels (17) and units with TOC values 0.5–2.0 wt% were identified as sapropelitic (20). Methane was the dominant headspace hydrocarbon present; the generally low concentrations locally reached as high as 883 ppmv, which is well within safe operational limits.

Paleomagnetic analysis at Site U1591 focused on measurement and demagnetization of archive section halves to determine magnetostratigraphic age controls. The upper 63 m of Lithostratigraphic Unit I carried normal polarity remanences acquired during the Brunhes Chron. Scattered inclinations then prevented magnetostratigraphic correlations within Unit II from 185 to 480 mbsf; from 480 to 770 mbsf, however, the quality of data improved and eight reversal boundaries could be tied precisely to the Geomagnetic Polarity Timescale (within the Pliocene), with a further four tentative correlations also possible. Data in the evaporite sequence of Unit III were less conclusive.

We present a very preliminary synthesis of Site U1591. Correlation of the sequence with seismic stratigraphy must await full analysis. Overall, we can confirm volcanic activity in the CSK volcanic field to have started in the Pliocene. Lithostratigraphic Unit III is an evaporite sequence dominated by anhydrite and is of Messinian age. Unit II consists of oozes with volcanic and tuffaceous horizons and ranges from Early Pliocene to mid-Pleistocene in age; it contains several slumped horizons and layers of reworked benthic fauna. Unit I is dominated by volcanic and tuffaceous lithologies, including a thick pumice layer with chemical affinities to Christiana Volcano. Seawater depths during emplacement of Units II and I ranged 300–1000 m.

## 4.4. Site U1592

### 4.4.1. Background and scientific objectives

Site U1592 is located ~10 km southeast of Anhydros Island within the Anafi Basin in a water depth of 693 mbsl. The aim at the site was to penetrate the entire volcano-sedimentary fill as far as the Alpine basement to reconstruct the evolution of the Anafi Basin: history of subsidence, the presence of volcanic event layers in the basin sediments, and links between volcanism and crustal tectonics.

The Anafi Basin potentially records the full volcanic history of Santorini (and any older centers) since rift inception but was envisaged to probably contain few eruptive products from Kolumbo Volcano. Drilling would enable reconstruction of the volcanic, sedimentary, and tectonic histories of the Anafi Basin, allowing us to compare its evolution with that of the Anhydros Basin. The site was also chosen to develop a core-log-seismic integration stratigraphy and compare it with the recently published seismic stratigraphy for the basin (Preine et al., 2022a, 2022b) and the paleotectonic reconstruction of the region (Nomikou et al., 2016b, 2018). The site transects six seismic packages of the Anafi rift basin, as well as the onlap surfaces between them (Nomikou et al., 2016b, 2018; Preine et al., 2022a, 2022b).

The Anafi Basin is crossed by many seismic profiles obtained in campaigns between 2006 and 2019, many of them multichannel (Hübscher et al., 2015; Nomikou et al., 2016b, 2018). It is included within the area of the 2015 PROTEUS seismic tomography experiment, when subbottom profiling, gravity, and magnetic data were also recorded (Hooft et al., 2017). The basin bathymetry has been studied in several marine campaigns, and fault distributions and throws have been mapped (Nomikou et al., 2016b; Hooft et al., 2017).

Coring at Site U1592 in the Anafi Basin addressed science Objectives 1–4 and 6 of the *Expedition 398 Scientific Prospectus* (Druitt et al., 2022). It is complemented by Site U1589 in the Anhydros Basin because each basin taps a different sediment distributary branch of the Christiana-Santorini-Kolumbo volcanic system.

### 4.4.2. Operations

Operations at Site U1592 involved two holes with a switch to RCB for Hole U1592B, following slow progress by XCB. Hole U1592A was an APC, HLAPC, XCB advance to 339.2 mbsf. Hole U1592B was RCB cored to 527. 8 mbsf after an initial 293.0 m drilled interval. Logging was not attempted, as there were several sections of the same loose, unconsolidated layers that had been causing problems at earlier sites.

#### 4.4.2.1. Hole U1592A

On 14 January 2023, the rig crew proceeded to make up the APC/XCB BHA with a used bit. Hole U1592A was spudded at 0830 h from 700 mbrf at 36°33.9358′N, 25°45.6784′E. The recovered core was 5.1 m, giving a calculated seafloor depth of 693.1 mbsl. APC coring continued to Core 16H from 135.3 mbsf, but the last three cores suffered partial strokes. Coring switched to the HLAPC at Core 17F.

HLAPC coring continued into 15 January with Core 45F to 273.8 mbsf, where the barrel became stuck. Overpull to 50,000 lb was ineffective. In attempting to drillover the barrel, the drill pipe became stuck, with indications the hole was filling in. The drill pipe was worked free, and eventually the barrel was freed with 120,000 lb overpull. At 1330 h, an XCB barrel was dropped and coring reconvened with Core 46X from 273.8 mbsf. Coring continued into 16 January to Core 55X at 339.2 mbsf, the final depth for Hole U1592A. The rate of penetration (ROP) for the XBC was slowing to the 4 m/h range, so the decision was made to switch to RCB. At 0730 h on 16 January, XCB coring was terminated. The drill string was tripped out with the top drive from 339.2 to 285.5 mbsf. The top drive was racked back, and the pipe trip continued. The bit cleared the rotary table at 1120 h, ending Hole U1592A. On 16 January at 1120 h, the crew began assembling the RCB BHA with bit. Meanwhile, the vessel was offset 50 m southeast of Hole U1592A.

#### 4.4.2.2. Hole U1592B

Hole U1592B was spudded at 1600 h at 36°33.9164′N, 25°45.7027′E. The seafloor depth was again 693.1 mbsl by offset. A drill-ahead commenced and had made it to 286.8 mbsf by midnight. Liberal mud sweeps were used to keep the hole clean. The drill-down finished at 0100 h on 17 January at a depth of 293.0 mbsf. The center bit was recovered and an RCB barrel dropped. The driller started RCB coring with Core 2R from 293.0 mbsf. Cores 8R–13R were almost zero recovery and were assumed to be a pumice layer judging from the seismic profiles. Core 11R was a "punch" core, a 2 m advance with little to no rotation or pump, to try to recover some of the difficult pumice section. The recovery was still very poor, but measurable, as a handful of the pumice lapilli was recovered. Following Core 12R, the drill string became stuck, requiring several minutes, 100,000 lb overpull, and two mud sweeps to free. Coring continued into 18 January until 1545 h with Core 26R to 527.8 mbsf, the final depth for Hole U1592B. Average core recoveries were 71% (U1592A) and 50% (U1592B). The bit cleared the rotary table at 2001 h. The rig crew secured the floor for transit. The thrusters were raised beginning at 2048 h. The vessel was out of DP control at 2052 h. All thrusters were up and secure and the sea passage started at 2100 h, ending Site U1592.

### 4.4.3. Principal results

The recovered material at Site U1592 is unlithified sediment, dominated by volcanic and tuffaceous material in the upper 269 m with lesser nonvolcanic lithologies (Lithostratigraphic Unit I; 0–269 mbsf; Figure **F9**). Unit I subunit distinctions are corroborated by physical property data (Figure **F9**) such as MS and NGR.

- Unit I (0–269 mbsf) is a succession of volcanic layers and tuffaceous or nonvolcanic layers.
  - Subunit Ia (~13 m) consists of mainly pumice lapilli;
  - Subunit Ib (~18 m) consists of a repetitive sequence of nonvolcanic and volcanic sediments;
  - Subunit Ic (49 m) is a nonvolcanic-dominated interval with volcanic sediments at the top and base; and
  - Subunit Id (189 m) is an extensive thick ash interval at the base.
- Unit II (269–338 mbsf) is dominantly ooze and other nonvolcanic lithologies interspersed with minor volcanic and tuffaceous sediments.
- Unit III (404–494 mbsf) is ~90 m composed of dolomitic muds and sands with shell fragments.
- Unit IV (494–508 mbsf) is a thin (~15 m) unit of bioclastic limestone.
- Univ V (508–519 mbsf) is approximately 10 m of limestone basement and marble.

In the upper part of Unit V, near the boundary with the overlying bioclastic limestone of Unit IV, the limestones and marbles of Unit V are typically reddish yellow in color due to oxidation, but they transition downward to mainly nonoxidized, massive, white, and partly banded limestone and marble. Units II, III, IV, and V do not exhibit sufficient variation to warrant subunits.

Representative XRD spectra of the tuffaceous and volcanic lithologies show the usual characteristic hump at low °2θ, indicating the presence of volcanic glass. Mineral phases in tuffaceous lithologies include Ca-rich plagioclase and a range of other phases such as quartz, calcium carbonate (calcite and aragonite), clay minerals typical of the illite group and smectite group (montmorillonite), and glauconite. A distinguishing feature of the nonvolcanic sediments (sands and oozes) of Lithostratigraphic Unit III, compared to Unit I and Unit II lithologies, is the relatively high proportion of dolomite.

Bedding planes at Site U1592 mostly exhibited horizontal to subhorizontal dips throughout the core. The bedding dip in Lithostratigraphic Unit III (median dip = 7.0°) was greater than that in Unit II (median dip = 4.5°). The dip increased again from Unit II to Subunits Ib–Ic (4.5°–7.0°). One possibility is that the occurrence of volcanism triggered slumps in Subunits Ib–Ic and thus increased the median dip. A slump deposit was identified at the upper part (31–38 mbsf) of Lithostratigraphic Unit I. A large population of normal faults and deformation bands occurred in the interval 300–350 mbsf, just above a ~50 m recovery gap from which a small amount of pumice was recovered.

Site U1592 recovered Holocene to Early Pleistocene sediments (0 to ~0.91 Ma). Reworking of microfossils sourced from Pleistocene–Early Cretaceous sediments was observed throughout the entire cored interval, and reworked Eocene benthic foraminifera constituted a substantial bioclastic component of Lithostratigraphic Unit IV. Seven nannofossil biostratigraphic datums were recognized at Site U1592, representing a continuous Middle to Late Pleistocene sedimentary sequence. Foraminiferal faunas were sufficiently common to divide the Pleistocene into six Mediterranean planktonic foraminiferal biostratigraphic zones (Figure **F6**):

- MPle2b (0.00–0.53 Ma),
- MPle2a (0.53–0.94 Ma),
- MPle1c (0.94–1.21 Ma),
- MPle1b (1.21–1.37 Ma),
- MPle1a (1.37–1.79 Ma), and
- MPl6b (1.79–2.00 Ma).

Holocene to Pleistocene planktonic foraminifer faunas suggested large fluctuations in oceanicity (a proxy for relative paleowater depth) and highly variable planktonic abundances that ranged

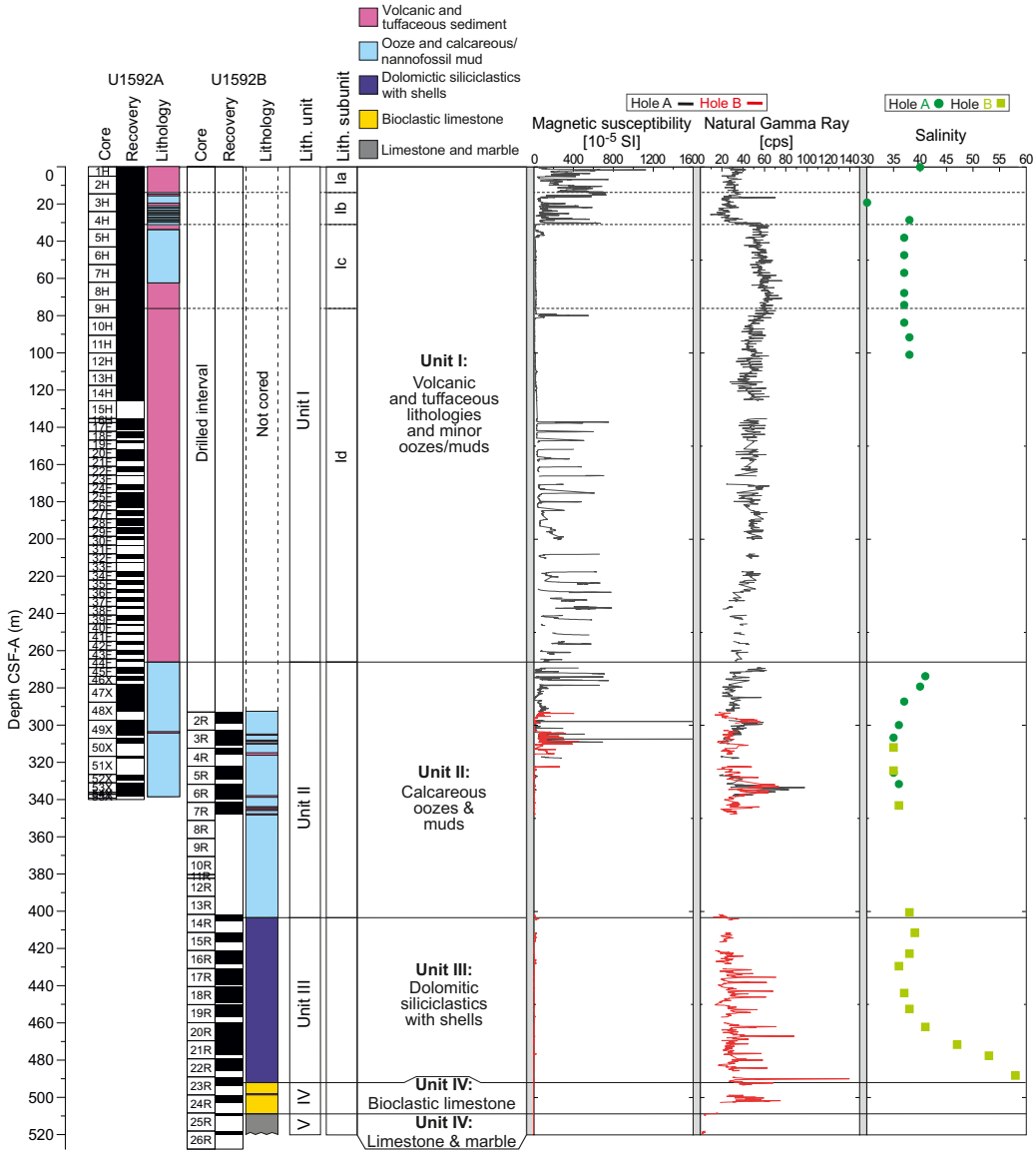


**Figure F9.** Simplified summary and overview for Site U1592, in the Anafi Basin, showing core recovery, stratigraphy, lithology, and units, whole-round measurements of MS and NGR, and salinity measurements from interstitial waters.

from 5.5% to 100%. Benthic foraminifer distributions were highly variable, indicating paleowater depths from inner shelf (<50 m) to lower bathyal (>1000 m).

Creation of a CCSF-A depth scale and construction of a splice for Holes U1592A and U1592B was not necessary because both holes had only a short overlap between 293 and 339 m (CSF-A scale). Within this overlapping interval, several correlations were established using MS and NGR measurements from WRMSL, as well as half-core images.

Physical properties at Site U1592 were correlated with lithology and respective units (Figure **F9**). The topmost volcaniclastic Lithostratigraphic Subunit Ia had low NGR counts and high MS relative to other volcaniclastic units. Volcaniclastic layers in Subunit Ic had lower MS and a factor of 2× higher NGR than Subunits Ia and Ib. Subunit Id exhibited large variations in MS and often had high MS compared to other sediments at this site. In Lithostratigraphic Unit II, which was dominated by nannofossil-rich oozes, *P*-wave velocity increased with depth, NGR was low, and MS was low except where thin volcaniclastic layers had high MS. The dolomitic and siliciclastic layers of Unit III often displayed cyclic variations in NGR that correlated with organic-rich layers. Limestones and marbles in Units IV and V had higher *P*-wave velocity and lower NGR than Units I–III. Overall, porosities ranged 3–83 vol% and bulk densities ranged 1.2–2.7 g/cm$^3$. Bulk density increased with depth but was lowest in volcaniclastic materials. Grain densities ranged 1.9–2.8 g/cm$^3$, with the lowest values in volcaniclastic subunits in the upper 280 m. Thermal conductivity increased with depth, except in the upper 150 m, as expected from the compaction of sediments. The limestones and marbles in Lithostratigraphic Units IV and V had higher thermal conductivities (>2 W/[m·K]) than other sediments at similar depths (1–2 W/[m·K]). Due to the instability of the formations encountered, downhole logging was not conducted.

Of the 9 volcanic units analyzed for major and trace elements by ICP-AES, 2 were classified as basaltic andesites, 2 as andesites, and 5 as dacites. Interstitial water salinity values ranged 30–58; the highest value of 58 was recorded near 490 mbsf (Figure **F9**). Values for alkalinity ranged 1.2–7.0 mM, and those of pH 7.6–8.0. The concentrations of bromide, $Cl^-$, B, $Na^+$, and $K^+$ followed similar trends to salinity. Calcium, $Mg^{2+}$, and $SO_4^{2-}$ correlated well with each other and showed an increase in the lowermost 75 m as salinity also increased. Trends for Li, Sr, Mn, Ba, and Si did not follow salinity. Both carbonate and TOC declined from 19 to 101 mbsf; the highest carbonate values were noted below 283 mbsf, reaching 58 wt%. Six organic-rich units were identified as sapropelitic (TOC = 0.5–2.0 wt%). Methane, ethane, and propane concentrations were below the detection limit in headspace gases.

Paleomagnetic analysis at Site U1592 focused on measurement and demagnetization of archive section halves to determine magnetostratigraphic age controls. The upper 82 m of the sequence sampled in Hole U1592A carried normal polarity remanences acquired during the Brunhes Chron. Beneath this, the cores recovered from Hole U1592A were unsuitable for paleomagnetic measurement. The interval ~270–348 mbsf in Hole U1592B was also normally magnetized and assigned to the Brunhes Chron. The Brunhes–Matuyama transition (0.773 Ma) was not recovered, but the sequence from 400 to 457 mbsf exhibited changes in magnetic polarity, allowing three reversal boundaries to be tied precisely to the Geomagnetic Polarity Timescale (corresponding to the start/end of the Jaramillo Subchron at 1.008/1.076 Ma and the start of the Cobb Mountain normal polarity subchron at 1.189 Ma in the Matuyama Chron). An additional tentative correlation to the base of the Cobb Mountain Subchron was also made by reference to a biostratigraphic marker. Samples below 460 mbsf exhibited mainly positive inclinations. However, this unit was dated biostratigraphically to the reversed polarity Matuyama Chron, suggesting that this interval was remagnetized during either the Jaramillo/Cobb Mountain Subchron or Brunhes Chron.

In summary, cores at Site U1592 in the Anafi Basin traversed a 1.8 My old basin fill sequence lying upon basement limestones. Lithostratigraphic Unit III consisted of dolomitic sands aged 1.8 to <0.92 Ma and recorded the initial marine transgression into the basin. This was followed by a gap in our record that recovered only a small amount of pumice. Given that core loss commonly coincided with well-sorted pumice layers, it is possible that a thick pumice layer formed the base of Lithostratigraphic Unit II. This was overlain by an interval with abundant faults and deformation bands. Following Unit II, Unit I consisted of about 180 m of ash deposited with sedimentation

rates exceeding ~1 m/ky, the origin of which is yet to be established. Finally, the top of Unit I contained volcaniclastic deposits from Santorini and Kolumbo Volcanoes. Correlation with the seismic stratigraphy of the Anafi Basin awaits detailed analysis of the data.

## 4.5. Site U1593

### 4.5.1. Background and scientific objectives

Site U1593 (formerly alternate prospectus Site CSK-04C) is located 8 km northwest of Kolumbo Volcano at a water depth of 402 mbsl.

The seismic profiles across the Kolumbo edifice reveal five units interpreted as Kolumbo-derived volcaniclastics (Eruption Units K1–K5 from the base up), with Eruption Unit K5 representing the 1650 eruption (Hübscher et al., 2015). The submarine cones northeast of Kolumbo postdate Eruption Unit K2 on seismic profiles, but their products are not expected to be prominent in our drill cores.

The aim of drilling on the flanks of Kolumbo Volcano was to penetrate the different seismically recognized volcanic eruption units from that volcano (K1, K2, K3, K5, or their thin, lateral equivalents), as well as many eruption units from Santorini and traces from the submarine cones northeast of Kolumbo. This would enable characterization of the products of the Kolumbo eruptions as well as construction of a coherent stratigraphy for Santorini and the submarine Kolumbo volcanic chain together.

Site U1593 lies at the foot of the Kolumbo edifice, 3 km northwest of Site U1590. Owing to the poor recovery at the latter site, we decided to also drill at Site U1593, which lies on the other side (northwest) of the Kolumbo Fault to Site U1590. This has two advantages. First, we could measure the offset across the Kolumbo Fault by correlating key marker layers from one site to the other. Second, the sequence at Site U1593 is more condensed that at U1590, offering us older recovery and potentially greater hole stability.

Like Site U1590, Site U1593 allowed us to drill Eruption Units K1, K2, K3, and K5, and therefore nearly the entire history of Kolumbo Volcano, within the proposed drilling target depth of 581 mbsf. These eruption units are not seismically distinguishable here (Hübscher et al., 2015); however, we expected to penetrate the more distal and thinner deposits of these units. Intercalated seismic units were believed to contain the products of Santorini eruptions, including potentially those of smaller magnitude than recorded at the more distal basin sites.

### 4.5.2. Operations

#### 4.5.2.1. Hole U1593A

After arrival on 18 January 2023, the vessel was switched to DP control at 2324 h. An APC/XCB BHA with bit was assembled, and Hole U1593A (36°34.5103′N, 25°24.8765′E) was spudded on 19 January at 0245 h from 409.0 mbrf. Recovery for Core 1H was 4.7 m, giving a calculated seafloor depth of 402.5 mbsl.

APC coring continued through Cores 2H–16H (4.7–147.2 mbsf). Indications of partial strokes on three consecutive cores plus high overpull on Core 16H led to a switch to the HLAPC. HLAPC coring commenced with Core 17F and continued through Core 38F (250.6 mbsf), the final depth for Hole U1593A. The drill string was tripped up with the top drive to 202.6 mbsf, the top drive was racked back, and the trip out continued to 404.9 mbrf. The bit cleared the seafloor at 0750 h on 20 January, ending Hole U1593A.

#### 4.5.2.2. Hole U1593B

The rig crew serviced the rig while the vessel was offset 50 m southeast. At 0940 h on 21 January, Hole U1593B (36°34.4916′N, 25°24.9000′E) was spudded from 412.0 mbrf. The recovery of 6.20 m gave a calculated seafloor depth of 404.0 mbsl. APC coring continued with Cores 2H–11H. HLAPC coring began with Core 12F at 101.2 mbsf and continued through Core 39F (232.8 mbsf), the final depth for Hole U1593B. The bit cleared the rotary table at 1409 h on 21 January, ending Hole U1593B.

### 4.5.2.3. Hole U1593C

At 1445 h, the vessel was offset 25 m north. Meanwhile, the crew started assembling the RCB BHA with a bit. Hole U1593C (36°34.5060′N, 25°24.8995′E) was spudded at 1752 h. The hole was advanced without recovery to 192.6 mbsf. At the 192 mbsf mark, the drill pipe started experiencing increasing torque. The drill string was worked up from 189.3 to 173.1 mbsf. During the attempt to work the drill string back to bottom, excessive torque was still observed. The drill string was pulled up again, from 192.6 to 123 mbsf, when there was a loss of rotation. Attempts to free the string with mud sweeps and circulation proved fruitless. Overpull on the drill string was increased to a final attempt at 150,000 lb, still with no success.

At 0830 h, the Schlumberger wireline was rigged up to sever the pipe. The drill string was severed at 37.0 mbsf at 1010 h on 22 January. The drill string immediately regained rotation and was tripped up with the top drive. The pipe cleared the rotary table at 1320 h. The drill floor was secured and thrusters were raised starting at 1646 h. The vessel was switched to bridge control at 1648 h. All thrusters were up and secured and the sea passage began at 1700 h, ending Site U1593.

In total we drilled to a maximum depth of 250.6 mbsf in three holes (U1593A–U1593C) with average core recoveries of 60%, 67%, and <1%, respectively.

## 4.5.3. Principal results

Cores from Site U1593 recovered a coherent stratigraphy from 0 to 251 mbsf (Figure **F10**). Hole U1593A consisted of Sections 398-U1593A-1H-1 through 38F-CC (0–251 mbsf). Hole U1593B consisted of Sections 398-U1593B-1H-1 through 39F-CC (0–232 mbsf). The recovered material was unlithified sediment, dominated by volcanic and tuffaceous sediments interspersed with minor amounts of nonvolcanic sediments in both holes. Six prominent correlatable deposits were identified in Holes U1593A and U1593B. Site U1593 had two lithostratigraphic units:

- Unit I was composed of four subunits:
  - Subunit Ia (0–24 mbsf) was mainly volcanic and tuffaceous lithologies (ash, lapilli, and lapilli-ash and tuffaceous mud/ooze) with small amounts of mud and organic-rich tuffaceous mud;
  - Subunit Ib (24–112 mbsf) was interspersed volcanic and nonvolcanic sediments;
  - Subunit Ic (117–219 mbsf) was almost entirely volcanic lithologies with minor ooze and tuffaceous ooze intervals; and

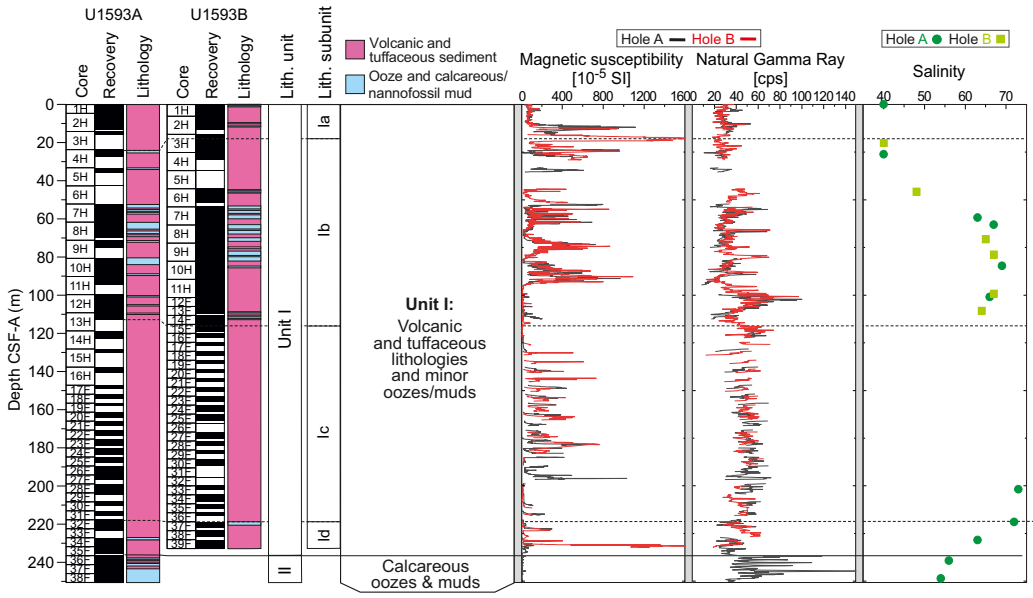


**Figure F10.** Simplified summary and overview for Site U1593, at the distal Kolumbo Volcano site, showing core recovery, stratigraphy, lithology, and units, whole-round measurements of MS and NGR, and salinity measurements.

- Subunit Id (219–232 mbsf) was an increased abundance of greenish gray and well-sorted nonvolcanic lithologies including ooze, organic-rich ooze, and crystal-rich tuffaceous ooze.
- Unit II (235–251 mbsf) had no subunits; it consisted mainly of nonvolcanic oozes or organic-rich oozes with intermittent intervals of tuffaceous ooze and ash.

XRD spectra of volcanic ashes showed a characteristic hump at low °2θ, indicating the presence of volcanic glass, which was less obvious in the tuffaceous mud samples. The only identified crystalline phase in the ashes was Ca-rich plagioclase. Oozes were characterized by calcite, aragonite, quartz, and clay minerals typical of the illite group as the main constituents.

Bedding planes were mostly horizontal to subhorizontal (median values = 3.6°–5.2°) throughout the core. Some slumps were documented in Lithostratigraphic Subunits Ib and Id and in Unit II.

Hole U1593A recovered Holocene to Early Pleistocene aged sediments (<1.078 Ma), and Hole U1593B recovered Late to Early Pleistocene sediments (<0.91? Ma). Foraminiferal faunas were sufficiently common to biostratigraphically divide the Pleistocene sediments into the three Mediterranean planktonic foraminiferal biostratigraphic zones (Figure **F6**):

- MPle2b (0.00–0.53 Ma),
- MPle2a (0.53–0.91 Ma), and
- MPle1c (0.91–1.21 Ma).

Benthic foraminiferal assemblages were highly variable between abundant to reworked/transported specimens and totally barren samples. The low abundances or complete absence of benthic foraminiferal faunas in most of the samples are possibly correlated with rapid emplacement of volcanoclastic sediments and/or inhospitable environmental conditions. Benthic foraminifers yielded few useful paleodepth data. Relative paleowater depths based on oceanicity (percentage of planktonic foraminifers) ranged widely from 0 to 1000 m.

Coarse volcanic deposits at Site U1593 typically had low grain densities and thermal conductivities compared to other sediments at this site. MS was highly variable in the volcaniclastic layers (Figure **F10**) and was sometimes very high (>1500 SI) and helped, together with core images, to correlate, where possible, between Holes U1593A and U1593B. The typical increases of bulk density, *P*-wave velocity, and thermal conductivity with increasing depth were not clearly documented at this site. Porosity values ranged 36%–70%, bulk density 1.1–2.1 g/cm$^3$, and grain density 1.1–2.8 g/cm$^3$, with the lowest values in the volcaniclastic subunits. Compared to typical sediments in which thermal conductivity exceeds 1 W/(m·K) deeper than 100 mbsf, thermal conductivity was low in volcaniclastic sediments at Site U1593. Due to the instability of the formations encountered, downhole logging was not conducted.

Holes U1593A and U1593B had an overlap almost over the entire depth to 232.8 mbsf and allowed stratigraphic correlation based mainly on the MS derived with the WRMSL. A preliminary splice was constructed that contained only minor gaps.

Of the volcanic units sampled, 1 was classified as a basalt, 1 as basaltic andesite, 3 as andesites, and 7 as dacites. Trace element data suggested derivation from both Kolumbo and Santorini. Interstitial water salinity ranged 40–73, with most values 60–70 (Figure **F10**). Most values for interstitial water alkalinity were 4–5.5 mM. Values for pH ranged 7.3–7.9 and generally decreased with depth. $Br^-$, $Cl^-$, B, $Na^+$, $K^+$, $Mg^{2+}$, $Ca^{2+}$, and $SO_4^{2-}$ all followed trends similar to salinity. Trends for Sr, Mn, Ba, and Si did not follow salinity as strongly as the major cations and anions, though Li generally did. Methane, ethane, and propane concentrations were below the detection limit in all measured samples

The upper 117 m of the sequence sampled in Hole U1592A carried normal polarity remanences acquired during Chron C1n (Brunhes). No cores suitable for paleomagnetic analysis were recovered in the 88 m below this (117–205 mbsf), but a 2 m interval with normal polarity at ~206 mbsf was also assigned to the Brunhes Chron. The Brunhes/Matuyama boundary (0.773 Ma) was assigned to the interval 207.5–218.0 mbsf and the interval displaying variable inclinations to Chron C1r.1r. The interval below 240 mbsf was assigned to Chron C1r.1n (Jaramillo).

In summary, Site U1593 recorded more than 1 My of rift fill and volcanism associated with Kolumbo and Santorini Volcanoes. The sequence was dominated by many volcanic and tuffaceous lithologies that will require a great deal of work to chemically fingerprint and to correlate across the study area. Our preliminary results suggest that Kolumbo had major phases of activity in both the mid-Pleistocene and Late Pleistocene. Water depths in the range 250–750 m appear to have been most common in this part of the rift system.

## 4.6. Site U1594

### 4.6.1. Background and scientific objectives

Site U1594 (Prospectus Site CSK-07B) is located in the southern basin of Santorini caldera. It lies at a water depth of 291 mbsl. Site U1595 addresses the same drilling objectives and lies southwest of U1594. Two additional sites (U1596 and U1597) lie in the northern caldera basin.

These four caldera sites were planned to sample intracaldera Seismic Units S1–S3, to test the published correlations between the two caldera basins, to penetrate below Unit S3 (Seismic Unit S4), and to address scientific Objectives 1, 4, 5, and 7 of the *Expedition 398 Scientific Prospectus* (Druitt et al., 2022). The seismic units were thought to probably consist of (S1) muds and sands from cliff mass wasting, (S2) volcaniclastics from Kameni Volcano, and (S3) consolidated coarse blocky tuffs, landslide debris, and/or flood gravels. Seismic Unit S4 may be intracaldera tuffs. The goals were to groundtruth the seismic units, document the processes, products, and potential impacts of the LBA eruption, reconstruct the eruptive history of Kameni Volcano, penetrate below Unit S3, and discover the nature of Unit S4. The combined approach of drilling in the northern and southern caldera basins would enable us to test several hypotheses regarding the LBA caldera-forming eruption of Santorini. By drilling both caldera basins and exploiting our dense seismic reflection coverage, we would gain access to the 3-D architecture of the entire caldera fill and would better understand the relative roles of downfaulting and downsagging in the LBA caldera collapse. We would also target the question of why the northern basin is 100 m deeper than the southern one, with thicker Seismic Unit S1 but thinner Seismic Unit S3. Finally, we would be able to test whether Seismic Unit S3 consists of flood debris from the caldera-flooding event (Nomikou et al., 2016a) or whether it represents LBA intracaldera tuffs (Johnson et al., 2015). Intracaldera Hole U1594A was sampled for the microbiological work of Objective 7.

### 4.6.2. Operations

On 22 January 2023 at 1830 h the vessel arrived at Site U1594 in the southern end of the Santorini caldera. All thrusters were down and secure at 1848 h. The vessel was switched to DP control, starting Site U1594 at 1850 h. The 15.0 nmi transit took 1.8 h at an average speed of 8.3 kt.

#### 4.6.2.1. Hole U1594A

Once given the "all clear," the rig crew made up an APC/XCB BHA with a bit. Hole U1594A (36°23.3368′N, 25°25.0290′E) was spudded on 22 January at 2310 h. The core was shot from 297.0 mbrf and recovered 4.2 m, establishing the seafloor at 291.0 mbsl.

APC coring continued into 23 January, with 94% recovery from Core 2H (4.2 mbsf) to 6H, with the bottom at 51.7 mbsf, the final depth for Hole U1594A. Excessive torque was observed, indicating a collapsing hole. The driller worked the drill string, but the tight conditions persisted. The drill string was pulled up with the top drive from 42.2 mbsf to ~100 m above seafloor. The bit cleared the seafloor at 0350 h.

The decision was made to offset to an alternate site in the southern caldera (Prospectus Site CSK-08B). The vessel was moved in DP mode, starting the 0.7 nmi passage at 0445 h, marking the end of Site U1594.

### 4.6.3. Principal results

The recovered core material at Site U1594 is unlithified sediment, dominated by volcanic material with minor amounts of mud and tuffaceous mud in the upper 1.5 m (Figure **F11**).

- Unit I (0–50 mbsf) consists predominantly of volcanic lithologies (>75% volcanic particles; glass shards, pumice, scoria, crystals) with small amounts of tuffaceous (25%–75% volcanic particles) and nonvolcanic sediments (<25% volcanic particles).
  - Subunit Ia (0–20 mbsf) is a volcanic-dominated succession of ash, lapilli-ash, and lapilli with a minor amount of mud.
  - Subunit Ib (20–50 mbsf) is a volcanic-dominated succession lapilli-ash and lapilli with lesser ash.

The volcanic ash samples from Hole U1594A show a characteristic hump at low °2θ on XRD, indicating the presence of volcanic glass. The only identified crystalline phases in the ash samples are Ca-rich plagioclase, augite, clay minerals of the illite group or smectite group (montmorillonite), and zeolite.

Very rare planktonic and benthic foraminifers as well as rare calcareous nannofossils indicated an age of younger than 0.265 Ma for the sequence, which is consistent with the known intracaldera geology.

Physical properties measurements showed a general trend of increasing *P*-wave velocity and MS (Figure **F11**) with increasing depth at the site. Porosity ranged 51–80 vol%, and bulk density ranged 1.2–1.6 g/cm$^3$. Bulk density did not obviously increase with depth. Grain density ranged 1.6–2.6 g/cm$^3$; more than 40% of discrete samples had grain densities <2.0 g/cm$^3$, and grain density decreased with increasing depth. Compared to typical sediments in which thermal conductivity is close to 1 W/(m·K) at these depths below seafloor, thermal conductivity was low in the volcaniclastic sediments. There was no apparent increase in thermal conductivity with increasing depth.

Of the samples analyzed by ICP-AES, all were dacites of Santorini trace element affinity. Interstitial water salinity was 40 throughout the hole (Figure **F11**). There was a slight increase in alkalinity from the mudline (2.6 mM) to a depth of 13 mbsf (5.7 mM), followed by a slight decrease in total alkalinity with depth to the base of the hole at 15 mbsf. Values for pH ranged 7.8–7.9. There were small variations in boron and major cations and anions in interstitial water, except Br$^-$, which remained constant with depth. There were larger variations in Li, Sr, Mn, Ba, and Si than for cations and anions. Methane, ethane, and propane concentrations were below the detection limit through all of the hole.

Since there was only a single hole, no stratigraphic correlation was possible at Site U1594 and, due to the instability of the formations encountered, downhole logging was not conducted. None of the cores recovered were suitable for paleomagnetic analysis.

For Site U1594, six whole-round core samples were collected for microbial community composition analysis.

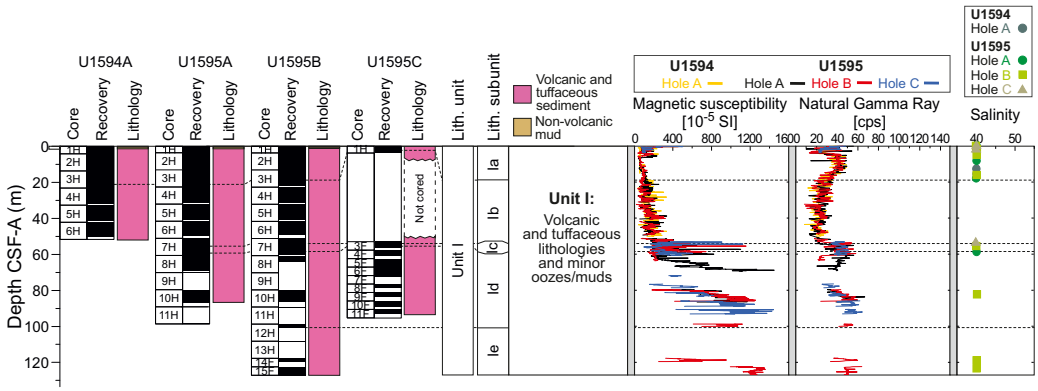


**Figure F11.** Combined simplified summary and overview for Sites U1594 and U1595, from the southern basin in the Santorini Caldera, showing core recovery, stratigraphy, lithology, and units, whole-round measurements of MS and NGR, and salinity measurements from interstitial waters.

To briefly summarize our findings at Site U1594, Lithostratigraphic Subunit 1a corresponds approximately to Seismic Unit S1, which consists of muds and ashes. Lithostratigraphic Subunit 1b corresponds approximately to Seismic Unit S2 and is mostly volcanic in nature. The volcanic material in Subunit 1b appears to be of Kameni origin, but confirmation must await detailed geochemical characterization.

## 4.7. Site U1595

### 4.7.1. Background and scientific objectives

Site U1595 (formerly Prospectus Alternate Site CSK-08B) is located in the southern basin of Santorini caldera at a water depth of 292 m. Site U1594 addresses the same drilling objectives and lies northeast of Site U1595. Two additional sites (U1596 and U1597) lie in the northern caldera basin.

These four caldera sites were planned to sample intracaldera Seismic Units S1–S3, to test the published correlations between the two caldera basins, to penetrate below Unit S3 (Seismic Unit S4), and to address Scientific Objectives 1, 4, 5, and 7 of the *Expedition 398 Scientific Prospectus* (Druitt et al., 2022). The seismic units were thought to probably consist of (S1) muds and sands from cliff mass wasting, (S2) compacted (possibly lithified) sandy volcaniclastics from Kameni Volcano, and (S3) consolidated coarse blocky tuffs, landslide debris, and/or flood gravels. Seismic Unit S4 may be intracaldera tuffs. The goals were to groundtruth the different seismic units, document the processes, products, and potential impacts of the LBA eruption, reconstruct the eruptive history of Kameni Volcano, penetrate below Unit S3, and discover the nature of Unit S4. The combined approach of drilling in the northern and southern caldera basins would enable us to test several hypotheses regarding the LBA caldera-forming eruption of Santorini. By drilling both caldera basins and exploiting our dense seismic reflection coverage, we would gain access to the 3-D architecture of the entire caldera fill and would better understand the relative roles of downfaulting and downsagging in the LBA caldera collapse. We would also target the question of why the northern basin is 100 m deeper than the southern one, with thicker Seismic Unit S1 but thinner Seismic Unit S3. Finally, we would be able to test whether Seismic Unit S3 consists of flood debris from the caldera-flooding event (Nomikou et al., 2016a) or whether it represents LBA intracaldera tuffs (Johnson et al., 2015). Intracaldera Holes U1596B and U1596C were sampled for the microbiological work of Objective 7.

### 4.7.2. Operations

#### 4.7.2.1. Hole U1595A

With the DP move completed at 0530 h on 23 January 2023, Hole U1595A (36°22.8955′N, 25°24.3630′E) was spudded at 0635 h. With a shot depth of 297.0 mbrf and a recovery of 3.6 m, the calculated seafloor depth was 291.6 mbsl.

APC coring continued to Core 11H at 98.6 mbsf, the final depth for Hole U1595A. At 1315 h, while preparing to shoot Core 11H, the hole packed off suddenly. The backpressure exceeded 3400 psi within 1–2 s. The relief valve on both mud pumps ruptured. The pressure spike also sent the sinker bars up, slamming into the oil saver, knocking it off and up into the top drive. Seawater rained down on the drill floor for several seconds. The coring line separated from the rope socket and came spooling out. With no core barrel in the pipe since operation was planned to switch to HLAPC, the sinker bars were lost in the hole.

The driller still had rotation with the pipe but no pressure. Lifting off the elevator showed the pipe to be vertically stuck as well. The mud pump relief valve discs were replaced, and the pumps were put back online. The driller started applying pressure, but the hole still appeared to be packing off, with intermittent pressure spikes to 2800 psi.

An attempt to free the oil saver using the forward coring line sinker bars to drive it down was unsuccessful. However, the drill string was worked free. The drill string was pulled out of the hole with the top drive from 89.1 mbsf to 271.2 mbrf, with the bit clearing the seafloor at 1636 h. With the drill string out of the hole, the rig crew was eventually able to remove the oil saver after ~2 h. The bit cleared the rotary table at 2131 h.

At 2300 h, the vessel began a DP move from Site U1595, ending the site, to Site U1596 (Proposed Site CSK-06B) in the northern portion of the Santorini caldera.

#### 4.7.2.2. Hole U1595B

The ship returned to Site U1595 at 0415 h, 50 m from Hole U1595A on 2 February 2023. The vessel was under DP control at 0440 h. The rig crew began assembling the BHA with a used bit. Core 1H was shot from 297.0 mbrf. Hole U1595B was spudded at 1010 h with 3.7 m of recovery. The seafloor depth was calculated at 291.4 mbsl. Coring continued with the APC from Core 2H to 13H. A 130,000 lb overpull was observed on Core 13H. The bit was advanced to 117.7 mbsf.

At 1900 h, the change was made to HLAPC with Cores 14F–15F to 127.1 mbsf, the final depth for Hole U1595B. Maximum overpull and high amps on the bit advance provided the incentive to leave the hole. The drill string was tripped up with bit clearing the seafloor at 2320 h, ending Hole U1595B.

#### 4.7.2.3. Hole U1595C

The vessel was again offset 50 m along the seismic line toward Prospectus Site CSK-18A. Hole U1595C (36°22.8674′N, 25°24.3062′E) was spudded at 0005 h on 3 February, with Core 1H shot from 297.0 mbrf. The recovery of 3.8 m established the seafloor at 291.3 mbsl. A center bit was dropped for a 49.2 m drilled interval. With the drill-down completed to 53.0 mbsf, coring was picked up again with the HLAPC for Cores 3F–11F to 95.3 mbsf.

After Core 11F, the plan was to drill ahead to 104 mbsf and resume coring. However, high torque led to the drill string stalling. A 100,000 lb overpull was applied with no success. The drill pipe was worked, and after about 20–30 min regained rotation. The decision was made to abandon the hole.

The string was pulled out of the hole with the top drive, clearing the seafloor at 1115 h. The bit cleared the rotary table at 1347 h. The rig floor was secured at 1415 h. Just after 1410 h, the 15 guests disembarked to the launch. The launch was away at 1430 h. The DP move to Site U1596 (Prospectus Site CSK-06B), in the northern caldera, began.

Overall, the core recoveries for Holes U1595A, U1595B, and U1595C were moderate, averaging 46%–73%.

### 4.7.3. Principal results

The material recovered from Site U1595 is unlithified sediment dominated by volcanic material with minor amounts of mud and tuffaceous mud in the upper 1 m (Figure **F11**).

- Lithostratigraphic Unit I (0–87 mbsf) in Hole U1595A consisted predominantly of volcanic lithologies (>75% volcanic particles; glass shards, pumice, scoria, crystals) with small amounts of tuffaceous (25%–75% volcanic particles) and nonvolcanic sediments (<25% volcanic particles). Four subunits were identified:
  - Subunit Ia (21 m thick) consisted predominantly of volcanic lithologies (ash, lapilli-ash, and lapilli) with minor amounts of tuffaceous sediment (tuffaceous mud) and nonvolcanic sediment (mud) in the upper section.
  - Subunit Ib (34 m thick) consisted entirely of volcanic lithologies including ash, lapilli-ash, and lapilli. The boundary between the bottom of Subunit Ia and the top of Subunit Ib was recognized by a distinct color change from dark gray to brown to grayish brown and the appearance of pumice lapilli. The boundary between these subunits was also recognized in physical properties with an increase in MS (Figure **F11**).
  - Subunit Ic (4 m thick) consisted primarily of intercalated thin ash, ash lapilli, and tuffaceous mud.
  - Subunit Id (27 m) consisted entirely of volcanic lithologies.

No calcareous nannofossils or planktonic foraminifers were found at Site U1595; very rare benthic foraminifers and ostracods were insufficient to permit paleoenvironmental analyses.

There was a general trend of increasing bulk density and MS with increasing depth at the site (Figure **F11**). Porosity ranged 34–77 vol% and bulk density 1.3–2.1 g/cm$^3$. Bulk density did not obviously increase with depth. Grain density ranged 1.6–2.7 g/cm$^3$; one-fifth of discrete samples had

grain densities <2.0 g/cm$^3$. Compared to typical sediments in which thermal conductivity is close to 1 W/(m·K) at these depths below seafloor, thermal conductivity was low in the volcaniclastic sediments. Due to the instability of the formations encountered, downhole logging was not conducted.

To establish the CCSF-A depth scale, Holes U1595A–U1595C were analyzed for physical properties using the WRMSL for MS and GRA density and the NGRL for NGR intensity, as well as section-half photos once the cores were split into working and archive halves. Correlation was very challenging at this site, and only the MS data allowed several reliable correlations, whereas NGR and GRA density measurements were strongly overprinted by the irregular distribution of core material in cores with low recovery and a high content of water.

Only five core sections from two cores recovered at Site U1595 were suitable for paleomagnetic analysis using the superconducting rock magnetometer (SRM). The interval analyzed was assigned to the Brunhes Chron, consistent with the age of the Santorini caldera.

Of two volcanic units sampled, both were classified as dacites of Santorini affinity. Interstitial water salinity was 40 throughout the hole (Figure **F11**), total alkalinity was 2.5–9.7 mM, and pH was 6.9–7.8. Bromide, $Cl^-$, $Na^+$, $K^+$, $Mg^{2+}$, and $SO_4^{2-}$ decreased with depth, whereas B and $Ca^{2+}$ were elevated in the deepest sample at 59 mbsf. Trends for Li, Sr, Mn, Ba, and Si showed more variation than the major cations and anions. Methane, ethane, and propane concentrations are below the detection limit through all of Hole U1595A.

In total, 98 subsamples were collected for microbiological analysis from 14 whole-round core samples.

To briefly summarize our findings at Site U1595, Lithostratigraphic Subunit 1a corresponds approximately to Seismic Unit S1, which consists of muds and ashes. Lithostratigraphic Subunit 1b corresponds approximately to Seismic Unit S2 and is mostly volcanic in nature. The volcanic material in Subunit 1b appears to be of Kameni origin as proposed by Johnston et al. (2015), but confirmation must await detailed geochemical characterization. Subunits 1c and 1d correspond approximately to Seismic Unit S3. This shows that Seismic Unit S3 is composed of lithic-pumice sands and gravels rather than intracaldera tuff from the LBA eruption.

## 4.8. Site U1596

### 4.8.1. Background and scientific objectives

Site U1596 (Alternate Prospectus Site CSK-06B) is located in the northern basin of Santorini caldera at a water depth of 382 m. Site U1597 addresses the same drilling objectives and lies southeast of Site U1596. Two additional sites (U1594 and U1595) lie in the southern caldera basin.

These four caldera sites were planned to sample intracaldera Seismic Units S1–S3, to test the published correlations between the two caldera basins, to penetrate below Unit S3 (Seismic Unit S4), and to address Scientific Objectives 1, 4, 5, and 7 of the *Expedition 398 Scientific Prospectus* (Druitt et al., 2022). The seismic units were thought to probably consist of (S1) muds and sands from cliff mass wasting, (S2) compacted (possibly lithified) sandy volcaniclastics from Kameni Volcano, and (S3) consolidated coarse blocky tuffs, landslide debris, and/or flood gravels. Seismic Unit S4 may be intracaldera tuffs. The goals were to groundtruth the different seismic units, document the processes, products, and potential impacts of the LBA eruption, reconstruct the eruptive history of Kameni Volcano, penetrate below Unit S3, and discover the nature of Unit S4. The combined approach of drilling in the northern and southern caldera basins would enable us to test several hypotheses regarding the LBA caldera-forming eruption of Santorini. By drilling both caldera basins and exploiting our dense seismic reflection coverage, we would gain access to the 3-D architecture of the entire caldera fill and would better understand the relative roles of downfaulting and downsagging in the LBA caldera collapse. We would also target the question of why the northern basin is 100 m deeper than the southern one, with thicker Seismic Unit S1 but thinner Seismic Unit S3. Finally, we would be able to test whether Seismic Unit S3 consists of flood debris from the caldera-flooding event (Nomikou et al., 2016a) or whether it represents LBA intracaldera

tuffs (Johnson et al., 2015). Intracaldera Hole U1596B was sampled for the microbiological work of Objective 7.

## 4.8.2. Operations

### 4.8.2.1. Hole U1596A

The DP move to Site U1596 was completed at 0330 h on 24 January 2023 while the crew completed assembling the BHA. At 0430 h, the BHA was lowered and Hole U1596A (36°26.5378′N, 25°22.5130′E) was spudded at 0650 h. The recovery of 3.9 m gave a calculated seafloor depth of 382.0 mbsl. Coring continued to Core 5H at 41.9 mbsf, the final depth for U1596A. Excessive torque was encountered before shooting Core 6H. The decision was made to pull out and offset to the primary site, CSK-05C.

The drill string was pulled from 32.4 mbsf to ~80 m above the seafloor. The DP move started at 1102 h, ending Site U1596 for the first time.

### 4.8.2.2. Hole U1596B

On 3 February, the ship revisited Site U1596 at a location 50 m northwest of Hole U1596A, at 1615 h. The 4.8 nmi DP move from Site U1595 took 1.7 h at a speed of 2.8 kt. The APC/XCB BHA was again assembled with a used bit. Hole U1596B (36°26.5568′N, 25°22.4875′E) was spudded at 1915 h. A recovery of 4.2 m gave a calculated mudline as 381.9 mbsl. APC coring continued to Core 5H at 42.2 mbsf, the final depth for the hole. The core recovery for the two holes (U1596A and U1596B) was 87%–91%.

The drill string was pulled clear of the hole with the top drive. On 4 February at 0105 h, the bit cleared the rotary table, the drill floor was secure at 0145 h. The vessel was brought under bridge control at 0148 h. All thrusters were brought up and secured. The sea passage to Site U1600 started at 0154 h, ending Site U1596.

## 4.8.3. Principal results

Cores from Site U1596 recovered a coherent stratigraphy from 0 to 40 mbsf. This site consisted of two holes, Hole U1596A and U1596B. The sequence was classified as a single lithostratigraphic unit (Figure F12):

- Unit I (0–40 mbsf) consisted of a massive, fine grained, dark gray ash in the upper ~10 m transitioning into a slightly lighter colored, brownish gray ash with lapilli. This was followed downhole by a lapilli-ash and lapilli interval that continued for the remainder of the hole. Three intervals of tuffaceous mud and one interval of mud were observed within the upper section.
  - Subunit Ia (18 m thick) consisted primarily of fine-grained ash with minor tuffaceous mud and mud.
  - Subunit Ib (32 m thick) was mainly lapilli-ash and lapilli.

Bedding dips ranged 1°–4° (average = 2.4°).

No calcareous nannofossils or planktonic foraminifers were found at Site U1596; the very rare benthic foraminifers and ostracods abundances were insufficient to permit paleoenvironmental analyses.

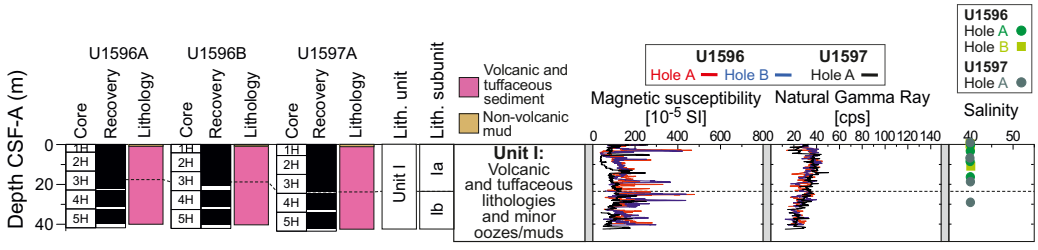


**Figure F12.** Combined simplified summary and overview for Sites U1596 and U1597, from the northern basin in the Santorini Caldera, showing core recovery, stratigraphy, lithology, and units, whole-round measurements of MS and NGR, and salinity measurements from interstitial waters.

There was a general trend of increasing *P*-wave velocity and MS and decreasing NGR with increasing depth at the site (Figure **F12**). Porosity ranged 52–74 vol% and bulk density 1.2–1.6 g/cm$^3$. Bulk density did not obviously increase with depth. Grain density ranged 1.6–2.5 g/cm$^3$; more than 70% of discrete samples had grain densities <2.0 g/cm$^3$. Compared to typical sediments in which thermal conductivity is close to 1 W/(m·K) at these depths below seafloor, the mean value of 0.83 W/(m·K) was low in the volcaniclastic sediments.

Similar to site U1595, correlation was very challenging at this site and only the MS data allowed several reliable correlations, whereas NGR and GRA density measurements were strongly overprinted by the irregular distribution of core material in cores. A preliminary CCSF-A depth scale was constructed but must await further refinement during onshore analysis. Because of the instability of formations encountered downhole logging was not conducted. None of the cores recovered at this site were suitable for paleomagnetic analysis.

Interstitial water salinity was 40 throughout the holes (Figure **F12**). Total alkalinity (2.5–4.3 mM) increased with depth to 8.4 mbsf before decreasing to the base of the hole. Values for pH showed variation within the sampled depths, ranging 7.6–7.9, with the highest value recorded in the mudline sample. Only small variations in $Br^-$, $Cl^-$, B, $Na^+$, and $Ca^+$ were detected. Lithium, Sr, Fe, Mn, Ba, and Si all increased with depth, reaching maxima at either 2.9 mbsf (Sr, Mn, Ba) or 8.4 mbsf (Li, Fe, Si). Methane, ethane, and propane concentrations were below the detection limit. Concentrations of heavier hydrocarbons (*iso*-butane, *n*-butane, and *n*-pentane, and so on) were also below the detection limit throughout the hole.

In total, 14 subsamples were collected for microbiological analysis from two whole-round core samples, and 11 samples were collected from the mudline of the Core 398-U1596B-1H for microbial community composition analysis.

Site U1596 was drilled in its upper part in order particularly to assess any potential technical problems in drilling deeper. It was partly a reconnaissance exercise. It enabled us to discover that Lithostratigraphic Subunits Ia and Ib, which correspond approximately to Seismic Units S1 and S2, were the same in the northern caldera basin as in the southern one. The upper two seismic units in the northern and southern basins therefore correlate.

## 4.9. Site U1597

### 4.9.1. Background and scientific objectives

Site U1597 (formerly Proposed Site CSK-05C) is located in the northern basin of Santorini caldera at a water depth of 382 m. Site U1596 addresses the same drilling objectives and lies northwest of Site U1597. Two additional sites (U1594 and U1595) lie in the southern caldera basin.

These four caldera sites were planned to sample intracaldera Seismic Units S1–S3, to test the published correlations between the two caldera basins, to penetrate below Unit S3 (Seismic Unit S4), and to address Scientific Objectives 1, 4, 5, and 7 of the *Expedition 398 Scientific Prospectus* (Druitt et al., 2022). The seismic units were thought to probably consist of (S1) muds and sands from cliff mass wasting, (S2) compacted (possibly lithified) sandy volcaniclastics from Kameni Volcano, and (S3) consolidated coarse blocky tuffs, landslide debris, and/or flood gravels. Seismic Unit S4 may be intracaldera tuffs. The goals were to groundtruth the different seismic units, document the processes, products, and potential impacts of the LBA eruption, reconstruct the eruptive history of Kameni Volcano, penetrate below Unit S3, and discover the nature of Unit S4. The combined approach of drilling in the northern and southern caldera basins would enable us to test several hypotheses regarding the LBA caldera-forming eruption of Santorini. By drilling both caldera basins and exploiting our dense seismic reflection coverage, we would gain access to the 3-D architecture of the entire caldera fill and would better understand the relative roles of downfaulting and downsagging in the LBA caldera collapse. We would also target the question of why the northern basin is 100 m deeper than the southern one, with thicker Seismic Unit S1 but thinner Unit S3. Finally, we would be able to test whether Seismic Unit S3 consists of flood debris from the caldera-flooding event (Nomikou et al., 2016a) or whether it represents LBA intracaldera tuffs (Johnson et al., 2015).

### 4.9.2. Operations

The revised plan was to be very conservative, while learning the nature of the formation to aid in planning the future caldera work. The immediate foreseen work was limited to 1–2 holes, 40–50 mbsf each.

#### 4.9.2.1. Hole U1597A

Hole U1597A (36°26.2494′N, 05°22.7326′E) was spudded on 24 January 2023 at 1240 h. With a recovery of 5.6 m, the depth of the seafloor was calculated as 382.3 mbsl. Coring continued with APC to Core 5H, a final depth of 43.6 mbsf, and core recovery of 94%. Again, excessive torque started building. The drill string was tripped up with the top drive and the bit cleared the seafloor at 1547 h. The bit cleared the rotary table at 1728 h.

The floor was secured for transit. The thrusters were raised starting at 1815 h. The vessel was switched to bridge control at 1818 h. All thrusters were up and secure and the start of the sea passage began at 1824 h, ending Site U1597 (Proposed Site CSK-05C).

### 4.9.3. Principal results

A single hole, U1597A, was drilled at this site to a depth of 42 mbsf. The recovered material was unlithified sediment, dominated by volcanic material. A single lithostratigraphic unit was identified (Figure **F12**):

- Unit I: consisted of a fine to coarse grained dark gray ash interval in the upper ~10 m, partly accompanied by lapilli-sized clasts, and a slightly lighter colored ash and lapilli-ash interval that continued for the remainder of the hole. Subunits within Unit I were defined by changes in grain size, color, and componentry.
  - Subunit Ia (24 m thick) consisted of fine to coarse grained dark gray ash and lapilli-ash with minor intervals of lapilli, mud, or tuffaceous mud.
  - Subunit Ib (18 m thick) was mainly dark gray, fine- to coarse-grained ash and lapilli-ash.

As reported in previous site reports, on XRD the volcanic ash samples from Hole U1597A showed a characteristic hump at low °2θ, indicating the presence of volcanic glass. The only identified crystalline phases in the ash samples were Ca-rich plagioclase, clay minerals of the illite group, and zeolite.

No sedimentary structures were identified at Site U1597. Although there were some bedding planes, core-induced disturbance prevented measurements.

No calcareous nannofossils or benthic foraminifers were found at this site. Very rare planktonic foraminifers and ostracods occurred but were of insufficient quantity to permit paleoenvironmental analyses.

Physical properties measurements showed that there was a layer at 1–5 mbsf with distinctly higher *P*-wave velocity and lower bulk density than volcaniclastic deposits at shallower and greater depths. Overall, there was a general trend of decreasing NGR with increasing depth (Figure **F12**). Porosity ranged 58–70 vol% and bulk density 1.3–1.6 g/cm$^3$. Bulk density did not obviously increase with depth. Grain density ranged 1.7–2.5 g/cm$^3$; more than 20% of discrete samples had grain densities <2.0 g/cm$^3$. Compared to typical sediments in which thermal conductivity was close to 1 W/(m·K) at these depths below seafloor, the mean value of 0.81 W/(m·K) was low in volcaniclastic sediments at Site U1597.

Since there was only a single hole, no stratigraphic correlation was possible at Site U1596, and due to the instability of the formations encountered, downhole logging was not conducted. None of the cores recovered were suitable for paleomagnetic analysis.

Interstitial water salinity was 40 throughout the hole, and no significant variations were recorded (Figure **F12**). Total alkalinity (2.4–6.6 mM) increased with depth to 18.1 mbsf before decreasing to the base of the hole. Values for pH showed variation within the sampled depths, ranging 7.6–7.7, with the values increasing with depth. Bromide, $Cl^-$, $Na^+$, and $Mg^{2+}$ all increased with depth, while B decreased. Potassium and $Ca^{2+}$ were inversely correlated, with $K^+$ decreasing to a minimum of

5.7 mM at 18.1 mbsf and $Ca^{2+}$ increasing to a maximum of 15 mM at the same depth. Interstitial water values of Li were inversely correlated with Sr, Mn, and Ba, while Fe and Si both increased with depth to their maxima at 18.1 mbsf before slightly decreasing downhole. Methane, ethane, and propane concentrations were below the detection limit through all of the hole. Concentrations of heavier hydrocarbons (*iso*-butane, *n*-butane, and *n*-pentane) were also below the detection limit.

Site U1597 was drilled in its upper part in order to assess any potential technical problems in drilling deeper. It enabled us to discover that Lithostratigraphic Subunits Ia and Ib, which correspond approximately to Seismic Units S1 and S2, were the same in the northern caldera basin as in the southern one. The upper two seismic units in the northern and southern basins therefore correlate.

## 4.10. Site U1598

### 4.10.1. Background and scientific objectives

Site U1598 (formerly alternate Prospectus Site 14A) is located ~8 km northwest of Christiana Island and ~20 km southwest of Santorini in a water depth of 521 mbsl. The drill site targeted the Pliocene–Quaternary volcano-sedimentary fill of the Christiana Basin in two holes.

Christiana Basin formed by subsidence along an east-northeast–west-southwest fault system in the Pliocene to Early Pleistocene, before the changing tectonic regime activated the current northeast–southwest rift system in which the Christiana-Santorini-Kolumbo volcanic field lies (Tsampouraki-Kraounaki and Sakellariou, 2018; Preine et al., 2022b, 2022c). Christiana Basin is deeper than the Anhydros and Anafi Basins; its volcano-sedimentary fill potentially records the earlier volcanic history of the CSK volcanic field (including the products of Christiana and early Santorini), as well as younger Santorini and possibly Milos Volcano to the west along the Aegean volcanic arc. The now-extinct Christiana Volcano produced lavas and tuffs of unknown ages (Aarbourg and Frechen, 1999), but an ignimbrite found on Christiana, Santorini, and the nonvolcanic island of Anafi, called the Christiani Ignimbrite, has the geochemical fingerprint of Christiana magmas (Keller et al., 2010).

Site U1598 was chosen to complement the previously drilled Site U1591. The aim was to retarget a thick pumice layer found at Site U1591 (top ~65 mbsf), for which we had insufficient recovery for our scientific aims, to increase our recovery of the interval. This pumice layer was thought to possibly be the submarine equivalent of the Christiani Ignimbrite. The site address scientific Objectives 1–4 and 6 of the *Expedition 398 Scientific Prospectus* (Druitt et al., 2022).

### 4.10.2. Operations

The vessel arrived at Site U1598 on 24 January 2023 at 1945 h. The vessel was under full DP control at 2015 h, ending the transit and marking the start of Site U1598.

#### 4.10.2.1. Hole U1598A

The APC/XCB BHA with a bit was assembled. Hole U1598A (36°18.2937′N, 25°7.7155′E) was spudded at 2350 h on 24 January from 527.0 mbrf. Core 1H recovered 3.7 m, establishing the seafloor at 521.5 mbsl. Coring continued into 25 January to Core 8H from 60.7 mbsf. The switch was made to the HLAPC with Cores 9F–10F at 79.6 mbsf. High torque was observed when drilling; the drill string was worked, but to be conservative, the decision was made to pull out of the hole. The drill string was tripped up and out of the hole with the bit clearing the seafloor at 0715 h, ending Hole U1598A.

#### 4.10.2.2. Hole U1598B

The vessel was offset 50 m southwest of Hole U1598A. Hole U1598B (36°18.2747′N, 25°7.6929′E) was spudded at 0805 h, using the offset water depth of 532.8 mbrf. A drill-ahead section was completed to 75.6 mbsf. At 1015 h on 25 January, coring commenced with the HLAPC for Cores 2H–6F at 98.8 mbsf, the final depth for Hole U1598B. Excessive torque was again observed, and the decision made to abandon the hole. Core recoveries for Holes U1598A an U1598B were 69% and 34%, respectively.

The string was pulled out of the hole with the top drive, and the bit cleared the seafloor at 1430 h. The top drive was racked back, and the pipe trip up continued to 127 mbrf. The bit cleared the rotary table at 1645 h. The rig floor was secured. The thrusters were raised starting at 1720 h. The vessel was switched to bridge control at 1725 h. All thrusters were up and secured and the sea passage to Site U1599 started at 1730 h on 25 January, ending Site U1598.

### 4.10.3. Principal results

The recovered material at Site U1598 was unlithified in both Holes U1598A and U1598B and was characterized by predominantly volcanic lithologies comprising a single lithostratigraphic unit, as at Site U1591 (Figure **F13**).

- Unit I (0–76.41 mbsf) in Hole U1598A; (to 95.68 mbsf) in Hole U1598B consisted primarily of intercalated volcanic and tuffaceous lithologies, punctuated by intervals of calcareous mud and ooze. As at Site U1591, Unit I was divided into three subunits:
  - Subunit Ia (24 m thick) was composed primarily of lapilli-ash with minor ash and lapilli; other components included tuffaceous mud/sand, calcareous mud, organic-rich calcareous mud, and minor ooze.
  - Subunit Ib (30 m thick) was composed of ooze and organic-rich ooze/calcareous mud, punctuated by tuffaceous mud/ooze and ash.
  - Subunit Ic (20 m thick) was composed mainly of pumice lapilli, lapilli-ash, and ash, with minor lithic lapilli layers.

Bedding planes throughout the sequence dipped at 1°–12° (mean = 5°); however, steeper inclinations (22°–33°) developed in slumps at the bottom of Lithostratigraphic Subunit Ia.

When analyzed by XRD, tuffaceous mud showed the characteristic amorphous hump at low °2θ indicating the presence of volcanic glass. Identified minerals in muds and oozes were calcite, aragonite, quartz, and clay minerals of the illite group; Ca-rich plagioclase, dolomite, halite, and pyrite, were also identified.

Two nannofossil biostratigraphic datums were recognized at Site U1598, representing a continuous Pleistocene sedimentary sequence. The presence of *Emiliania huxleyi* indicated a Middle Pleistocene to Holocene age (≤0.265 Ma) within Zones MNN21a and 21b; the last appearance datum of *Pseudoemiliania lacunosa* defined the NN19/20 boundary. Foraminiferal faunas biostratigraphically divided the Pleistocene into two Mediterranean planktonic foraminiferal biostratigraphic zones (Figure **F6**):

- Zone MPle2b (0.00–0.53 Ma) and
- Zone MPle2a (0.53–0.94 Ma).

The oceanicity data for Site U1598 generally indicated fluctuations from extraneritic to oceanic conditions (100 to >1000 mbsl) through the study section; benthic foraminifer distributions indicated an uppermost to upper bathyal (300–700 m) paleowater depths in the <42 mbsf range.

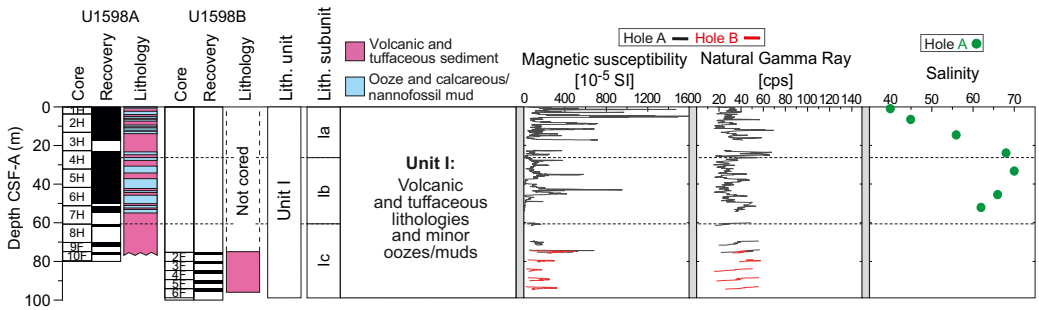


**Figure F13.** Simplified summary and overview for Site U1598, from the western Christiana Basin, showing core recovery, stratigraphy, lithology, and units, whole-round measurements of MS and NGR, and salinity measurements from interstitial waters.

Holes U1598A and U1598B overlapped between 75.3 and 79.4 m; however, in this short interval no reliable correlation could be identified. Due to the instability of formations encountered downhole, logging was not conducted.

Physical properties measurements revealed that MS was highly variable within the volcaniclastic deposits at this site and could exceed 2500 SI in some volcaniclastic layers (Figure **F13**). There was no clear systematic increase in *P*-wave velocity with increasing depth in whole-round measurements. Discrete sample *P*-wave velocities ranged 1.50–2.45 km/s (mean = 1.61 km/s). Sample porosities ranged 50–74 vol%, bulk densities 1.05–1.79 g/cm$^3$, and grain densities 1.10–2.79 g/cm$^3$; most of the low grain densities were found in lapilli layers deeper than 60 mbsf. The mean thermal conductivity was 1.06 W/(m·K) with no apparent increase with depth.

Interstitial water salinity ranged 40–70, with the maximum occurring at 34 mbsf before salinity decreased to the base of the hole (Figure **F13**). Total alkalinity was 2.5–6.8 mM, and values for pH ranged 7.3–7.8, with the highest value at the mudline. Similar to other sites, $Br^-$, $Cl^-$, B, $Na^+$, $K^+$, $Mg^{2+}$, $Ca^{2+}$, and $SO_4^{2-}$ trends resembled those of salinity, but not Li, Sr, Mn, Ba, or Si. Sediment carbonate contents ranged 21–42 wt%; three organic-rich sediment layers were identified as sapropelitic and one as a sapropel. Headspace methane, ethane, and propane concentrations were below the detection limit through all of Hole U1598A. A single volcaniclastic unit analyzed by ICP-AES was classified as dacite.

No paleomagnetic reversals were present in the data set; the sampled interval was therefore assigned to the Brunhes Chron (C1n, <0.773 Ma), which is compatible with available biostratigraphic age constraints.

Site U1598, corresponding to the shallow levels of Site U1591, resembled the upper ~100 m of the latter site and provided no particular extra conclusions. However, it succeeded in its objective to provide better sampling of the thick pumice lapilli layer of Lithostratigraphic Subunit 1c. This pumice, tentatively correlated with the Christiani Ignimbrite onland, is now well sampled in the Christiana Basin.

## 4.11. Site U1599

### 4.11.1. Background and scientific objectives

Site U1599 is located ~6 km north of Anafi Island within the upper reaches of the Anafi Basin in a water depth of 591 mbsl. Permission to drill there was requested, and granted, by the IODP EPSP during the expedition.

Site U1592 was situated on the axis of the Anafi Basin and penetrated a thick basin fill, including mass transported material. In contrast, Site U1599 is located on the southeast margin of the basin. It was chosen to offer a condensed sequence of tephra without quantities of mass wasting debris. The same six Seismic Units U1–U6 (from the bottom up; Preine et al., 2022a, 2022b) present at Site U1592 are present at Site U1599. Site U1599 is included within the area of the 2015 PROTEUS seismic tomography experiment, when subbottom profiling, gravity, and magnetic data were also recorded (Hooft et al., 2017).

Drilling at Site U1599 would enable us to reconstruct a near-complete stratigraphy of volcanic tephra from Santorini and Kolumbo, consistent with both onshore and offshore constraints and pinned by chronological markers from biostratigraphy and magnetostratigraphy. Benthic foraminifers from fine-grained sediments could provide estimates of ancient water depths and, via integration with seismic profiles and chronologic data, of time-integrated basin subsidence rates. Drilling in the Anafi Basin addressed science Objectives 1–4 and 6 of the *Expedition 398 Scientific Prospectus* (Druitt et al., 2022). It was complemented by Site U1589 in the Anhydros Basin because each basin taps a different sediment distributary branch of the Christiana-Santorini-Kolumbo volcanic system.

Although not anticipated in the expedition proposal, biological samples were collected from Hole U1599C. Drilling addressed science Objectives 1–4, 6, and 7 of the *Expedition 398 Scientific Prospectus* (Druitt et al., 2022).

## 4.11.2. Operations

### 4.11.2.1. Hole U1599A

The crew made up the APC/XCB BHA with bit. The BHA was run in to 585.7 mbrf. On 26 January 2023, following 12.75 h of awaiting approval for the site, the go-ahead was given at 1315 h. The APC was fired for Core 1H from 599.0 mbrf. Once retrieved, it was discovered the core barrel had parted at the mid-connection. The pipe tally and the precision depth recorder (PDR) were verified. A second attempt was made with the APC, unfortunately with the same result—a parted core barrel.

An XCB barrel was dropped. Hole U1599A (36°26.9592′N, 25°46.8005′E) was spudded at 1535 h with a solid tag at 602.5 mbrf. After retrieving, the barrel had zero recovery, but it was obvious the coring system had been in the ground.

Still unsure of the stiffness of the formation, the switch was made to HLAPC for Core 2F from 9.7 mbsf. The 97% recovery showed the material was suitable for piston coring. It was assumed there was some tightly compacted layer at the mudline.

Coring was switched to APC for Cores 3H–9H at 71.4 mbsf. The formation stiffened up quickly, forcing the change to HLAPC at Core 10F and all the way to Core 44F to 245.4 mbsf, the final depth for Hole U1599A. There was an unsuccessful overpull of 60,000 lb on Core 44F. An attempt was made to drillover the barrel for ~30 min. The driller aired down the compensator and applied 100,000 lb overpull, which freed the barrel. The decision was made to terminate the hole.

The string was pulled up with top drive from 240.7 to 185.4 mbsf, and the bit cleared the seafloor at 2145 h, ending Hole U1599A.

### 4.11.2.2. Hole U1599B

The vessel was offset 50 m northeast of Hole U1599A. Seafloor was tagged at 604.0 mbsf. Hole U1599B (36°26.9764′N, 25°46.8237′E) was spudded at 2330 h on 27 January 2023 with Core 1X to 9.7 mbsf. Coring was switched to APC from Cores 2H–11H at 95.2 mbsf. Overpulls of 35,000 and 30,000 lb were seen on Cores 10H and 11H, respectively. Coring was again switched, this time to HLAPC, for Core 12F from 104.7 mbsf to 40F at 241.0 mbsf, the final depth for Hole U1599B.

The drill string was tripped up with the top drive, with the bit clearing the seafloor at 0100 h, clearing the rotary table at 0255h. The drill floor was secured and the thrusters were raised starting at 0324 h. All thrusters were up and secure, the vessel under bridge control, and the sea passage started at 0336 h.

### 4.11.2.3. Hole U1599C

Hole U1599C (36°26.9389′N, 25°46.7762′E) was spudded on 30 January at 1925 h. A seafloor depth of 604.0 mbrf was used by offset. A drill-ahead without recovery progressed to 223.0 mbsf at 0445 h. RCB coring commenced with Core 2R on 30 January and proceeded to 1 February and Core 25R to 455.5 mbsf. The drill string was tripped from 455.5 to 404.9 mbsf. The top drive was racked back, and the pipe trip up continued to 55.6 mbsf.

Next, the rig crew pulled the upper guide horn (UGH) in preparation for launching a free fall funnel (FFF). The FFF was assembled and welded in the moonpool. The FFF was launched at 2005 h and immediately chased with the vibration isolated television (VIT) camera at 2015 h.

Once at the seafloor, the VIT camera verified the FFF had landed successfully. The pipe was tripped up, out of the hole, 55.6 mbsf to 516.7 mbrf with the camera observing. The bit cleared the seafloor at 2117 h and seemed to leave the FFF undisturbed.

The VIT was back on deck at 2209 h. The rig crew then reinstalled the UGH and reassembled the rig floor. The pipe trip continued to 145.0 mbrf. The bit cleared the rotary table at 0025 h. The rig floor was secured. The vessel was switched to bridge control at 0130 h on 2 January. All thrusters were up and secure, with the start of the sea passage to Site U1595 at 0142 h, ending Site U1599 for the time being.

After returning on 5 February 2023, the crew made up the RCB BHA with the bit used previously. Winds were forecast to rise above 40 kt, with gusts over 50 kt, exceeding shallow operations limits. The vessel began waiting on weather (WOW) with the pipe down beginning at 0915 h on 6 February. The ship was offset 5.5 nmi west in DP mode to deeper water, away from the Anafi Island, which was on the leeward side.

At 1840 h on 6 February, in anticipation of the weather coming down, the ship started the DP move back over Hole U1599C. The move was completed at 0100 h on 7 February, and the vessel went back to work, following 39.75 h of WOW.

The VIT was deployed. While the camera system was being lowered, the vessel was maneuvered for reentry for about 30 min, reentering Hole U1599C at 0230 h. The VIT was retrieved and back on deck at 0345 h.

The pipe was tripped in to 56.6 mbsf, and the top drive was assembled. A wash barrel was dropped. The trip in with the top drive progressed to 410.0 mbsf, where an obstruction was found. The wash barrel was recovered, a center bit was dropped, and the hole was reamed down to 455.5 mbsf.

At 1300 h on 7 February, RCB coring commenced with Core 26R from 455.5 mbsf and continued into 9 February, to Core 50R at 697.8 mbsf, the final depth for Hole U1599C.

The drill string was tripped with the top drive, the bit cleared the rotary table at 2030 h. The rig floor was secured, with all equipment put away, at 2130 h.

The thrusters were raised, and the vessel brought under bridge control at 2134 h. All thrusters were up and secure, with the start of the sea passage to Heraklion, Greece, at 2142 h, marking the end of Site U1599.

On 10 February, the vessel arrived at the pilot station at 0700 h, with the pilot on board at 0706 h. Tugboats connected at 0715 h. The first line ashore was at 0736 h, ending Expedition 398. The science party disembarked at 1200 h.

In total, Expedition 398 drilled 7.34 km, cored an interval of 5.72 km, and recovered 3.35 km of sediments and basement rock.

### 4.11.3. Principal results

The recovered material in Holes U1599A and U1599B was divided into three lithostratigraphic units. Lithostratigraphic Unit IV was only recovered in Hole U1599C and was 145 m thick (the hole was terminated before the lower boundary was recovered) (Figure **F14**).

- Unit I (upper ~220 m) was nonlithified sediment with mixed volcanic, tuffaceous, and nonvolcanic material.
  - Subunit Ia (45 m thick) consisted of intercalated volcanic sediments with oozes;
  - Subunit Ib (74 m thick) consisted of mixed intervals of ash, (organic-rich) ooze, ooze with dispersed ash pods, and a lapilli-dominated interval;
  - Subunit Ic (33 m thick) consisted of a sequence dominated by (organic-rich) oozes with volcanic and tuffaceous intervals; and
  - Subunit Id (70 m thick) was a volcanic-dominated succession consisting of white lapilli, lapilli-ash, and ash with ooze intervals.,
- Unit II (~25 m) was ooze interspersed with minor volcanic and tuffaceous sediment. It was composed dominantly of oozes with intermittent ash layers. The upper boundary of Unit III was defined by the appearance of consolidated dolomitic marl.
- Unit III (~300 m) consisted of dolomitic marl with organic-rich intervals.
  - Subunit IIIa consisted of dolomitic marl and organic-rich dolomitic marl,
  - Subunit IIIb was an organic-rich dolomitic marl, and
  - Subunit IIIc consisted of dolomitic marl and organic-rich dolomitic marl.
- Unit IV (~145 m) consisted of micrite and calcareous sandstones. It began with calcareous mudstone with interbedded sandstone layers and a few tuffs, then transitioned downhole into

a micrite-dominated succession with interbedded calcareous sandstone. Some sandstone intervals contained ash.

Bedding dips at the site were mostly <30°, except in Lithostratigraphic Unit IV and Subunit IIIa, where they reached up to 70°. Sand dikes, faults, and sediment-filled veins were also common Unit IV and Subunit IIIa.

Calcareous nannofossils and planktonic foraminifers provided good resolution in the Holocene through Upper Pliocene sediments at Site U1599; however, significant reworking within the lower section required the use of first occurrence datums for primary age control. Ages provided by ben-

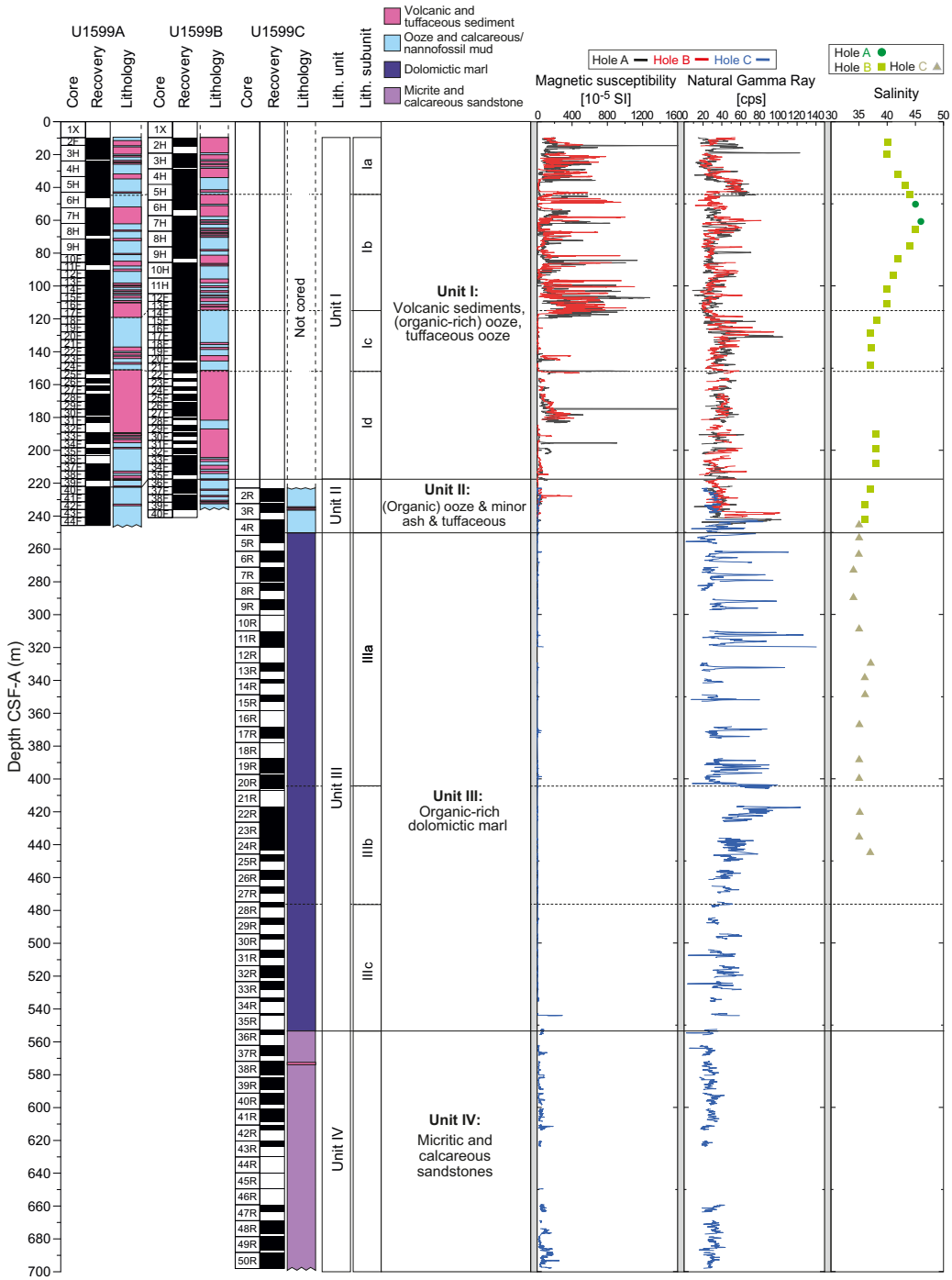


**Figure F14.** Simplified summary and overview for Site U1599, drilled close to Anafi, showing core recovery, stratigraphy, lithology, and units, whole-round measurements of MS and NGR, and salinity measurements from interstitial waters.

thic foraminifers were also consistent with those of planktonic foraminifers and calcareous nannofossils. Ten nannofossil biostratigraphic datum planes and two calcareous nannofossil zones were recognized, representing a discontinuous Pleistocene–Miocene sedimentary sequence. Lithostratigraphic Unit IV was assigned to the Non-Distinctive Zone (Miocene?) or older due to the absence of normal marine planktonic foraminiferal assemblages, and where present, faunas were dwarfed and exhibited very poor preservation. The microfossil component within this section was primarily composed of rare, moderately preserved Ostracoda. There was a significant quantity of carbonaceous plant matter and charcoal present within this interval.

Benthic foraminiferal distributions were variable, indicating paleowater depths from uppermost bathyal (200–400 m) to lower bathyal (>1000 m). Oceanicity (% planktonic foraminifers) values were generally in agreement with benthic foraminiferal paleowater depth indicators in intervals where reworking was low or absent.

To establish the CCSF-A depth scale, Holes U1599A–U1599C were analyzed for physical properties using the WRMSL for MS and GRA density, and images were taken once the cores were split. The MS data were the most reliable physical parameter for correlations.

Physical properties whole-round measurements showed that MS was highly variable within the volcaniclastic deposits of Lithostratigraphic Unit I and could be very high, exceeding 2500 SI. High values of MS corresponded to volcaniclastic layers. MS in Lithostratigraphic Unit III was much lower than that of Units I and II and lower than Unit IV. NGR was more variable in Unit III than in volcaniclastic-dominated Units I and II and the micrites of Unit IV. There was no systematic increase in whole-round GRA bulk density and *P*-wave velocity with increasing depth in Unit I. Discrete measurement porosities ranged 30–78 vol%, density 1.25–2.18 g/cm$^3$, and grain density 1.74–2.81 g/cm$^3$. Most of the low grain densities were found in lapilli layers at depths between 120 and 230 mbsf. Overall, there was a general trend of decreasing porosity and increasing bulk density with increasing depth. Owing to hole instability issues, no wireline logging was possible at this site.

Of 9 volcanic units analyzed by ICP-AES for major and trace elements, 1 was classified as a basalt, 1 as an andesite, and 7 as dacites. Interstitial water salinity ranged 34–46 throughout Holes U1599A, U1599B, and U1599C, with the highest value at 61.6 mbsf. Alkalinity values ranged 1.3–7.9 mM, and pH ranged 7.5–8.2. Ca, Mg, K, Li, and $SO_4$ followed similar trends and had similar local maxima as salinity, but Br, Cl, B, Na, Sr, Mn, Ba, and Si did not. A total of 19 organic-rich sediment units were identified as sapropelitic from TOC measurements, and 11 were identified as sapropels. Headspace methane concentrations in Hole U1599C increased between 266 and 311 mbsf, reaching a maximum of 816.3 ppmv at 275.7 mbsf. Methane, ethane, and propane concentrations were below the detection limit in all other samples.

Paleomagnetic analysis at Site U1599 focused on measurement and demagnetization of archive section halves to determine magnetostratigraphic ages controls. Three reversal boundaries could be tied with confidence to the Geomagnetic Polarity Timescale as follows: (i) the Brunhes–Matuyama transition (0.773 Ma) occurred at 228.3 mbsf (CCSF scale); (ii) the top of the Jaramillo Subchron (C1r.1n; 1.008 Ma) was observed at 250.0 mbsf; and the base of the Jaramillo Subchron (1.076 Ma) occurred at 260.5 mbsf. No magnetostratigraphic correlations were possible deeper than 260.5 mbsf (CCSF scale) due to a combination of degradation of the record by diagenetic alteration and lack of available independent biostratigraphic markers to aid correlation.

A total of 35 whole-round core samples were collected for microbiological study from Hole U1599C.

In summary, Site U1599 proved to be an excellent choice with which to access a condensed (sedimentation rate ~20 cm/ky prior to 0.5 Ma; ~50 cm/ky since 0.5 Ma) succession containing tephra layers from Santorini, Kolumbo, and possibly Christiana. A total of 21 biostratigraphic datums and 3 magnetostratigraphic datums allowed construction of a detailed age-depth model that will ultimately allow fine-scale dating of the many tephra layers observed. The site provides an excellent complement to the adjacent basin sequences (Sites U1589, U1592, and U1599).

## 4.12. Site U1600

### 4.12.1. Background and scientific objectives

Site U1600 is located 10 km south of Anhydros Island within a small graben atop the Anhydros Horst. Anhydros Horst separates the Anhydros Basin to the west from the Anafi Basin to the east (Nomikou et al., 2018; Hooft et al., 2017). The water depth is 326 mbsl. Permission to drill there was requested as proposed Site CSK-24A and granted by the IODP EPSP during the expedition. Three holes were drilled, U1600A–U1600C.

The site was chosen because of its situation on the Anhydros Horst immediately east of the Kolumbo chain of volcanoes and for the well-stratified nature of the graben fill on seismic profiles. It seemed like a likely site at which to drill a condensed sequence of muds and tephra for chronology, sheltered from the large-scale mass wasting of the main basins. Site U1600 is included within the area of the 2015 PROTEUS seismic tomography experiment, when subbottom profiling, gravity, and magnetic data were also recorded (Hooft et al., 2017).

Drilling at Site U1600 would enable us to reconstruct a near-complete volcanic stratigraphy consistent with both onshore and offshore constraints and pinned by chronological markers from biostratigraphy and magnetostratigraphy. Benthic foraminifers from fine-grained sediments could provide estimates of ancient water depths and, via integration with seismic profiles and chronologic data, of time-integrated basin subsidence rates. Although not anticipated in the expedition proposal, biological samples were collected from Hole U1600C. Drilling on the Anhydros Horst addressed science Objectives 1–4, 6, and 7 of the *Expedition 398 Scientific Prospectus* (Druitt et al., 2022).

### 4.12.2. Operations

#### 4.12.2.1. Hole U1600A

With the "all clear" given, the rig crew started assembling the APC/XCB BHA with the same bit used previously. Hole U1600A (proposed Site CSK-24A; 36°32.6277′N, 25°39.0553′E) was spudded with Core 1H on 29 January 2023 at 0710 h. The recovery of 4.0 m gave a calculated seafloor of 326.2 mbsl. Coring continued with APC from Cores 2H–4H. Prior to Core 4H, two misfires (pins did not shear) were experienced with the APC. An XCB barrel was run as a deplugger. Core 4H fired on the third attempt with good recovery, but with 45,000 lb overpull and a completely fractured liner.

The switch was made to HLAPC with Cores 5F–10F at 60.7 mbsf. Core 10F had overpull of 50,000 lb. Coring continued with Cores 11X–13X at 84.4 mbsf, the final depth for Hole U1600A. The recovery for the XCB was extremely poor, and the decision was made to repeat the piston section with Hole U1600B. The drill string was pulled up with the top drive, clearing the seafloor at 1905 h, ending Hole U1600A.

#### 4.12.2.2. Hole U1600B

The ship was positioned 50 m southwest of Hole U1599A. Hole U1600B (36°32.6092′N, 25°39.0311′E) was spudded with Core 1H on 29 January at 2005 h. Recovery of 6.8 m established the water depth at 326.3 mbsl. Coring was switched to HLAPC, from Cores 2F–19F at 91.4 mbsf, the final depth for Hole U1600B.

The drill string was tripped up with the top drive on 30 January, clearing the seafloor at 0735 h. The bit cleared the rotary table at 0900 h. The drill floor was secured for transit.

The crew started raising the thrusters at 0954 h. The vessel was under bridge control at 0956 h. All the thrusters were up and secure and the sea passage started at 1000 h, ending Hole U1600B.

#### 4.12.2.3. Hole U1600C

The vessel returned to Site U1600 on 4 February 2023. Once on site, the rig crew assembled the RCB BHA with a used bit. Hole U1600C (36°32.5890′N, 25°39.0067′E) was spudded at 0655 h. A drill-ahead was done to 75.0 mbsf. RCB coring was initiated with Cores 2R from 75.0 mbsf to 14R at 188.5 mbsf on 5 February, the final depth for Hole U1600C. After confirming that the basement was reached, the string was tripped up with the top drive and the bit cleared the seafloor at 0410 h.

The bit cleared the rig floor at 0525 h. The drill floor was secured at 0548 h, the vessel was switched to bridge control, and the thrusters raised starting at 0550 h. All thrusters were up and secure, starting the sea passage at 0600 h, ending Site U1600. Holes U1600A–U1600C achieved a total penetration of 188.5 mbsf, with average hole core recoveries between 37% and 69%.

### 4.12.3. Principal results

The recovered material from Site U1600 is unlithified in Holes U1600A and U1600B, with a gradual transition to more consolidated material toward the bottom of Hole U1600B (Figure **F15**). Hole U1600C consists of more consolidated sediments; however, the change from sediment to sedimentary rock was clearly identified at ~166 mbsf. Lithostratigraphic units are described below.

- Unit I (upper 92 m) was dominated by volcanic and tuffaceous lithologies with minor intermittent intervals of nonvolcanic muds and sands. All cores were rich in bioclasts (shells and shell fragments), including the volcanic intervals.
  - Subunit Ia was a primarily volcanic-dominated succession of ash, lapilli-ash, and lapilli with tuffaceous ooze/mud intercalated with a minor amount of calcareous mud;
  - Subunit Ib was primarily bioclastic ash and lapilli;
  - Subunit Ic was primarily calcareous tuffaceous sand with shells; and
  - Subunit Id was primarily lapilli.
- Unit II (77–172 mbsf), observed at the bottom 14 m of Hole U1600B and in the upper 87 m of Hole U1600C, is a continuation of the calcareous muds and sands present in Unit I but with two important distinctions: (1) these sediments are devoid of any volcanic and tuffaceous intervals, whereas Unit I has abundant volcanic and tuffaceous intervals, and (2) the sediments are almost entirely organic rich. All of Hole U1600C is designated as Unit II until a sharp discontinuity with basement rock at 172.1 mbsf.
- Unit III, defined after the sharp discontinuity at 172.1 mbsf, is composed of moderately to completely serpentinized peridotites.

Bedding measurements mostly exhibited horizontal to subhorizontal dips, ranging 1°–15° (mean = 4°). Major increases in the bedding dip were identified (upward) from Lithostratigraphic Units II to Subunit Id, with median dips increasing from 4° to 11°. In contrast, from Lithostratigraphic Subunit Id to Subunit Ia, the median dip decreased from 11° to 2°. Mineral veins were abundant in Lithostratigraphic Unit III.

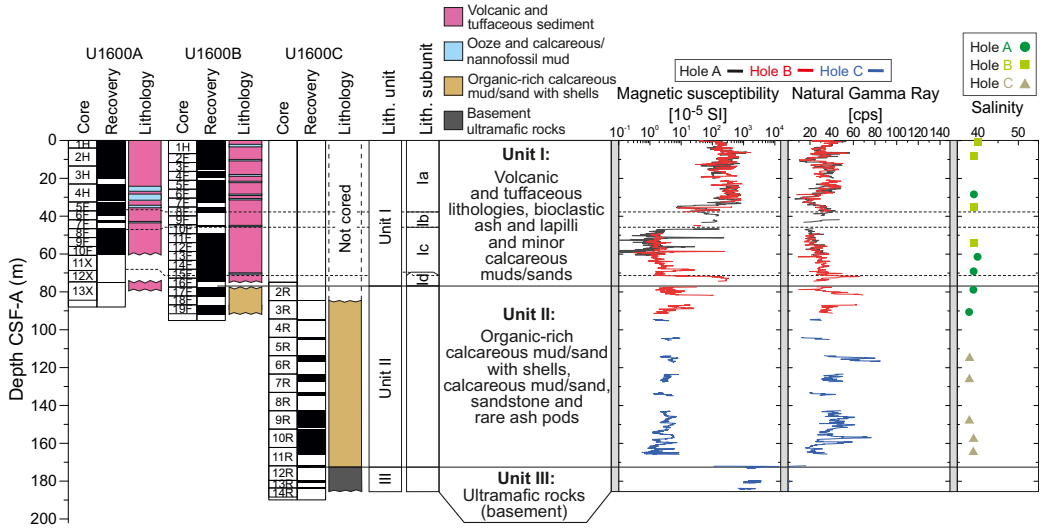


**Figure F15.** Simplified summary and overview for Site U1600, drilled on the Anhydros Horst structure, showing core recovery, stratigraphy, lithology, and units, whole-round measurements of MS and NGR, and salinity measurements from interstitial waters.

Four nannofossil biostratigraphic datums were recognized at Site U1600, representing a continuous Middle–Late Pleistocene sedimentary sequence (CN Zones MNN21b-21a, MNN20-19, MNN18-16b, and MNN16a). Foraminiferal faunas were sufficiently common to biostratigraphically divide the Pleistocene into the majority of Pleistocene Mediterranean planktonic foraminiferal biostratigraphic zones determined via both primary and secondary marker species (Figure **F6**):

- MPle2b (0.00–0.53 Ma),
- MPle2a (0.53–0.94),
- MPle1c (0.94–1.21 Ma),
- MPle1b-a (1.21–1.79 Ma),
- MPl6b (1.79–2.00 Ma),
- MPl6 (2.00–2.09 Ma), and
- MPl5b (2.09–2.41 Ma).

Planktonic foraminifer abundances were highly variable, ranging 0%–94%. Benthic foraminiferal distributions were also variable, indicating paleowater depths from 200 to >1000 m.

To establish the CCSF-A depth scale, we analyzed Holes U1600A and U1600B for physical properties using the WRMSL for MS and GRA density and the NGRL for NGR intensity, as well as photos once the cores were split into working and archive halves. The MS data proved to be the most reliable physical parameter for correlations. Since Hole U1600C had no overlap with Holes U1600A and U1600B, no correlation was possible.

Whole-round physical properties measurements showed that MS was high and variable in the volcaniclastic deposits but was exceptionally high in the basement (>10,000 SI) (Figure **F15**). Two high *P*-wave velocity layers, around 17 and 71 mbsf, corresponded to lapilli-ash layers; overall, there was no clear systematic increase *P*-wave velocity with increasing depth. Discrete measurements of *P*-wave velocity on working-half core sections showed similar downhole variations as those measured on whole-round cores. In basement rocks deeper than 166 mbsf, *P*-wave velocity ranged 3.37–5.29 km/s. Above basement in the upper 166 mbsf, porosity ranged 40–83 vol%, bulk density ranged 1.24–2.00 g/cm$^3$, grain density ranged 1.82–2.77 g/cm$^3$ (with the lowest values in volcaniclastic subunits), and mean thermal conductivity was 1.16 W/(m·K). The two basement samples from Lithostratigraphic Unit III have thermal conductivities markedly higher at 3.1 and 2.2 W/(m·K). Due to the instability of formations encountered downhole, logging was not conducted.

Of the volcaniclastic units analyzed by ICP-AES, one was classified as a basalt, one as basaltic andesite, two as andesites, and three as dacites. Interstitial water salinity values ranged 38–40, with the highest recorded value of 40 at the mudline and at a depth of 61.5 mbsf (Figure **F15**). Alkalinity ranged 2.53–3.3 mM and pH 7.5–7.9. Interstitial water concentrations of $Br^-$, $Cl^-$, and $Na^+$ showed mutually similar trends and generally decreased with depth. Other elements exhibited more complex variations with depth. Carbonate values in sediment samples were highest in Lithostratigraphic Unit I, peaking at 82 wt% at 54 mbsf, which was characterized by volcanic and tuffaceous material but contained calcareous oozes. Carbonate values decreased while TOC increased in Lithostratigraphic Unit II, which was characterized by organic-rich calcareous mud/sand. Four organic-rich layers were identified as sapropels and seven were identified as sapropelitic. Methane, ethane, and propane concentrations were below the detection limit in all measured headspace samples.

The upper 40 m of the sequence at Site 1600 carried normal polarity remanences acquired during Chron C1n (Brunhes). We assigned the Brunhes/Matuyama boundary (0.773 Ma) to the interval 40.0–55.3 mbsf where no data were available, and this interval must also span Chrons C1r.1r and C1r.1n. Several reversals were recognized by reference to biostratigraphic markers below this level. Very limited data were available below 165.8 mbsf.

Microbiological analysis was conducted on three whole-round samples from Site U1600. The whole-round samples were split into 21 subsamples. Most of the microbiological analyses will be

conducted on shore, but first culturing experiments indicate the presence of an iron oxidizing bacterium, most possibly *Mariprofundus ferroxydans*.

In summary, Site 1600 proved to be an excellent choice with which to access a condensed (sedimentation rate ~5 cm/ky) succession containing tephra layers from Santorini, Kolumbo, and possibly Christiana. A total of 20 biostratigraphic datums, combined with magnetostratigraphic controls, allowed construction of a detailed age-depth model that will ultimately allow fine-scale dating of the many tephra layers observed. This includes some pumice layers older than a million years that offer access to the ancestral roots of the CSK volcanoes. The site provides an excellent complement to the adjacent basin sequences (U1589, U1592, and U1599).

# 5. Preliminary scientific assessment

## 5.1. Drilling summary

Despite a number of technical problems, Expedition 398 went a long way toward achieving its objectives. One obstacle was the unstable nature of some of the drilled formations that caused holes to be prematurely abandoned. The worst lithologies were thick pumice layers and thick ash layers. The pumice layers had low strength and appeared to avalanche into the hole, causing the drill string to jam. However, it was judged that the worst offender was the fine-grained ash layers, some of them many meters thick. These ashes appeared to liquefy when drilled, allowing them in some cases to close the hole and jam the drill bit. The combination of these two lithologies restricted the depths to which we could drill at several sites. At Site U1589 the hole collapsed during wireline logging, and at Sites U1590, U1593, and U1595 collapse occurred during drilling. At three sites in the caldera (U1594, U1596, and U1597) we were unable to penetrate further than 40–50 m without problems. As a result of hole instability, we were unable to wireline log at any site except Site U1589, where only one rapid pass was made, and attempts to carry out thermal measurements at all sites except Site U1589 were not possible. At several sites we were forced to pull out prematurely when the drill bit began to stick.

Owing to a combination of these issues, we found ourselves with extra time. We therefore requested permission from the IODP EPSP and Greek Foreign Ministry to drill at two new Sites U1599 and U1600, which was granted during the expedition. These two sites were chosen to be situated within condensed sequences on the edges of the basins, where complete successions could be expected and a greater abundance of mud would stabilize the holes.

The final total of 12 drilling sites provided an excellent combination of successions with which to address the expedition objectives (Druitt et al., 2022). Basin Sites U1589, U1591, U1592, and U1593 provided the opportunity to groundtruth the basin seismic stratigraphy and to link volcanism and tectonics and possibly also sea level. These sites suffered, however, from multiple hiatuses and abundant mass wasting. Therefore, Sites U1599 and U1600 at the basin edges were drilled to provide a most complete and continuous sequence and complement the basin sites to achieve a most complete time series for sediments and eruptive events. Sites U1590 and U1593 both drilled through proximal sequences of Kolumbo pumice layers, allowing us to characterize them, and since they lay each side of the Kolumbo Fault enabled us to determine the displacement across the fault using biostratigraphic datums. Finally, we drilled at all four caldera sites (U1594–1597), giving us a thorough coverage of the intracaldera fill. Unfortunately, the inability to wireline log at all except one site (U1589) limited our ability do real-time core-seismic integration, which must now await detailed analysis of volcanic stratigraphy and chronology.

## 5.2. Meeting the objectives of the expedition

### 5.2.1. Objective 1

Objective 1 (arc volcanism in an active rift environment) was to reconstruct the volcanic history of the CSK volcanic field and its development in space and time. The recovered cores provided us with the volcanic material we need to achieve this goal.

- We successfully drilled through the different units of the Anhydros (Site U1589) and Anafi (Site U1592) Basins as seen on seismic profiles, including many units from Santorini and Kolumbo Volcanoes.
- We drilled on the flanks of Kolumbo Volcano (Sites U1590 and U1593) and traversed several thick pumice layers, although the lack of detailed wireline logging and detailed core-seismic integration have so far limited our ability to correlate the layers in detail to the seismic stratigraphy of Kolumbo.
- Basin margin Sites U1599 and U1600 provided condensed sequences in calmer depositional environments, with preservation of large numbers of tephra ranging from mafic to felsic in composition, ideal for reconstructing a complete record of volcanism of the CSK volcanic field.
- Christiana Basin Site U1591 provided a succession from Miocene to recent with many visible tephra layers, as well as tephra preserved in burrows, offering samples of the earliest stages of the CSK volcanic field and of Milos Volcano to the west.
- Within the caldera at Site U1595, we penetrated a 125 m sequence of tephra and pumice layers that records the history of Kameni Volcano since close to its inception following the LBA eruption 3600 y ago.

Pyroclastic deposits occur in the cores both as fallout tephra and as volcaniclastic turbidites. Magnetic susceptibility turned out to be a good proxy for certain types of volcaniclastic layers but not for all. For example, the deposits of the Thera Pyroclastic Formation of Santorini were recognized by their high MS, although some ash layers had lower MS signals. Liquefaction of ash-rich intervals during core retrieval commonly caused homogenization, blurring the stratigraphic record and destroying sedimentary structures.

Preliminary findings related to Objective 1 include the discovery of a large mid-Pleistocene eruption (possibly the Christiani Ignimbrite of Keller et al., 2010) from a submarine center close to Christiana Volcano. The main phase of construction of Christiana Volcano itself has been shown to be Late Pliocene to Middle Pleistocene. Both Santorini and Kolumbo have unexpectedly long volcanic histories, stretching back over a million years. Owing to poor recovery, we were unable to directly sample the oldest eruptive units of Kolumbo Volcano (K1 and K2), and we will have to rely on basin-margin Sites U1599 and U1600 for this. The cores could confirm the seismostratigraphic correlations of (Preine et al. (2022a, 2022b, 2022c) between the Christiana Basin, Anafi Basin, and western Anhydros Basin. However, correlations to the eastern Anhydros Basin have now been disproven. An unexpected feature of all the tephra in our cores was their fresh nature; this will allow glass major and trace element chemical fingerprinting to be done at all levels of all our cores, simplifying the task of tephra correlation.

The volcanic record was chronologically pinned by large numbers of biostratigraphic datums from foraminifer and nannofossils assemblages. Magnetostratigraphy was less useful in our sequences owing to the widespread diagenetic sulfide phase, greigite, which significantly complicated the recognition of magnetic reversals. Large numbers of sapropels offer the possibility of using astronomically tuned markers to provide a timeline for some drilled intervals with particularly good recovery.

In-depth postcruise work of the shipboard and shore-based scientists will now (1) chemically fingerprint (major and trace element compositions) the main tephra and pumice layers from all cores, using pilot samples taken onboard and those to be collected at the postcruise sampling party, and use established trace element ratios to correlate packages of tephra and major pumice layers across the volcanic field (e.g., Kutterolf et al., 2021a, 2021b; Flaherty et al., 2022); (2) radiometrically date key volcanic layers using $^{40}Ar/^{39}Ar$ on biotite, amphibole, and plagioclase, and/or U-Pb, U-Th, or (U-Th)/He on zircon, to provide absolute ages of volcanic layers, building on the existing biostratigraphic and magnetostratigraphic constraints from the expedition; (3) seek well-dated marker tephra in our cores, such as the 0.39 Ma Campanian eruption. X-ray fluorescence (XRF) scanning of archive-half sections at the IODP Gulf Coast Repository in summer of 2023 will aid in identification of cryptotephra, as will planned scanning using a visible/near-infrared spectrometer at the IODP Bremen Repository in May 2023. Another postcruise objective is to refine the shipboard stratigraphic correlation and establish the scaled CCSF-B depth scale. Afterward,

detailed velocity analysis will allow a more precise core-(log)-seismic integration to more reliably integrate core data with the seismostratigraphic framework.

### 5.2.2. Objective 2

Objective 2 (the volcano-tectonic connection) aimed, once Objective 1 had been largely achieved, to carry out core-seismic integration and to establish links between volcanism and rift pulses in the Anhydros and Anafi Basins. This would test published interpretations based on seismic data (Preine at al., 2022a, 2022b) and feed into modeling of causal relationships and feedbacks. So far, the expedition has provided certain observations relevant to Objective 2:

- The fault west of Kolumbo Volcano has a larger offset than previously known, suggesting that it may be a major structure of the volcanic field and might exert strong control on magmatism at Santorini and Kolumbo.
- There is clear evidence for an association between ash-rich layers and major rift pulses inferred from seismic profiles, notably the presence of volcanic and tuffaceous units on onlap surfaces. However, whether these relate to eruptions, mass wasting of previously deposited pyroclastics, or both has to be established by detailed laboratory analysis of glass and mineral populations in the volcanic layers. Structural observations also identified numerous intervals of slumping and debris flows. The cores and biostratigraphic age constraints support a previously published idea that a major rift pulse in the Anafi Basin preceded the Thera Pyroclastic Formation (Preine et al., 2022a), although with some details modified.

The cores also provide the opportunity to study the possible relationships between volcanism and sea level (e.g., McGuire et al., 1997; Satow et al., 2021). Some cores such as those of Sites U1591 and U1599 contain thick intervals with well-preserved ash layers, sapropels, and sets of biostratigraphic and magnetostratigraphic datums. Such levels will form the basis for detailed tephra chemical fingerprinting, cryptotephra detection, sapropel chronology, and oxygen isotope chronology to tease out relationships between volcanic activity and sea level.

### 5.2.3. Objective 3

Objective 3 (arc magmatism in a region of extending crust) aims, once Objectives 1 and 2 have been achieved, to use glass major elements, trace elements, and radiogenic isotopes to track different magma batches of the volcanic field in space and time, linking to previous work (Klaver et al., 2016a, 2016b). The cores have provided us with ample samples to achieve this goal. This work will enable us to discover to what extent crustal rift pulses cause tapping of different melt batches stored in the crust and mantle, as well to explore the extent to which rifting lowers the pressure on the mantle wedge sufficiently to cause decompression melting, diluting the existing flux melting component of primary magma generation (Bailey et al., 2009; Sternai et al., 2017; Flaherty et al., 2022).

### 5.2.4. Objective 4

Objective 4 (unraveling an iconic caldera-forming eruption) aimed to groundtruth the seismic stratigraphy in order to identify the products of the LBA eruption, thereby allowing much more precise calculation of eruptive volume for this iconic event. We drilled through the LBA deposits outside of the caldera at several sites (U1589–U1593 and U1598–U1600); once chemical analysis has confirmed identification of the LBA deposits in these cores, we can proceed with this objective. A preliminary observation is that the LBA deposits are rather thinner than envisaged by some previous authors (e.g., Sigurdsson et al., 2006), leading toward lower estimates of erupted volume (Pyle, 1990). The cores also provide many sections through the offshore continuations of LBA pyroclastic flows, allowing distinction between fallout and turbidite facies and establishment of facies models for these kinds of deposits through detailed sedimentological and textural work. We discovered that lithic clasts in the LBA turbidites are typically centimeter sized, ruling out the thermal remnant magnetism approach proposed by Druitt et al. (2022). Inside the caldera, we failed to reach the level of LBA intracaldera tuff due to the hole instability issues discussed above. However, we confirmed that Seismic Unit S1 consists mostly of mud/ash and that Seismic Unit S2 consists of material derived from the submarine phase of Kameni, as proposed by Johnston et al. (2015). We also discovered that Seismic Unit S3 is not intracaldera tuff but consists of sands and

gravels related either to marine currents or to the caldera flooding event proposed by Nomikou et al. (2016a). By penetrating through Unit S1 to Unit S2 in both the northern and southern caldera basins, we confirmed the intracaldera stratigraphy of Johnston et al. (2015) is the same across the whole caldera.

### 5.2.5. Objective 5

Objective 5 (volcanic hazards from submarine silicic eruptions) addresses the submarine silicic eruptions of the CSK Volcanoes and the implications of hazards related to such eruptions. Many of the main discoveries made during Expedition 398 related to this objective.

- We discovered a thick and extensive submarine pumice layer related to a mid-Pleistocene explosive eruption from near Christiana Volcano and identified its source.
- We cored at least four pumice deposits from Kolumbo Volcano, tracing the history of this volcano back at least a million years.
- We cored into the intracaldera fill of Santorini caldera, showing that Seismic Unit S2 does indeed come from the Kameni Volcano, as previously postulated (Johnston et al., 2015). This unit therefore provides a time series record of the volcanic and magmatic history of Kameni Volcano since its submarine inception 3600 years ago. Recovery of vegetation traces within these deposits may permit $^{14}C$ dating of the eruptive layers. Detailed sedimentological, textural, and petrological studies of these different submarine tuffs are planned (e.g., Rotella et al., 2015; Carey et al., 2018)

### 5.2.6. Objective 6

Objective 6 (transition from continental to marine environments in the southern Aegean) benefited from a wealth of new observations and data. In the Anhydros (Site U1589) and Anafi (Site U1592) Basins we penetrated the basin fills to basement limestones/marbles of Eocene age. In so doing, we passed through sequences of siliciclastics overlying the basement, including dolomitic ones in Anafi, and recovered benthic foraminifer assemblages recording the early basin flooding and subsequent seawater depths as each basin evolved through successive rift pulses. These two basins turned out to be Late Pleistocene in age rather than Pliocene as previously envisaged (Nomikou et al., 2018). An unexpected feature of these basins was the very high sedimentation rates recorded in some intervals (up to 1 m/ky or more), probably due to large mass wasting events accompanying and following rift pulses. This is consistent with the low measured temperature gradient, steep vertical gradients in pore water chemistry, and fresh glassy tephra in the Anhydros Basin. On the horst separating the Anhydros and Anafi Basins (Site U1600) we bottomed out in serpentinites, which shows that the basement geology of the CSK rift-horst system is very complex. In the Christiana Basin we penetrated the Pliocene–Quaternary basin fill and bottomed out in 120 m of anhydrite-bearing Miocene sediments, providing a valuable example of a marginal Messinian sequence for the general geological community. In drilling the basins, we encountered and documented many sapropel sequences (e.g., De Lange et al., 2008); this opens up the possibility of studying the influence of ash-derived nutrients on sapropel formation.

The cores from these three basins offer excellent opportunities for detailed studies of basin development in the southern Aegean using paleoenvironmental indicators and subsidence modeling and supported by dense age-depth curves from biostratigraphy, magnetostratigraphy, and, in the future, radiometric dating of volcanic minerals. Use of astronomically tuned sapropel records may further refine the age-depth curves (Rohling et al., 2015; Grant et al., 2016).

### 5.2.7. Objective 7

Objective 7 (biological systems reaction to volcanic eruptions and seawater acidification) focused on two intracaldera sites (U1595 and U1596), one site in the Anafi Basin (Site U1599), and one site on the Anhydros Horst (Site U1600), where multiple thin iron-rich layers and one thicker such layer may reflect the presence of bacteria (possibly the iron oxidizing bacterium *Mariprofundus ferroxydans*) and were sampled for culture-based analysis, genetic characterization of microorganisms present, and metagenomic analysis. These samples provide a potentially rich source of information on deep ecosystems, both inside and outside of the caldera. Laboratory-based biochemical and genetic and metagenomic characterization of these layers is now planned.

# 6. Outreach

Expedition 398 had two Outreach Officers, one on board and one onshore. The officers communicated the science objectives of the expedition from the ship to the general public via live ship-to-shore educational tours and coordinated media interviews, social media, and blog posts. The Onshore Outreach Officer also ran in-person outreach activities in collaboration with Greek colleagues from the National Kapodistrian University of Athens (NKUA) and the support of the Municipality of Thira before the beginning of the expedition, developing expedition-specific materials in English and Greek for the "In Search of Earth's Secrets" traveling exhibit. This exhibit was on display for a week in October 2022 at the Bellonio Cultural Center on Santorini.

## 6.1. Educational outreach

The Onboard Outreach Officer hosted live ship-to-shore video tours over Zoom for formal and informal groups all over the world. These events introduced students and members of general audiences to the scientific goals of Expedition 398 and the broader history, significance, and process of scientific ocean drilling.

Broadcasts began with an introduction to the *JOIDES Resolution*, an explanation of the importance of scientific ocean drilling, and a description of the scientific goals of the expedition. In many cases, a scientist who shared a non-English language with the audience hosted the tour. Participants received a 45 min tour of the ship that included the bridge, lifeboats, derrick, rig floor, catwalk, and laboratories. Viewers learned about the core flow process from scientists in each laboratory including physical properties, core description, paleomagnetism, biostratigraphy, and geochemistry. Tours ended with question-and-answer sessions with scientists and the Onboard Outreach Officer.

Over the course of the expedition, the Onboard Outreach Officer facilitated 59 live tours with institutions including primary and secondary schools, colleges and universities, professional societies, laboratory groups, and informal community groups. Student audiences ranged from pre-K to graduate students. Every member of the Science Party on Expedition 398 assisted with the tours in some capacity—either leading a tour themselves or sharing 2–3 min summaries of their work as tours stopped at their workstation—and many of the scientists recruited tour audiences in their home countries. One of the shipboard Greek scientists was instrumental in coordinating tours in Greece, reaching the Department of Geology in Athens and Thessaloniki and many high schools and elementary schools not only from Santorini but from many different places in Greece as well as the UNESCO Associated Schools Network in Greece, resulting in two tours that were each attended by ~1000 students simultaneously.

Tours were conducted in 7 different languages, reaching 6479 people in Greece, Japan, China, France, Germany, the United Kingdom, and the United States. Demand for broadcasts was very high, with 2–4 taking place on most weekdays once students returned to school after the holidays.

The broadcasts were wholly successful, with positive feedback from event organizers. Below are some reactions from teachers and students:

> *"Through the tour of the ship and the presentation of all the laboratories inside the ship and the facilities outside, including of course the drilling ship, the different specialties of scientists, the quick and quite explanatory presentation of the work of each specialty separately and the way they cooperate with each other, Mrs. Nomikou made me feel like one of these worthy scientists!"*

> *"First, I couldn't imagine the drilling vessel before the tour. But it was fun learning a lot about it. I am happy to see one of my unknown worlds."*

> *"The tour leading us to the ocean drilling, to see what's like on the JR, was so interesting. I would like to be on board and study the physical props on the JR in the future!"*

> *"Amazing experience!!! I feel like I was part of the research team. The tour was detailed, descriptive, scientifically accurate, with a commanding sense of immediacy and*

*professionalism. The ship and the laboratories are organized, orderly and electronically equipped. The drilling rig is imposing. I was impressed by the excellent coexistence and interaction of the scientists of different disciplines and the cooperation of all the people involved in the mission. In addition, the fact that the safety of all those involved is at the top of the mission is very important. I thank Mrs. Nomikou for her detailed and illustrative tour and I wish the team much success, health, strength, perseverance and persistence in achieving your goals for the promotion of Greek researchers."*

*"Yes, that was so good... strong connection, lots of student engagement, and Sara did a great job of throwing out lots of tiny hooks of interest that will keep students and teachers coming back for more. Expertly done!"*

*"This is honestly way better than NASA."*

## 6.2. Media outreach

While at sea, a priority for Outreach was sharing Expedition 398 science with the media. This included pitching stories about the expedition to shore-based journalists and hosting several international news and documentary crews and science writers on the ship for 2 days while inside the Santorini caldera.

To generate coverage during the expedition, the Onboard Outreach Officer researched and pitched 51 reporters including journalists at national publications and those at local publications where expedition scientists are based. This effort, together with the efforts of one of the Greek scientists from NKUA, resulted in 9 news items on Greek live TV, radio, prerecorded interviews, and newspapers. During the expedition, these efforts reached more than 200,000 people across the Aegean and all of Greece (Table **T2**). The stories already published were in Greek national news outlets and local US outlets, with 5 stories still in preparation. This outreach also built relationships with journalists at national publications around the world who will write stories as Expedition 398 research is published.

Before hosting news and documentary crews on the ship, the Onboard Outreach Officer prepared an expedition-specific media training course that was offered twice so that day- and night-shift crews could attend. This covered the current news landscape, basic and advanced tips for giving media interviews, and special guidelines for geoscientists talking to journalists in a confined field setting.

**Table T2.** Published stories that interviewed Expedition 398 scientists. Audience size was estimated by Cision, a public relations software application. * = a Skai TV reporter told us the audience size for their live interview.

| Outlet | Link | Format | Audience |
|---|---|---|---|
| Action24 Greece | https://youtu.be/oH0_tg5VseU<br>https://m.youtube.com/watch?v=LQ0bj3d2Tr0&feature=share | Live TV | Unknown |
| Abilene Reflector-Chronicle | http://www.abilene-rc.com/news/kansan-offers-tours-of-aegean-sea-research-vessel/article_8c321fae-8b7b-11ed-aa5a-0ba293ce77a0.html | Print | 3,800 |
| Cascadia Daily News | https://www.cascadiadaily.com/news/2023/jan/08/western-geology-professor-taking-part-in-volcanic-expedition/ | Print | 20,000 |
| Creta Live | https://www.cretalive.gr/kriti/oso-meletas-ta-ifaisteia-toso-mporeis-na-problepseis-mia-mellontiki-ekrixi-toys?fbclid=IwAR28PcsYBDMWyxctIyzi39K38F7iANeyDoiDcEePKr9nGQwbZp-Vg8WK6S4 | Newspaper | |
| Creta TV | https://m.youtube.com/watch?v=1IXEq0BfCVE&embeds_euri=https%3A%2F%2Fif-cdn.com%2F&feature=emb_logo | Live TV | |
| Kathimerini | https://www.kathimerini.gr/society/562227586/sta-sothika-toy-koloympo-to-ploio-poy-ereyna-ta-mystika-tis-kalnteras/ | Print | 95,007 |
| ERT TV | https://www.ertnews.gr/video/ta-mystika-toy-vythoy-tis-santorinis/ | Live TV | Unknown |
| KGMI | https://kgmi.com/podcasts/susan-debari-volcano-expedition/ | Live Radio | 20,018 |
| Fairbanks News-Miner | https://www.newsminer.com/news/education/uaf-researcher-participating-in-historical-greek-volcanic-study/article_7169ccfe-9F7d-11ed-9106-1f274eddae39.html | Print | 47,975 |
| Skai TV | https://www.youtube.com/watch?v=TLzOhOqqspE&feature=youtu.be<br>https://www.youtube.com/watch?v=WTZHu2kx1Wo | Live TV | 12,000* |
| TA NEA | https://www.tanea.gr/print/2023/02/14/greece/pote-tha-ksypnisei-to-ifaisteio-tis-santorinis/ | Newspaper | Unknown |
| Xinhua News/China Geological Museum | https://my-h5news.app.xinhuanet.com/xhh-pc/article/?id=c8e7c0664b872c0cfbd2d25874e6620c&timestamp=36547 | Live TV | 2,500,000 |

During the 2 days with media on board, we had the mayor of Santorini and his deputy, the commander of the port police authority, 2 eminent scientists, and a 12 documentarians and journalists visit from four outlets: GAP Filming/COSMOTE, Skai TV, K22 Films, and GEO Magazine. The Onboard Outreach Officer, Expedition Project Manager (EPM), Co-Chief Scientists, and one of the Greek scientists from NKUA hosted the journalists, and in total, 13 members of the Science Party and JRSO staff and 3 Siem crew members gave interviews. One story has already been published from this effort, and two documentaries will be released next year (Table **T2**).

## 6.3. Social media outreach

The Outreach Officers maintained five websites during the expedition: Twitter, Facebook, Instagram, the *JOIDES Resolution* Expedition 398 web page, and an asynchronous learning module developed in collaboration with Reach the World. From 11 December to 8 February, posts across all social media accounts earned 352,000 impressions and 304 new followers, with an overall engagement rate of 7.07%.

- 85 posts to Twitter resulted in 164,000 impressions and 101 new followers.
- 43 posts to Facebook resulted in 130,000 impressions and 100 new fans.
- 66 posts to Instagram resulted in 58,000 impressions and 103 new followers.

A total of 12 blog posts were written during Expedition 398, 4 on the *JOIDES Resolution* web page and 8 on the Reach the World page. These blogs covered topics including the scientific objectives and methods of the expedition, life at sea, and crew member interviews.

## 6.4. Onshore outreach

To educate and inform tourists and residents of Santorini about the work of the *JOIDES Resolution*, which would be visible off the island's shores in the winter, the Onshore Outreach Officer, one of the expedition's Co-Chiefs, one of the Greek scientists, and several students from the American University in Athens helped run an exhibit on Santorini during 16–23 October 2022 with support from the Municipality of Thira and NKUA colleagues. The exhibit was a combination of the successful US Science Support Program (USSSP) traveling exhibit "In Search of Earth's Secrets" and additional materials specific to the expedition, including banner stands, a brochure, a booklet, and a 3D-printed model of the bathymetry around Santorini. Most of these materials were translated into Greek as well.

The exhibit reached a broad audience of 1823 people, including 8 primary schools, 3 junior high schools, 1 high school, 1 nursery school, a technical high school, and an adult education class. The opening ceremony of the exhibit, featuring presentations from Expedition 398 scientists and USSSP staff, was successful and drew a crowd of about 100 people. The exhibit also provided an opportunity for media outreach, with expedition scientists and USSSP staff taking part in several TV and documentary interviews to complement later follow-up filming on the *JOIDES Resolution* during its time in the caldera.

## 6.5. Ongoing media relations

Much of the pitching work started by the Onboard Outreach Officer will continue onshore. Several stories with national publications are in progress, and new rounds of pitching will kick off as Expedition 398 science is published. To help future audio journalists cover *JOIDES Resolution* expeditions and publications, the Onboard Outreach Officer has recorded a collection of sounds from the *JOIDES Resolution*. After the expedition, these will be organized into a library and released on the *JOIDES Resolution* Soundcloud page for free use by audio producers covering *JOIDES Resolution* science in the future. The GEO Magazine article is scheduled to be published in the summer of 2023, and the K22 Films and GAP Filming/Cosmote documentaries will be released in the first quarter of 2024.

# References


Aarburg, S., and Frechen, M., 1999. Die pyroklastischen Abfolgen der Christiana-lnseln (Süd-Ägäis, Griechenland). In Becker-Haumann, R., and Frechen, M. (Eds.) Terrestrische Quartargeologie. 260–276.

Acocella, V., 2007. Understanding caldera structure and development: an overview of analogue models compared to natural calderas. Earth-Science Reviews, 85(3–4):125–160. **https://doi.org/10.1016/j.earscirev.2007.08.004**

Acocella, V., and Funiciello, F., 2010. Kinematic setting and structural control of arc volcanism. Earth and Planetary Science Letters, 289(1–2):43–53. **https://doi.org/10.1016/j.epsl.2009.10.027**

Athanassas, C.D., Bourlès, D.L., Braucher, R., Druitt, T.H., Nomikou, P., and Léanni, L., 2016. Evidence from cosmic ray exposure (CRE) dating for the existence of a pre-Minoan caldera on Santorini, Greece. Bulletin of Volcanology, 78(5):35. **https://doi.org/10.1007/s00445-016-1026-3**

Bachmann, O., and Huber, C., 2016. Silicic magma reservoirs in the Earth's crust. American Mineralogist, 101(11):2377–2404. **https://doi.org/10.2138/am-2016-5675**

Bailey, J.C., Jensen, E.S., Hansen, A., Kann, A.D.J., and Kann, K., 2009. Formation of heterogeneous magmatic series beneath north Santorini, South Aegean island arc. Lithos, 110(1):20–36. **https://doi.org/10.1016/j.lithos.2008.12.002**

Brandl, P.A., Hamada, M., Arculus, R.J., Johnson, K., Marsaglia, K.M., Savov, I.P., Ishizuka, O., and Li, H., 2017. The arc arises: the links between volcanic output, arc evolution and melt composition. Earth and Planetary Science Letters, 461:73–84. **https://doi.org/10.1016/j.epsl.2016.12.027**

Bruins, H.J., MacGillivray, J.A., Synolakis, C.E., Benjamini, C., Keller, J., Kisch, H.J., Klügel, A., and van der Plicht, J., 2008. Geoarchaeological tsunami deposits at Palaikastro (Crete) and the late Minoan IA eruption of Santorini. Journal of Archaeological Science, 35(1):191–212. **https://doi.org/10.1016/j.jas.2007.08.017**

Brüstle, A., Friederich, W., Meier, T., and Gross, C., 2014. Focal mechanism and depth of the 1956 Amorgos twin earthquakes from waveform matching of analogue seismograms. Solid Earth, 5(2):1027–1044. **https://doi.org/10.5194/se-5-1027-2014**

Budetta, G., Condarelli, D., Fytikas, M., Kolios, N., Pascale, G., Rapolla, A., and Pinna, E., 1984. Geophysical prospecting on the Santorini Islands. Bulletin Volcanologique, 47(3):447–466. **https://doi.org/10.1007/BF01961218**

Camilli, R., Nomikou, P., Escartín, J., Ridao, P., Mallios, A., Kilias, S.P., Argyraki, A., Andreani, M., Ballu, V., Campos, R., Deplus, C., Gabsi, T., Garcia, R., Gracias, N., Hurtós, N., Magí, L., Mével, C., Moreira, M., Palomeras, N., Pot, O., Ribas, D., Ruzié, L., Sakellariou, D., and and the Caldera Science Team, 2015. The Kallisti Limnes, carbon dioxide-accumulating subsea pools. Scientific Reports, 5(1):12152. **https://doi.org/10.1038/srep12152**

Cantner, K., Carey, S., and Nomikou, P., 2014. Integrated volcanologic and petrologic analysis of the 1650AD eruption of Kolumbo submarine volcano, Greece. Journal of Volcanology and Geothermal Research, 269:28–43. **https://doi.org/10.1016/j.jvolgeores.2013.10.004**

Carey, R., Soule, S.A., Manga, M., White, J.D.L., McPhie, J., Wysoczanski, R., Jutzeler, M., Tani, K., Yoerger, D., Fornari, D., Caratori-Tontini, F., Houghton, B., Mitchell, S., Ikegami, F., Conway, C., Murch, A., Fauria, K., Jones, M., Cahalan, R., and McKenzie, W., 2018. The largest deep-ocean silicic volcanic eruption of the past century. Science Advances, 4(1):e1701121. **https://doi.org/10.1126/sciadv.1701121**

Carey, S., Nomikou, P., Bell, K.C., Lilley, M., Lupton, J., Roman, C., Stathopoulou, E., Bejelou, K., and Ballard, R., 2013. $CO_2$ degassing from hydrothermal vents at Kolumbo submarine volcano, Greece, and the accumulation of acidic crater water. Geology, 41(9):1035–1038. **https://doi.org/10.1130/G34286.1**

Cashman, K.V., Sparks, R.S.J., and Blundy, J.D., 2017. Vertically extensive and unstable magmatic systems: a unified view of igneous processes. Science, 355(6331):eaag3055. **https://doi.org/10.1126/science.aag3055**

Cembrano, J., and Lara, L., 2009. The link between volcanism and tectonics in the southern volcanic zone of the Chilean Andes: a review. Tectonophysics, 471(1–2):96–113. **https://doi.org/10.1016/j.tecto.2009.02.038**

Christakis, C.A., Polymenakou, P.N., Mandalakis, M., Nomikou, P., Kristoffersen, J.B., Lampridou, D., Kotoulas, G., and Magoulas, A., 2018. Microbial community differentiation between active and inactive sulfide chimneys of the Kolumbo submarine volcano, Hellenic Volcanic Arc. Extremophiles, 22(1):13–27. **https://doi.org/10.1007/s00792-017-0971-x**

De Lange, G.J., Thomson, J., Reitz, A., Slomp, C.P., Speranza Principato, M., Erba, E., and Corselli, C., 2008. Synchronous basin-wide formation and redox-controlled preservation of a Mediterranean sapropel. Nature Geoscience, 1(9):606–610. **https://doi.org/10.1038/ngeo283**

Dimitriadis, I., Karagianni, E., Panagiotopoulos, D., Papazachos, C., Hatzidimitriou, P., Bohnhoff, M., Rische, M., and Meier, T., 2009. Seismicity and active tectonics at Coloumbo Reef (Aegean Sea, Greece): monitoring an active volcano at Santorini Volcanic Center using a temporary seismic network. Tectonophysics, 465(1–4):136–149. **https://doi.org/10.1016/j.tecto.2008.11.005**

Dimitriadis, I., Papazachos, C., Panagiotopoulos, D., Hatzidimitriou, P., Bohnhoff, M., Rische, M., and Meier, T., 2010. P and S velocity structures of the Santorini–Coloumbo volcanic system (Aegean Sea, Greece) obtained by nonlinear inversion of travel times and its tectonic implications. Journal of Volcanology and Geothermal Research, 195(1):13–30. **https://doi.org/10.1016/j.jvolgeores.2010.05.013**

Dominey-Howes, D.T.M., Papadopoulos, G.A., and Dawson, A.G., 2000. Geological and historical investigation of the 1650 Mt. Columbo (Thera Island) eruption and tsunami, Aegean Sea, Greece. Natural Hazards, 21(1):83–96. **https://doi.org/10.1023/A:1008178100633**

Druitt, T., Kutterolf, S., and Höfig, T.W., 2022. Expedition 398 Scientific Prospectus: Hellenic Arc Volcanic Field. International Ocean Discovery Program. **https://doi.org/10.14379/iodp.sp.398.2022**

Druitt, T.H., 2014. New insights into the initiation and venting of the Bronze-Age eruption of Santorini (Greece), from component analysis. Bulletin of Volcanology, 76(2):794. **https://doi.org/10.1007/s00445-014-0794-x**

Druitt, T.H., and Vougioukalakis, G.E. (Eds.), 2019. The South Aegean Volcanic Arc. Elements, 15(3). **http://elementsmagazine.org/past-issues/south-aegean-volcanic-arc/**

Druitt, T.H., Edwards, L., Mellors, R.M., Pyle, D.M., Sparks, R.S.J., Lanphere, M., Davies, M., and Barreirio, B., 1999. Santorini Volcano. Memoir - Geological Society of London, 19. **http://pubs.er.usgs.gov/publication/70094778**

Druitt, T.H., and Francaviglia, V., 1992. Caldera formation on Santorini and the physiography of the islands in the late Bronze Age. Bulletin of Volcanology, 54(6):484–493. **https://doi.org/10.1007/BF00301394**

Duggen, S., Olgun, N., Croot, P., Hoffmann, L., Dietze, H., Delmelle, P., and Teschner, C., 2010. The role of airborne volcanic ash for the surface ocean biogeochemical iron-cycle: a review. Biogeosciences, 7(3):827–844. **https://doi.org/10.5194/bg-7-827-2010**

Elburg, M.A., Smet, I., and De Pelsmaeker, E., 2014. Influence of source materials and fractionating assemblage on magmatism along the Aegean arc, and implications for crustal growth. Geological Society Special Publication, 385(1):137–160. **https://doi.org/10.1144/SP385.1**

Farner, M.J., and Lee, C.-T.A., 2017. Effects of crustal thickness on magmatic differentiation in subduction zone volcanism: a global study. Earth and Planetary Science Letters, 470:96–107. **https://doi.org/10.1016/j.epsl.2017.04.025**

Feuillet, N., 2013. The 2011–2012 unrest at Santorini rift: stress interaction between active faulting and volcanism. Geophysical Research Letters, 40(14):3532–3537. **https://doi.org/10.1002/grl.50516**

Flaherty, T., Druitt, T.H., Francalanci, L., Schiano, P., and Sigmarsson, O., 2022. Temporal variations in the diversity of primitive melts supplied to the Santorini silicic magmatic system and links to lithospheric stresses. Contributions to Mineralogy and Petrology, 177(8):79. **https://doi.org/10.1007/s00410-022-01941-6**

Flaherty, T., Druitt, T.H., Tuffen, H., Higgins, M.D., Costa, F., and Cadoux, A., 2018. Multiple timescale constraints for high-flux magma chamber assembly prior to the Late Bronze Age eruption of Santorini (Greece). Contributions to Mineralogy and Petrology, 173(9):75. **https://doi.org/10.1007/s00410-018-1490-1**

Freundt, A., Schindlbeck-Belo, J.C., Kutterolf, S., and Hopkins, J.L., 2021. Tephra layers in the marine environment: a review of properties and emplacement processes. In Di Capua, A., De Rosa, R., Kereszturi, G., Le Pera, E., Rosi, M. and Watt, S.F.L.. (Eds.), Volcanic Processes in the Sedimentary Record: When Volcanoes Meet the Environment. Geological Society Special Publication, 520. **https://doi.org/10.1144/SP520-2021-50**

Friedrich, W.L., 2009. Santorini: Volcano, Natural History, Mythology: Aarhus, Denmark (Aarhus University Press).

Fuller, S., Carey, S., and Nomikou, P., 2018. Distribution of fine-grained tephra from the 1650?CE submarine eruption of Kolumbo volcano, Greece. Journal of Volcanology and Geothermal Research, 352:10–25. **https://doi.org/10.1016/j.jvolgeores.2018.01.004**

Grant, K.M., Grimm, R., Mikolajewicz, U., Marino, G., Ziegler, M., and Rohling, E.J., 2016. The timing of Mediterranean sapropel deposition relative to insolation, sea-level and African monsoon changes. Quaternary Science Reviews, 140:125–141. **https://doi.org/10.1016/j.quascirev.2016.03.026**

Hanert, H.H., 2002. Bacterial and chemical iron oxide deposition in a shallow bay on Palaea Kameni, Santorini, Greece: microscopy, electron probe microanalysis, and photometry of in situ experiments. Geomicrobiology Journal, 19(3):317–342. **https://doi.org/10.1080/01490450290098405**

Heath, B.A., Hooft, E.E.E., Toomey, D.R., Papazachos, C.B., Nomikou, P., Paulatto, M., Morgan, J.V., and Warner, M.R., 2019. Tectonism and its relation to magmatism sround Santorini Volcano from upper crustal P wave velocity. Journal of Geophysical Research: Solid Earth, 124(10):10610–10629. **https://doi.org/10.1029/2019JB017699**

Hooft, E.E.E., Heath, B.A., Toomey, D.R., Paulatto, M., Papazachos, C.B., Nomikou, P., Morgan, J.V., and Warner, M.R., 2019. Seismic imaging of Santorini: subsurface constraints on caldera collapse and present-day magma recharge. Earth and Planetary Science Letters, 514:48–61. **https://doi.org/10.1016/j.epsl.2019.02.033**

Hooft, E.E.E., Nomikou, P., Toomey, D.R., Lampridou, D., Getz, C., Christopoulou, M.-E., O'Hara, D., Arnoux, G.M., Bodmer, M., Gray, M., Heath, B.A., and VanderBeek, B.P., 2017. Backarc tectonism, volcanism, and mass wasting shape seafloor morphology in the Santorini-Christiana-Amorgos region of the Hellenic Volcanic Arc. Tectonophysics, 712–713:396–414. **https://doi.org/10.1016/j.tecto.2017.06.005**

Hübscher, C., Ruhnau, M., and Nomikou, P., 2015. Volcano-tectonic evolution of the polygenetic Kolumbo submarine volcano/Santorini (Aegean Sea). Journal of Volcanology and Geothermal Research, 291:101–111. **https://doi.org/10.1016/j.jvolgeores.2014.12.020**

Johnston, E.N., Sparks, R.S.J., Nomikou, P., Livanos, I., Carey, S., Phillips, J.C., and Sigurdsson, H., 2015. Stratigraphic relations of Santorini's intracaldera fill and implications for the rate of post-caldera volcanism. Journal of the Geological Society (London, UK), 172(3):323–335. **https://doi.org/10.1144/jgs2013-114**

Jolivet, L., Faccenna, C., Huet, B., Labrousse, L., Le Pourhiet, L., Lacombe, O., Lecomte, E., Burov, E., Denèle, Y., Brun, J.-P., Philippon, M., Paul, A., Salaün, G., Karabulut, H., Piromallo, C., Monié, P., Gueydan, F., Okay, A.I., Oberhänsli, R., Pourteau, A., Augier, R., Gadenne, L., and Driussi, O., 2013. Aegean tectonics: strain localisation, slab tearing and trench retreat. Tectonophysics, 597–598:1–33. **https://doi.org/10.1016/j.tecto.2012.06.011**

Karstens, J., Crutchley, G., Elger, J., Kühn, M., Schmid, F., Dalla Valle, G., Preine, J., and Nomikou, P., 2019. R/V Poseidon Cruise Report 538: THESEUS Tsunami hazard of explosive submarine eruptions: Kiel, Germany (GEOMAR Helmholtz Centre for Ocean Research Kiel). **https://doi.org/10.3289/cr_pos538**

Keller, J., Dietrich, V., Reusser, E., Gertisser, R., and Aarburg, S., 2010. Recognition of a major ignimbrite in the early evolution of the Santorini Group: the Christiani Ignimbrite. Presented at the Cities on Volcanoes Conference, Tenerife, Spain, January 2010.

Kilias, S.P., Nomikou, P., Papanikolaou, D., Polymenakou, P.N., Godelitsas, A., Argyraki, A., Carey, S., Gamaletsos, P., Mertzimekis, T.J., Stathopoulou, E., Goettlicher, J., Steininger, R., Betzelou, K., Livanos, I., Christakis, C., Bell, K.C., and Scoullos, M., 2013. New insights into hydrothermal vent processes in the unique shallow-submarine arc-volcano, Kolumbo (Santorini), Greece. Scientific Reports, 3(1):2421. **https://doi.org/10.1038/srep02421**

Klaver, M., Carey, S., Nomikou, P., Smet, I., Godelitsas, A., and Vroon, P., 2016a. A distinct source and differentiation history for Kolumbo submarine volcano, Santorini volcanic field, Aegean arc. Geochemistry, Geophysics, Geosystems, 17(8):3254–3273. **https://doi.org/10.1002/2016GC006398**

Klaver, M., Davies, G.R., and Vroon, P.Z., 2016b. Subslab mantle of African provenance infiltrating the Aegean mantle wedge. Geology, 44(5):367–370. **https://doi.org/10.1130/G37627.1**

Kokkalas, S., and Aydin, A., 2013. Is there a link between faulting and magmatism in the south-central Aegean Sea? Geological Magazine, 150(2):193–224. **https://doi.org/10.1017/S0016756812000453**

Kutterolf, S., Freundt, A., Druitt, T.H., McPhie, J., Nomikou, P., Pank, K., Schindlbeck-Belo, J.C., Hansteen, T.H., and Allen, S., 2021a. The medial offshore record of explosive volcanism along the central to eastern Aegean Volcanic Arc, part 2: Tephra ages and volumes, eruption magnitudes and marine sedimentation rate variations. Geochemistry, Geophysics, Geosystems, 22(12):e2021GC010011. **https://doi.org/10.1029/2021GC010011**

Kutterolf, S., Freundt, A., Hansteen, T.H., Dettbarn, R., Hampel, F., Sievers, C., Wittig, C., Allen, S.R., Druitt, T.H., McPhie, J., Nomikou, P., Pank, K., Schindlbeck-Belo, J.C., Wang, K.-L., Lee, H.-Y., and Friedrichs, B., 2021b. The medial offshore record of explosive volcanism along the central to eastern Aegean Volcanic Arc: 1. tephrostratigraphic correlations. Geochemistry, Geophysics, Geosystems, 22(12):e2021GC010010. **https://doi.org/10.1029/2021GC010010**

Kutterolf, S., Jegen, M., Mitrovica, J.X., Kwasnitschka, T., Freundt, A., and Huybers, P.J., 2013. A detection of Milankovitch frequencies in global volcanic activity. Geology, 41(2):227–230. **https://doi.org/10.1130/G33419.1**

Le Pichon, X., and Kreemer, C., 2010. The Miocene-to-Present kinematic evolution of the eastern Mediterranean and Middle East and its implications for dynamics. Annual Review of Earth and Planetary Sciences, 38(1):323–351. **https://doi.org/10.1146/annurev-earth-040809-152419**

Loughlin, S.C., Sparks, S., Brown, S.K., Jenkins, S.F., and Vye-Brown, C. (Eds.), 2015. Global Volcanic Hazards and Risk: Cambridge (Cambridge University Press). **https://doi.org/10.1017/CBO9781316276273**

Lowe, D.J., 2011. Tephrochronology and its application: a review. Quaternary Geochronology, 6(2):107–153. **https://doi.org/10.1016/j.quageo.2010.08.003**

Makris, J., Papoulia, J., and Yegorova, T., 2013. A 3-D density model of Greece constrained by gravity and seismic data. Geophysical Journal International, 194(1):1–17. **https://doi.org/10.1093/gji/ggt059**

McGuire, J., Plank, T., Barrientos, S., Becker, T., Brodsky, E., Cottrell, E., French, M., Fulton, P., Gomberg, J., Gulick, S., Haney, M., Melgar, D., Penniston-Dorland, S., Roman, D., Skemer, P., Tobin, H., Wada, I., and Wiens, D., 2017. The SZ4D Initiative: Understanding the Processes that Underlie Subduction Zone Hazards in 4D. Vision Document Submitted to the National Science Foundation. The IRIS Consortium. **http://www-udc.ig.utexas.edu/external/becker/sz4dmcs/ftp/sz4d.pdf**

McGuire, W.J., Howarth, R.J., Firth, C.R., Solow, A.R., Pullen, A.D., Saunders, S.J., Stewart, I.S., and Vita-Finzi, C., 1997. Correlation between rate of sea-level change and frequency of explosive volcanism in the Mediterranean. Nature, 389(6650):473–476. **https://doi.org/10.1038/38998**

McVey, B.G., Hooft, E.E.E., Heath, B.A., Toomey, D.R., Paulatto, M., Morgan, J.V., Nomikou, P., and Papazachos, C.B., 2019. Magma accumulation beneath Santorini volcano, Greece, from P-wave tomography. Geology, 48(3):231–235. **https://doi.org/10.1130/G47127.1**

National Academies of Sciences, Engineering, and Medicine, 2017. Volcanic Eruptions and Their Repose, Unrest, Precursors, and Timing: Washington, DC (The National Academies Press). **https://doi.org/10.17226/24650**

Newman, A.V., Stiros, S., Feng, L., Psimoulis, P., Moschas, F., Saltogianni, V., Jiang, Y., Papazachos, C., Panagiotopoulos, D., Karagianni, E., and Vamvakaris, D., 2012. Recent geodetic unrest at Santorini Caldera, Greece. Geophysical Research Letters, 39(6):L06309. **https://doi.org/10.1029/2012GL051286**

Nomikou, P., Carey, S., Papanikolaou, D., Croff Bell, K., Sakellariou, D., Alexandri, M., and Bejelou, K., 2012. Submarine volcanoes of the Kolumbo volcanic zone NE of Santorini caldera, Greece. Global and Planetary Change, 90–91:135–151. **https://doi.org/10.1016/j.gloplacha.2012.01.001**

Nomikou, P., Druitt, T.H., Hübscher, C., Mather, T.A., Paulatto, M., Kalnins, L.M., Kelfoun, K., Papanikolaou, D., Bejelou, K., Lampridou, D., Pyle, D.M., Carey, S., Watts, A.B., Weiß, B., and Parks, M.M., 2016a. Post-eruptive flooding of Santorini caldera and implications for tsunami generation. Nature Communications, 7(1):13332. **https://doi.org/10.1038/ncomms13332**

Nomikou, P., Hübscher, C., and Carey, S., 2019. The Christiana–Santorini–Kolumbo volcanic field. Elements, 15(3):171–176. **https://doi.org/10.2138/gselements.15.3.171**

Nomikou, P., Hübscher, C., Papanikolaou, D., Farangitakis, G.P., Ruhnau, M., and Lampridou, D., 2018. Expanding extension, subsidence and lateral segmentation within the Santorini - Amorgos basins during Quaternary: implications for the 1956 Amorgos events, central - south Aegean Sea, Greece. Tectonophysics, 722:138–153. **https://doi.org/10.1016/j.tecto.2017.10.016**

Nomikou, P., Hübscher, C., Ruhnau, M., and Bejelou, K., 2016b. Tectono-stratigraphic evolution through successive extensional events of the Anydros Basin, hosting Kolumbo volcanic field at the Aegean Sea, Greece. Tectonophysics, 671:202–217. **https://doi.org/10.1016/j.tecto.2016.01.021**

Nomikou, P., Papanikolaou, D., Alexandri, M., Sakellariou, D., and Rousakis, G., 2013. Submarine volcanoes along the Aegean volcanic arc. Tectonophysics, 597–598:123–146. **https://doi.org/10.1016/j.tecto.2012.10.001**

Nomikou, P., Parks, M.M., Papanikolaou, D., Pyle, D.M., Mather, T.A., Carey, S., Watts, A.B., Paulatto, M., Kalnins, M.L., Livanos, I., Bejelou, K., Simou, E., and Perros, I., 2014. The emergence and growth of a submarine volcano: the Kameni islands, Santorini (Greece). GeoResJ, 1–2:8–18. **https://doi.org/10.1016/j.grj.2014.02.002**

Okal, E.A., Synolakis, C.E., Uslu, B., Kalligeris, N., and Voukouvalas, E., 2009. The 1956 earthquake and tsunami in Amorgos, Greece. Geophysical Journal International, 178(3):1533–1554. **https://doi.org/10.1111/j.1365-246X.2009.04237.x**

Oulas, A., Polymenakou, P.N., Seshadri, R., Tripp, H.J., Mandalakis, M., Paez-Espino, A.D., Pati, A., Chain, P., Nomikou, P., Carey, S., Kilias, S., Christakis, C., Kotoulas, G., Magoulas, A., Ivanova, N.N., and Kyrpides, N.C., 2016. Metagenomic investigation of the geologically unique Hellenic Volcanic Arc reveals a distinctive ecosystem with unexpected physiology. Environmental Microbiology, 18(4):1122–1136. **https://doi.org/10.1111/1462-2920.13095**

Pallikarakis, A., Triantaphyllou, M.V., Papanikolaou, I., Dimiza, M.D., Reicherter, K., and Migiros, G., 2018. Age constraints and paleoenvironmental interpretation of a borehole sedimentary sequence along the eastern part of the Corinth Isthmus, Greece. Journal of Coastal Research, 34(3):602–617. **https://doi.org/10.2112/JCOASTRES-D-16-00191.1**

Papazachos, C.B., 2019. Deep structure and active tectonics of the South Aegean Volcanic Arc. Elements, 15(3):153–158. **https://doi.org/10.2138/gselements.15.3.153**

Parkes, R.J., Cragg, B.A., and Wellsbury, P., 2000. Recent studies on bacterial populations and processes in subseafloor sediments: a review. Hydrogeology Journal, 8(1):11–28. **https://doi.org/10.1007/PL00010971**

Parks, M.M., Moore, J.D.P., Papanikolaou, X., Biggs, J., Mather, T.A., Pyle, D.M., Raptakis, C., Paradissis, D., Hooper, A., Parsons, B., and Nomikou, P., 2015. From quiescence to unrest: 20years of satellite geodetic measurements at Santorini volcano, Greece. Journal of Geophysical Research: Solid Earth, 120(2):1309–1328. **https://doi.org/10.1002/2014JB011540**

Pe-Piper, G., and Piper, D.J.W., 2005. The South Aegean active volcanic arc: relationships between magmatism and tectonics. In Fytikas, M., and Vougioukalakis, G.E. (Eds.), The South Aegean Active Volcanic Arc: Present Knowledge and Future Perspectives. Developments in Volcanology, 7: 113–133. **https://doi.org/10.1016/S1871-644X(05)80034-8**

Piper, D.J.W., and Perissoratis, C., 2003. Quaternary neotectonics of the South Aegean arc. Marine Geology, 198(3–4):259–288. **https://doi.org/10.1016/S0025-3227(03)00118-X**

Polymenakou, P.N., Nomikou, P., Zafeiropoulos, H., Mandalakis, M., Anastasiou, T.I., Kilias, S., Kyrpides, N.C., Kotoulas, G., and Magoulas, A., 2021. The Santorini volcanic complex as a valuable source of enzymes for bioenergy. Energies, 14(5):1414. **https://doi.org/10.3390/en14051414**

Preine, J., Hübscher, C., Karstens, J., and Nomikou, P., 2022a. Volcano-tectonic evolution of the Christiana-Santorini-Kolumbo rift zone. Tectonics, 41(11):e2022TC007524. **https://doi.org/10.1029/2022TC007524**

Preine, J., Karstens, J., Hübscher, C., Crutchley, G.J., Druitt, T.H., Schmid, F., and Nomikou, P., 2022b. The hidden giant: how a rift pulse triggered a cascade of sector collapses and voluminous secondary mass-transport events in the early evolution of Santorini. Basin Research, 34(4):1465–1485. **https://doi.org/10.1111/bre.12667**

Preine, J., Karstens, J., Hübscher, C., Nomikou, P., Schmid, F., Crutchley, G.J., Druitt, T.H., and Papanikolaou, D., 2022c. Spatio-temporal evolution of the Christiana-Santorini-Kolumbo volcanic field, Aegean Sea. Geology, 50(1):96–100. **https://doi.org/10.1130/G49167.1**

Preine, J., Schwarz, B., Bauer, A., and Hübscher, C., 2020. When there is no offset: a demonstration of seismic diffraction imaging and depth-velocity model building in the southern Aegean Sea. Journal of Geophysical Research: Solid Earth, 125(9):e2020JB019961. **https://doi.org/10.1029/2020JB019961**

Pyle, D.M., 1990. New estimates for the volume of the Minoan eruption. In Hardy, D.A., Thera and the Aegean World III (Volume 2). London (Thera Foundation), 113–121.

Pyle, D.M., and Elliott, J.R., 2006. Quantitative morphology, recent evolution, and future activity of the Kameni Islands volcano, Santorini, Greece. Geosphere, 2(5):253–268. **https://doi.org/10.1130/GES00028.1**

Rabillard, A., Jolivet, L., Arbaret, L., Bessière, E., Laurent, V., Menant, A., Augier, R., and Beaudoin, A., 2018. Synextensional granitoids and detachment systems within cycladic metamorphic core complexes (Aegean Sea, Greece): toward a regional tectonomagmatic model. Tectonics, 37(8):2328–2362. **https://doi.org/10.1029/2017TC004697**

Rohling, E.J., Marino, G., and Grant, K.M., 2015. Mediterranean climate and oceanography, and the periodic development of anoxic events (sapropels). Earth-Science Reviews, 143:62–97. **https://doi.org/10.1016/j.earscirev.2015.01.008**

Rotella, M.D., Wilson, C.J.N., Barker, S.J., Schipper, C.I., Wright, I.C., and Wysoczanski, R.J., 2015. Dynamics of deep submarine silicic explosive eruptions in the Kermadec arc, as reflected in pumice vesicularity textures. Journal of Volcanology and Geothermal Research, 301:314–332. **https://doi.org/10.1016/j.jvolgeores.2015.05.021**

Royden, L.H., and Papanikolaou, D.J., 2011. Slab segmentation and late Cenozoic disruption of the Hellenic arc. Geochemistry, Geophysics, Geosystems, 12(3):Q03010. **https://doi.org/10.1029/2010GC003280**

Sachpazi, M., Laigle, M., Charalampakis, M., Diaz, J., Kissling, E., Gesret, A., Becel, A., Flueh, E., Miles, P., and Hirn, A., 2016. Segmented Hellenic slab rollback driving Aegean deformation and seismicity. Geophysical Research Letters, 43(2):651–658. **https://doi.org/10.1002/2015GL066818**

Satow, C., Gudmundsson, A., Gertisser, R., Ramsey, C.B., Bazargan, M., Pyle, D.M., Wulf, S., Miles, A.J., and Hardiman, M., 2021. Eruptive activity of the Santorini Volcano controlled by sea-level rise and fall. Nature Geoscience, 14(8):586–592. **https://doi.org/10.1038/s41561-021-00783-4**

Satow, C., Tomlinson, E.L., Grant, K.M., Albert, P.G., Smith, V.C., Manning, C.J., Ottolini, L., Wulf, S., Rohling, E.J., Lowe, J.J., Blockley, S.P.E., and Menzies, M.A., 2015. A new contribution to the Late Quaternary tephrostratigraphy of the Mediterranean: Aegean Sea core LC21. Quaternary Science Reviews, 117:96–112. **https://doi.org/10.1016/j.quascirev.2015.04.005**

Schippers, A., Neretin, L.N., Kallmeyer, J., Ferdelman, T.G., Cragg, B.A., John Parkes, R., and Jørgensen, B.B., 2005. Prokaryotic cells of the deep sub-seafloor biosphere identified as living bacteria. Nature, 433(7028):861–864. **https://doi.org/10.1038/nature03302**

Schmincke, H.U., and Sumita, M., 1998. Volcanic evolution of Gran Canaria reconstructed from apron sediments: synthesis of VICAP project drilling. In Weaver, P.P.E., Schmincke, H.-U., Firth, J.V., and Duffield, W. (Eds.), Pro-

ceedings of the Ocean Drilling Program, Scientific Results. 157: College Station, TX (Ocean Drilling Program). **https://doi.org/10.2973/odp.proc.sr.157.135.1998**

Shaw, B., and Jackson, J., 2010. Earthquake mechanisms and active tectonics of the Hellenic subduction zone. Geophysical Journal International, 181(2):966–984. **https://doi.org/10.1111/j.1365-246X.2010.04551.x**

Sigurdsson, H.E., 2015. Encyclopedia of Volcanoes: New York (Elsevier). **https://doi.org/10.1016/C2015-0-00175-7**

Sternai, P., Caricchi, L., Garcia-Castellanos, D., Jolivet, L., Sheldrake, T.E., and Castelltort, S., 2017. Magmatic pulse driven by sea-level changes associated with the Messinian salinity crisis. Nature Geoscience, 10(10):783–787. **https://doi.org/10.1038/ngeo3032**

Syracuse, E.M., van Keken, P.E., and Abers, G.A., 2010. The global range of subduction zone thermal models. Physics of the Earth and Planetary Interiors, 183(1):73–90. **https://doi.org/10.1016/j.pepi.2010.02.004**

Templeton, A.S., 2011. Geomicrobiology of iron in extreme environments. Elements, 7(2):95–100. **https://doi.org/10.2113/gselements.7.2.95**

Tsampouraki-Kraounaki, K., and Sakellariou, D., 2018. Seismic stratigraphy and geodynamic evolution of Christiana Basin, South Aegean Arc. Marine Geology, 399:135–147. **https://doi.org/10.1016/j.margeo.2018.02.012**

Ulvrova, M., Paris, R., Nomikou, P., Kelfoun, K., Leibrandt, S., Tappin, D.R., and McCoy, F.W., 2016. Source of the tsunami generated by the 1650AD eruption of Kolumbo submarine volcano (Aegean Sea, Greece). Journal of Volcanology and Geothermal Research, 321:125–139. **https://doi.org/10.1016/j.jvolgeores.2016.04.034**

Vougioukalakis, G., Sparks, R.S., Druitt, T., Pyle, D., Papazachos, C., and Fytikas, M., 2016. Volcanic hazard assessment at Santorini Volcano: a review and a synthesis in the light of the 2011–2012 Santorini unrest. Bulletin of the Geological Society of Greece, 50(1):274–283. **https://doi.org/10.12681/bgsg.11728**

Walter, T.R., and Amelung, F., 2007. Volcanic eruptions following M ≥ 9 megathrust earthquakes: implications for the Sumatra-Andaman volcanoes. Geology, 35(6):539–542. **https://doi.org/10.1130/G23429A.1**

Wulf, S., Keller, J., Satow, C., Gertisser, R., Kraml, M., Grant, K.M., Appelt, O., Vakhrameeva, P., Koutsodendris, A., Hardiman, M., Schulz, H., and Pross, J., 2020. Advancing Santorini's tephrostratigraphy: new glass geochemical data and improved marine-terrestrial tephra correlations for the past ~360 kyrs. Earth-Science Reviews, 200:102964. **https://doi.org/10.1016/j.earscirev.2019.102964**